Innovations in In-Shoe Plantar Pressure Measurement Technology for Field Based Quantification of Running Gait

By

Samuel Carl William Blades

A Dissertation Submitted in Partial Fulfillment of the Requirements for the Degree of

DOCTOR OF PHILOSOPHY

In the Department of Exercise Sciences, Physical & Health Education

University of Victoria

Innovations in In-Shoe Plantar Pressure Measurement Technology for Field Based Quantification of Running Gait

By

Samuel Carl William Blades

Supervisory Committee

Dr. Marc Klimstra
Department of Exercise Science, Physical & Health Education

Dr. Sandra Hundza
Department of Exercise Science, Physical & Health Education

Dr. David Kennedy
Department of Exercise Science, Physical & Health Education

Dr. Stuart MacDonald
Faculty of Psychology

Abstract

Although substantial progress has been made in the field of running biomechanics, a significant portion of this research has been confined to laboratory settings. Data collection within the laboratory, while controlled, often lacks the ecological validity necessary to capture the complexities of athletes' performances in their natural training and competition environments. Given this need, in-shoe plantar pressure measurement technology is of primary importance due to its location of measurement and its unique capacity to deliver continuous measurements of both kinematic and kinetic biomechanical data. However, most commercially available in-shoe plantar pressure measurement systems (PPMS) are designed primarily for use in research settings and are thus unsuitable for field-based use due in part, to their high cost, low durability, and cumbersome hardware designs that can interfere with natural running gait. These limitations restrict researchers, athletes, coaches, and footwear designers from using PPMS to acquire valuable biomechanical data in training and competition environments. The development of a wearable, field-appropriate, in-shoe PPMS capable of providing lab-quality pressure data and its derivative biomechanical signals could address the current gap in measurement technology enabling significant advancements in running biomechanics research. The development of such a technology, however, is highly demanding due to many competing requirements such as low weight, high durability, imperceptible form factor, and cost-effectiveness while still providing lab-quality data.

The purpose of this dissertation is to present research that could aid in the development of a wearable, field-appropriate, in-shoe PPMS through the following research objectives. The first research objective was to determine the accuracy and performance of a low-cost, fully integrated pressure sensing insole relative to a research-grade PPMS using laboratory-standard equipment on bench-top and in-situ performance tests (Chapter 2). The second research objective was to

determine the optimal sparse sensor layout and plantar pressure distribution estimation method capable of measuring the complete plantar pressure distribution with lab quality accuracy (Chapter 3). The final research objective was to develop and determine the optimal foot contact event detection algorithms for use with plantar pressure data to enable highly accurate gait phase analysis (Chapter 4). The results presented in this dissertation demonstrate the feasibility of the development of a wearable, field-appropriate, PPMS that can provide accurate kinematic and kinetic data. The application of these findings can aid in the further development of wearable PPMS, leading to advancements in the field of running biomechanics and the sport of running.

Table of Contents

Supervisory Committee ii

Abstract iii

Table of Contents v

List of Tables ix

List of Figures x

List of Symbols, Abbreviations, and Nomenclature xii

Acknowledgements xv

Dedication xvii

Introduction 1

1. Background 5

1.1 Introduction 5

1.2 Applications of running gait biomechanics 5

1.3 Lab based measurement technologies 8

1.3.1 Motion capture 8

1.3.2 Force platforms & treadmills 9

1.3.3 Inertial measurement units 10

1.3.4 Pressure measurement systems 11

1.3.5 Limitations of research grade PPMS 13

1.4 Requirements for wearable PPMS 15

1.4.1 Matrix vs. discrete sensor configuration 15

1.4.2 Spatial Resolution 16

1.4.3 Sample rate 17

1.4.4 Pressure sensor response 17

1.5 Summary 19

2. Characterization of the Kinetyx® SI Wireless Pressure-Measuring Insole during Benchtop Testing and Running Gait 20

2.1 Introduction: 20

Materials and Methods 25

2.1.1 Part 1—Benchtop Tests 25

2.1.2 Benchtop Tests Data Analysis 27

2.1.3 Part 2—Running 28

2.2 Results 30

2.2.1 Results Part 1: 30

2.2.2 Results Part 2: 31

2.3 Discussion 32

2.4 Conclusions 36

3. Assessment of interpolation methods to reconstruct the complete plantar pressure distribution from sparse sensors during running 37

3.1 Introduction 37

3.2 Materials and Methods 41

3.2.1 Subjects 41

3.2.2 Data collection 41

3.2.3 Data analysis 42

3.2.4 Data analysis – interpolation 44

3.2.5 Data analysis – error metrics 47

3.3 Results 48

3.3.1 Effect of sensor layout 48

3.3.2 Effect of interpolation method 50

3.3.3 Stance Phase 52

3.3.4 Interaction effect of sensor layout, interpolation method and stance phase 53

3.4 Discussion 60

3.5 Conclusions 66

4. Evaluation of Different Pressure-Based Foot Contact Event Detection Algorithms across Different Slopes and Speeds 68

4.1 Introduction 68

4.2 Materials and Methods 71

4.2.1 Participants and Protocol 71

4.2.2 Post-Hoc Data Processing 72

4.2.3 Reference FCE Detection 74

4.2.4 Pressure Based FCE Detection 75

4.2.5 Data Analyses and Statistics 84

4.2.6 Algorithms across speed (level grade) 84

4.2.7 Algorithms across speed, across grades 84

4.3 Results 85

4.3.1 Algorithms across speeds (level grade) 86

4.3.2 Algorithm across speed and across grades 89

4.4 Discussion 91

4.5 Conclusions 95

5. Summary and Conclusions 96

5.1 Summary 96

5.2 Limitations 99

5.3 Future Directions 100

5.4 Conclusions 102

6. References 103

7. Appendices 119

7.1 Appendix A 119

7.2 Appendix B 120

7.3 Appendix C 126

7.4 Appendix D 127

List of Tables

Table 2-1 Research grade PPMS 26

Table 2-2 Benchtop testing results - Kinetyx® SI and Tekscan® F-Scan™ systems 31

Table 2-3 Running testing results 32

Table 3-1 Mean absolute error (MAE) across different layouts and interpolation methods 57

Table 3-2 Error metrics per layout and interpolation method 59

Table 4-1 Error metrics for foot contact event algorithms 86

List of Figures

Figure 1-1 Research grade plantar pressure measurement systems 12

Figure 2-1 Expanded view of the Kinetyx® SI System 22

Figure 2-2 Part 1 testing equipment 25

Figure 2-3 Normalized vGRF signals 29

Figure 2-4Mean loading plots from the running data 30

Figure 3-1 Overview of the data collection and data analysis methodology 42

Figure 3-2 (a) Time normalized and stacked vertical ground reaction force (vGRF) signals 43

Figure 3-3 Sparse sensor layouts 44

Figure 3-4 Illustration of the interpolation process 46

Figure 3-5 Error by layouts 49

Figure 3-6 Center of pressure errors by layout 50

Figure 3-7 Error by interpolation method 51

Figure 3-8 Center of pressure errors by interpolation method 52

Figure 3-9 Error by stance phase 53

Figure 3-10 Center of pressure error by stance phase 53

Figure 3-11 Pressure and center of pressure (COP) error plots at 10, 25, 50 and 75% of stance .. 55

Figure 3-12 Mean absolute error (MAE) across different layouts and interpolation methods 56

Figure 3-13 Error results by error metric 58

Figure 4-1 Novel® Pedar™ pressure insole system 72

Figure 4-2 (a) Data processing 74

Figure 4-3 FCE-1 – reference system 75

Figure 4-4 FCE-1 77

Figure 4-5 FCE-2 78
Figure 4-6 FCE-3 79
Figure 4-7 FCE-4 80
Figure 4-8 FCE-5 81
Figure 4-9 FCE-6 82
Figure 4-10 FCE-7 83
Figure 4-11 Error metric results 88
Figure 4-12 Error metric results – grade 90
Figure 7-1 Root mean squared error (RMSE) 120
Figure 7-2 Max absolute error (MaxAE) 121
Figure 7-3 Percent difference in contact area (CA) 122
Figure 7-4 Error in medial-lateral center of pressure (COPx) 123
Figure 7-5 Error in anterior-posterior center of pressure (COPy) 124
Figure 7-6 Error in distance between estimated center of pressure and reference (COPdist) 125

List of Symbols, Abbreviations, and Nomenclature

%: Percent 42

3D: Three Dimensional 1

ANOVA: Analysis of Variance 48

CA: Contact Area 47

COP: Center of Pressure 12

COPx AE: Absolute Error in the Center of Pressure in the Medial-Lateral Direction 47

COPy AE: Absolute Error in the Center of Pressure in the Anterior-Posterior Direction 47

cubic: Bicubic 45

FCE: Foot Contact Event 68

GCT: Ground Contact Time 68

Hz: Hertz - Cycles per Second 8

IC: Initial Foot Contact 17

ICC: Interclass Correlation Coefficients 27

IDW: Inverse Distance Weighting 45

IMU: Inertial Measurement Unit 10

kg: Kilogram 28

kPa: Kilopascal 13

LFTD: Linear Force Testing Device 26

m: Meter 28

m/s: Meters per Second 28

MAE: Mean Absolute Error 47

MaxAE: Maximum Absolute Error 47

min: Minute 28

min/km: Minutes per Kilometer 41

mm: Millimeter 39

ms: Millisecond 84

N: Newton 74

NN: Natural Neighbor Interpolation 45

PBPT: Pneumatic Bladder Pressure Tester 26

PCC: Pearson's Correlation Coefficient 27

PPD: Plantar Pressure Distribution 12

PPMS: Plantar Pressure Measurement Systems 1

P_{sum}: Sum of Pressure 29

RBF: Radical Basis Function 45

RE: Running Economy 7

RMANOVA: Repeated Measures Analysis of Variance 48

RMSE: Root Mean Squared Error 16

RRI: Running Related Injuries 5

s: Second 28

SR: Stride Rate 68

ST: Swing Time 68

TO: Toe Off 17

vGRF: Vertical Ground Reaction Force 2

VO_{2max}: Volume of Maximal Oxygen 7

Acknowledgements

I want to extend my deepest appreciation to the following individuals and entities as this dissertation would not have been possible without their support and patience:

My supervisor, Dr. Marc Klimstra. Thank you for your patience and support and the trust that you placed in me. In particular, I want to thank you for your encouragement, and support throughout my doctoral process and as I pursued my professional development in sport wearable technology.

My supervisory committee members, Dr. Sandra Hundza, Dr David Kennedy, and Dr. Stuart MacDonald. Thank you for your patience, perspectives, and insights. Your advice and willingness to support me have played a critical role in my doctoral work.

My former lab mates at the Motion and Mobility Rehabilitation Laboratory (MMRL), in particular Dr. Matt Jenson and Dr. Drew Commandeur: thank you for enthusiasm, knowledge and advice.

To all my former colleagues at Kinetyx Sciences Inc., especially Omar Suleman, Maryam Hajizadeh, Hunter Marriott and Erin Eastick, whose collective intelligence, love of sport science and wearable sensor technology positively impacted me and this work.

My funding source, Mitacs Canada.

My parents, David Blades & Edith Blades. For providing endless hours of love and support. I truly couldn’t have done it without you.

To my sons, Benji, Simeon and Noam. For your many words of encouragement and years of support.

To my wife Celine, whose unwavering support and love guided me throughout my PhD. Your strength, patience, and encouragement have been my greatest assets. This achievement is not just a reflection of my efforts, but a testament to our collective pursuits, and the dedication you have shown in me. I owe you more than words can express.

Dedication

For my children, Benjamin, Simeon, Noam, and Ellington.
May you always find joy in movement,
and be inspired to change lives for the better,
as you all have done for me.

Introduction

> Running is a simple framework in which to explore the complexities of being human.
>
> Dr. Geoff Burns

Quantitative biomechanical research has typically been performed in laboratories using measurement technologies such as 3D motion capture cameras, plantar pressure measurement systems, force plates, and instrumented treadmills [1]. Laboratory-based running biomechanics research investigates a broad range of topics with goals of helping runners reduce the risk of injury and/or improving running performances [2,3]. While highly accurate and controlled, research conducted in laboratory settings using these measurement devices may fail to capture the dynamics of athletes' performances in their natural training and competition environments. For example, frequently used laboratory research equipment such as treadmills, have been shown to produce different running biomechanics when compared to overground running [4,5]. These discrepancies underscore the need for field-based running research which has been identified as one of the potential reasons for the number of inconclusive or conflicting research findings present in areas of running biomechanics research, in particular for the research investigating mechanisms of injury [2,3]. To that end, special attention has been given to technologies such as in-shoe plantar pressure measurement that could measure key aspects of running gait biomechanics outside of laboratories in real-world training and competition settings [1,6–8]. In-shoe plantar pressure measurement systems (PPMS) are unique in their ability to provide continuous kinematics and kinetics of running gait [6,8,9]. PPMS are of particular interest in running biomechanics research because they

provide detailed information of how forces are applied across the plantar surface of the foot, and with the ground or footwear which determine how forces are transmitted to the ground during forward propulsion [10,11]. Although research-grade in-shoe PPMS are commercially available, these systems were designed primarily for accuracy rather than wearability [12] and in addition to their high cost, and low durability, many systems employ a cumbersome hardware-design or form factor which has been shown to alter running gait [13]. Additionally, many of these systems are complex to use. Taken together, these properties render research grade PPMS unsuitable for field-based applications [6]. For pressure sensing technology to be viable beyond the laboratory, it needs to be designed with a form factor that is lightweight, imperceptible, highly durable, cost-effective and with a sufficient battery life to operate throughout extended training sessions and competitions [6,12].

A wearable PPMS designed to meet these requirements, which is also capable of providing research-grade pressure data, would be a critical research tool that could be used to address the current void in field-based running biomechanics research [10,14]. However, the design and development of such a system is highly challenging due to the many competing requirements. For example, it has been suggested that a wearable PPMS could overcome some of the limitations associated with research grade systems by using a reduced or sparse number of pressure sensing elements [15–17]. Specifically, it has been proposed that a sparse sensor count results in decreased power consumption (i.e. battery size and weight), decreased raw data files sizes, reduced production costs, improved durability and improved overall form factor [15,17–19]. However, this presents a dilemma since a reduced sensor count would also severely compromise the accuracy in plantar pressure measurement. For example, Ciniglio et al. [18] evaluated a reduced 16-sensor layout to measure the plantar pressure distribution and derivative biomechanical metrics during walking and jumping tasks. They found that a 16-sensor layout under-estimated mean and peak

pressure, vertical ground reaction force (vGRF), and contact area across all trials and tasks [18]. Thus, competing design requirements such as low-weight, high-durability, imperceptible form factor, and low cost, conflict with design requirements for high accuracy, high reliability, high spatial resolution, and high memory storage; present serious difficulties towards the development of a wearable, field-appropriate PPMS capable of providing research grade data. Although recent attempts to develop such a device have been made [6,20], many of these devices still fail to meet all the necessary requirements, typically compromising accuracy, form factor, durability, or sensor resolution. Consequently, wearable field-appropriate PPMS for use in running have yet to become widely adopted for research or sport applications. Thus, research is needed to resolve the competing requirements enabling the development of wearable PPMS for use in running.

First, to meet the low-cost requirement, research is needed to assess the viability of inexpensive resistive pressure sensors for use in running. Additionally, to address the need for an imperceptible hardware design that is low in cost and highly durable, the minimal number and layout for pressure sensing elements needs to be determined. Given the optimal layout, research is needed to develop and validate algorithms that could estimate the complete plantar pressure distribution from the reduced sensor layout. Finally, research is needed to evaluate the optimal algorithm to accurately quantify foot contact events from in-shoe plantar pressure data.

Therefore, the purpose of this dissertation is to address key design requirements which could aid in the development of a wearable PPMS for the field-based quantification of running gait. The results of this body of work contribute to the scientific literature by providing methods to develop a field-appropriate PPMS that can provide a critical and missing tool for researchers, athletes, coaches, and practitioners, enabling accurate field-based measures of running gait kinematics and kinetics.

Chapter 1 of this dissertation provides an overview of conceptually and methodologically relevant literature that pertains to the research presented in Chapters 2, 3, and 4. This chapter will briefly, discuss the relevance and applications of field-based running biomechanics in the areas of running performance and running injury. Additionally, this chapter will provide a high-level overview of current gait measurement technology followed by a detailed technical overview of plantar pressure measurement technology. Finally, this chapter will review the requirements for a wearable field-appropriate PPMS.

Chapter 2 presents research on the characterization and evaluation of the pressure sensor response from inexpensive resistive pressure sensors contained within a fully embedded insole. This evaluation compares the sensor response characteristics relative to a research grade PPMS on bench-top laboratory equipment as well as during treadmill running.

Chapter 3 presents research that evaluates the optimal number of pressure sensing elements and spatial interpolation methods necessary to derive the complete plantar pressure distribution and center of pressure from a reduced pressure count relative to a gold standard PPMS.

Chapter 4 presents research on different pressure-based foot contact event detection algorithms and the assessment of each algorithm for their accuracy relative to a gold standard foot contact event detection method and measurement equipment.

Chapter 5 summarizes the findings of this dissertation and discusses the implications of this dissertation for research in biomechanics, the sport of running, and insights for future research in running gait technologies.

1. Background

1.1 Introduction

This chapter presents an overview of previous research and technical content relevant to the studies presented in Chapters 2, 3, and 4. The first part of this chapter provides an overview of applications for field-based measurement of running gait mechanics as they relate to running injuries and running performance. The second part of this chapter presents an overview of current lab-based measurement technologies and their limitations for field-based quantification of running gait. This is followed by a description of research-grade plantar pressure measurement technology and its design elements as they relate to the quantification of running gait mechanics including a discussion of the limitations of this technology. The final part of this chapter explains the requirements necessary for a wearable, field-appropriate PPMS.

1.2 Applications of running gait biomechanics

Distance running is a popular form of physical activity used to enhance physical fitness and combat the health risks associated with a sedentary lifestyle [21,22], and it has been the topic of considerable biomechanical research. While running offers a multitude of health benefits, the prevalence of running related injuries (RRI) is substantial, with approximately 30-58% of all runners experiencing some form of running-related injury in a given year [22,23]. It has been proposed that a combination of running gait biomechanics and training load play a primary role in the development of RRI [24]. For example, biomechanical measures such as step length, stride rate, foot strike index, foot strike angle, tibial vibrations, breaking forces, vertical loading rates, and peak rearfoot eversion have all been investigated for their relationship to the development of

RRI [3,25–27]. While this body of research has made important advancements towards an understanding of the biomechanical etiology of RRI, there are still many conflicting results [3,26]. For example, vertical loading rates have received considerable attention for their links to the development of RRI, however, research on this metric has produced largely inconclusive results [26,28]. One explanation for the inconclusive results is that most of these research investigations were conducted in laboratory settings [3,24]. In contrast, field-based evaluations of running gait may yield more conclusive results as they enable analysis of a runner's biomechanics within the athletes' diverse training conditions, including various surfaces, different shoe types, gradients, and changing environmental conditions [3]. In addition to research applications, field-based gait measurement systems, capable of presenting real-time feedback of running gait kinetics and/or kinematics could be an effective strategy for reducing high-risk factors for RRIs [7,26]. By continuously monitoring various parameters such as foot strike pattern, stride length, ground contact time, and other relevant biomechanical metrics, field-appropriate gait measurement devices could provide immediate feedback that was once only available in laboratory settings [24]. Such devices could provide runners and clinicians with data that reflect the actual training conditions, thus offering a more realistic picture of a runner's biomechanics and workload. This in-field analysis can be particularly valuable for tailoring individual training programs, identifying early signs of potential overuse injuries, and supporting the recovery process by tracking progress in real-time [24]. However, before integrating wearable devices into a runner's training, the accuracy and validity of the data collected by the device must be considered and the device must be capable of providing reliable metrics that are consistent with laboratory-grade measurements.

Biomechanics researchers have explored not only injury-related studies but also the relationships between running biomechanical metrics and running performance; in particular, attention has been paid to determine if differences in running gait patterns could explain

differences in running economy [2]. Running economy (RE) is defined as the steady-state rate of oxygen consumption at a given speed during submaximal running [27] and has been shown to account for a large and considerable proportion of variation in distance-running performances and as a significant differentiator between elite and recreational runners [2]. Determinants of RE include training, environment, physiology, anthropometry, and running biomechanics [29]. Biomechanical factors which can influence RE can be designated as either intrinsic, pertaining to an individual's internal running biomechanics, or extrinsic, related to external influences [2]. Numerous researchers have investigated relationships between intrinsic running gait biomechanics and RE for their influence on running performance [2,30,31]. For example, Williams and Cavanagh (1987) [30] found that 54% of interindividual variations in submaximal running, volume of maximal oxygen (VO_{2max}) consumption could be accounted for by differences in intrinsic running gait mechanics. In 2016, Moore [31] conducted a comprehensive review of biomechanics research to summarize findings on the relationship between RE and modifiable biomechanical factors. The results of the review found support for a relationship between RE and stride length, vertical oscillation, leg stiffness, alignment of ground reaction forces (GRF) and leg axis during propulsion, lower limb moment of inertia, and reduced leg extension at toe off [2]. Conflicting results for intrinsic factors were found for ground contact time, impact force, swing time, and anterior-posterior forces [2]. Taken together, these results reveal that there is evidence for a relationship between running economy and running biomechanical factors, many of which could be continuously measured and monitored using a field-appropriate wearable PPMS. Further, the review by Moore, indicated that for several other biomechanical metrics, the results on their relationship to RE are often conflicting and that more controlled studies are required [2]. As previously noted, the conflicting results for these metrics may be due, in part, to the lack of accurate, field-based running biomechanics research.

1.3 Lab based measurement technologies

Various measurement technologies are employed in running gait research laboratories to provide valuable data for evaluating and modifying running mechanics. These insights, for example, can be used to enhance distance running performance and potentially reduce the likelihood of running-related injuries. The typical measurement technologies used in running gait biomechanics include motion analysis systems, force platforms, inertial motion sensors, and pressure measurement systems [32].

1.3.1 Motion capture

Motion analysis systems utilize a combination of video cameras and reflective markers to track the position of key anatomical joints and limb segments [33]. Recent advancements in motion analysis technology utilize infra-red cameras and reflective markers to derive a three-dimensional representation of the measured motion [34]. Motion capture is restricted to kinematic measures (position and motion) and can measure variables such as stride frequency and ground contact times at high spatial (0.5-2mm) and temporal resolution (100-500 Hz). Although considered a highly accurate method of measuring kinematics, [35] motion analysis presents several limitations for running gait analysis. First, 3D motion capture is incapable of directly measuring kinetic metrics such as ground reaction forces, and plantar pressure distribution. Second, 3D motion capture requires the measurements be completed in a laboratory, often on a treadmill, and thus, the measurements may not be a true representation of the intended motion to be studied, namely overground running [20]. Finally, 3D motion analysis is highly time consuming and can be cost prohibitive [1] for non-research applications. Thus, despite the ubiquity of motion analysis as a laboratory-based technology for measuring running gait kinematics, it remains unavailable and

impractical as a field-appropriate research tool or as a running gait measurement technology for the vast number of runners who may benefit from information regarding their running biomechanics.

1.3.2 Force platforms & treadmills

Force platforms are another form of measurement technology used in running gait biomechanics. Force platforms can measure all three components of the ground reaction forces generated by a body moving across them [36]. To measure the applied forces, force platforms use several force transducers built into a solid plate [34]. Although force platforms are considered the gold standard of gait kinetics [34], the data they generate are of limited practical value beyond research applications because force platforms typically can only record one foot strike at a time [36,38]. Further, force platforms do not provide information on the distribution of the load across the plantar surface and therefore have limited applicability to the structures of the foot [39]. An additional complication of force platforms is that participants may alter their running gait by targeting their stance foot onto the force platform [35]. To address these limitations, as early as 1990, several laboratories developed instrumented treadmills that measure the three components of the ground reaction force during treadmill running. This advancement was a significant improvement over force plates as it allowed for continuous measurements of ground reaction forces from multiple strides [40]. Although commercial instrumented force treadmills now exist, this technology is expensive and restricted to laboratory settings, and as such remains inaccessible to most distance runners who would benefit from information on their running kinetics. Further, there is evidence that running gait mechanics differ between treadmill and over-ground running. For example, Garcia-Parez et al., [4] found that treadmill running produced significantly longer contact times, and reduced plantar pressure loads at the heel, hallux, and medial metatarsals when

compared to overground running. Thus, researchers wanting to investigate the relationship between running gait and injury, or performance should employ research technologies that allow for continuous quantification of running gait during overground running. One such measurement technology is inertial sensors.

1.3.3 Inertial measurement units

Due to their small size, low weight, low-cost, and relative ease of implementation, inertial measurement units (IMU) are an attractive option for field-based measurement of running gait [7,41]. IMUs typically include a combination of accelerometers, gyroscopes, and magnetometers and can successfully derive running gait kinematics [42]. IMUs have been shown to be an accurate method of measuring temporal parameters of running gait including stride rate or cadence and stance time [43]. Recently, IMU-based running measurement systems have become commercially available and come in a variety of different form factors such as wrist mounted, chest mounted, hip mounted and shoe or foot mounted applications [7]. One example is the Garmin HRM-Pro chest strap (Garmin Ltd., Olathe, KS, USA), which uses an accelerometer embedded into the heart-rate strap to record and display in real-time via a paired watch: running cadence, vertical oscillation, and ground contact time [7]. Additionally, shoe mounted IMU sensor technologies have emerged, such as the Stryd® Run Pod (Boulder, Colorado, USA) and Coros® Pod 2 (COROS Wearables Inc., California, USA). These devices are gaining popularity and show promise for the field base measurement of running gait. However, research is still needed to determine their validity [7].

An important limitation of IMU-based measurement systems is that they are limited to purely kinematic measures and are thus unable to directly measure kinetic variables such as ground reaction forces or plantar pressure distributions [44]. Recent efforts have been made to address this

limitation of inertial sensors by using machine learning methods [44,45]. While these initial efforts are promising, the accuracy and generalizability of machine learning derived GRF signals remain a concern. For instance, Donahue and Hann [44] employed a Long Short-Term Memory (LSTM) machine learning technique to estimate GRF from foot-mounted inertial sensors. They validated their model's generalizability by testing it on data from participants not included in their training data set. However, their findings revealed a consistent underestimation of GRF by the model when applied to data from new participants, with the underestimation becoming more pronounced at higher running speeds [43]. This work demonstrated that estimation of GRF waveforms may have reduced accuracy at running velocities and grades outside of the conditions where the models were trained [44,45]. This limitation is particularly important in running sports such as trail running where athletes encounter extremely dynamic and diverse running conditions, surfaces, speeds, and grades. In these conditions, machine learning based methods are ineffective and direct measurement of running dynamics is required for running biomechanics researchers.

1.3.4 Pressure measurement systems

While important kinematic gait related parameters can be derived from wearable inertial sensors, gait researchers are also interested in the distribution of force over a given surface area, known as pressure [35]. In-shoe PPMS are an important measurement technology for quantifying foot-ground interactions during running gait. As the foot serves as the terminal point where propulsive forces are exchanged with the ground [35], measurement of ground reaction forces through plantar pressure can be used by researchers to assess the external loads acting on the body during overground running [39]. Unlike traditional laboratory measurement tools such as in-ground force plates, in-shoe PPMS enable the recording of consecutive steps across various activities and environments, and they offer crucial insights into the pressure distribution across the

plantar surface of the foot [8,36,46]. Plantar pressure distributions (PPD) from in-shoe systems, have been successfully used to calculate numerous biomechanical metrics including the vertical ground reaction force (vGRF) [47,48], the trajectory of the center of pressure (COP) [49–51], the timing of foot contact events [1,52], foot strike patterns [53,54], and other derivative metrics employed in research and sport applications. Beyond research applications, in-shoe plantar pressure data has garnered attention for its potential to provide real-time and summary-based feedback for injury prevention and management, as well as for training monitoring [12,21].

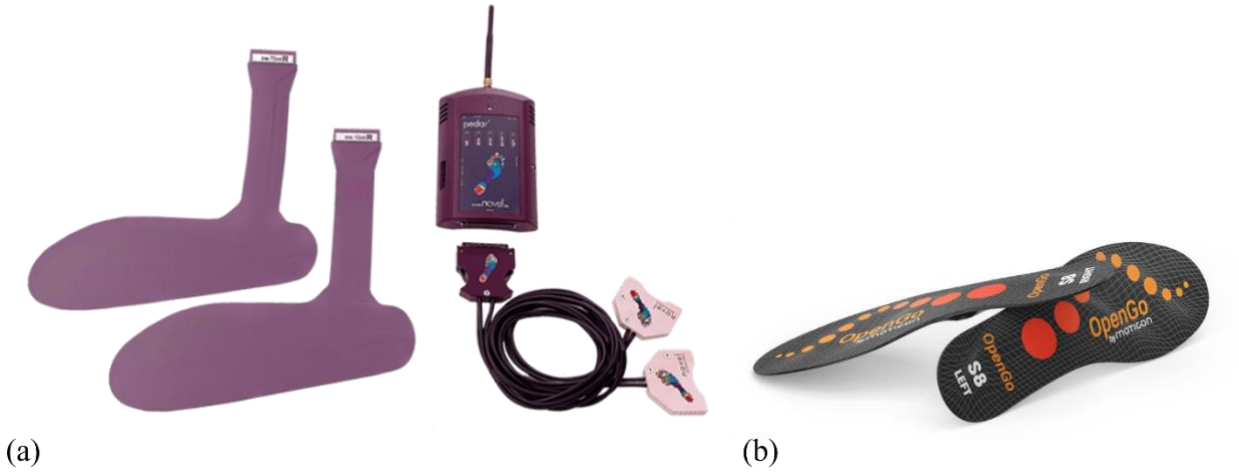

(a) (b)

Figure 1-1 Research grade plantar pressure measurement systems (a) The Pedar™ system by Novel®, is a 'gold-standard' research grade plantar pressure measurement system with 99 sensors in a matrix configuration, (b) OpenGo™ by Moticon® a fully integrated in-shoe plantar pressure measurement system with 16 discrete sensors.

In-shoe PPMS can be classified as containing either a matrix of pressure sensors that cover the entire insole (array-based) or containing discrete sensors, typically placed under important anatomical markers within the insole. Most research grade in-shoe pressure measurement systems, such as the Pedar™ system (Novel®, Munich, GER) and the F-Scan™ system (Tekscan® Boston, MA, USA) employ a matrix pressure array as they offer superior coverage and resolution over discrete sensors.

Additionally, in-shoe PPMS typically employ either resistive or capacitive pressure. In matrix resistive sensors such as the F-Scan™ system by Tekscan®, each sensor is made up of conductive material arranged in a grid of rows and columns. At every point where these rows and columns meet, there's a pressure-sensitive layer. When pressure is exerted on the surface of the sensor, it causes a change in the electrical resistance of this material. Electronic scanners linked to the sensors detect these changes in resistance and convert them into a digital signals [55]. On the other hand, capacitive sensors consist of two charged conductive plates separated by a dielectric elastic layer. When pressure is applied, the dielectric layer deforms, reducing the distance between the plates and subsequently altering the voltage across the plates in a manner proportional to the applied pressure.

Both the Pedar™ system and the F-Scan™, are considered 'gold standard' measurement systems and have been shown to be highly accurate across a range of pressures and loads [56]. The Pedar™ insole uses a matrix of 99 capacitive sensors with an effective sensor area of about 1.5 cm^2 and has a recommended measurement range of 20 - 600 kPa. Whereas the F-Scan™ insole consists of 960 resistive pressure sensors with a spatial resolution of 3.9 sensors per cm^2 with a pressure sensing range of 0-862 kPa.

1.3.5 Limitations of research grade PPMS

As previously noted, research-grade PPMS, such as the Pedar™ system, are designed for precision, and are used predominantly within controlled laboratory settings. Such systems are unsuitable for field based uses due in part to limitations in memory and battery capacity [7,15,17,18], cumbersome hardware designs [13], and low durability [57]. Importantly, research grade PPMS such as the Pedar™ and the F-Scan™ systems exceed the recommended weight for

body worn sensors in sports [12]. Further, both systems utilize cables and junction boxes to connect the pressure insoles to a waist mounted data loggers, which has been shown to also alter running gait mechanics and goes against the recommendations of researchers for body worn sensor systems [13]. Moreover, these systems often require operation and calibration by trained researchers, making them inaccessible to athletes, coaches, and others without specialized training. Thus, despite the potential of plantar pressure measurement technology for running biomechanics research and sport applications, the current research-grade PPMS cannot be considered 'wearable' and are impractical for field application.

To address these limitations a new generation of wearable PPMS are beginning to emerge [1]. For example, wearable in-shoe PPMS such as, Moticon® ReGo AG™ (München, Germany) [58], Arion™ (Eindhoven, Netherlands) [20], and Loadsol™ (Novel®, Munich, Germany) [59,60] have recently become available. These systems have made important first steps in the development of sensors capable of field-based quantification of running gait mechanics. However, their improved form factors over research grade PPMS, may compromise their ability to accurately quantify plantar pressure distribution during running. For example, the Arion™ PPMS, and the Moticon system the use discrete pressure insole with only 8 sensors [20] and 16 sensors [58] respectively. Such reduced sensor counts can have a significant impact on the device's ability to accurately measure the PPD [61]. Therefore, before these devices are used by researchers, the pressure sensor response of each system should first undergo an external validation study. Specifically, the pressure sensor response characteristics should first be assessed for their linearity, hysteresis, creep, and measurement error [56]. Additionally, given the reduced sensor counts employed by these systems, a validation study of their ability to measure the complete PPD, pressure derive metrics such as COP, and to detect foot contact event relative to gold standard

research grade systems is also warranted. Thus, while the development of these new systems appears promising, it's unknown if they can meet the requirements for a valid measurement system.

1.4 Requirements for wearable PPMS

Researchers have identified several important system requirements necessary for consideration during the development and assessment of a field-based plantar pressure measurement system for use in distance running. First, the design of the pressure measurement system should consider the speed and pressure range of the movements being recorded, which, in turn, will determine the sensor size, sample rate, and frequency response required [8]. The sensor system must be able to be worn on the body of the athlete without affecting the runner's gait and must be suitable to the runner's daily training environment. Harle et al. [12] identified several key design requirements for the fabrication of an in-shoe plantar pressure measurement system for sprinting, which include: sufficient sampling rate, careful ergonomics, hardware robustness, sensor reliability, and system cost. Other design considerations for an in-shoe system include low sensor response time, low power consumption, sufficient memory capacity, high wear resistance, especially to shear stress, wireless data transmission and the ability to accommodate several hours of continuous recording. The specifics of the sensor design requirements are addressed separately in the following section.

1.4.1 Matrix vs. discrete sensor configuration

Discrete in-shoe plantar pressure systems are defined by individually placed pressure transducers, typically placed under key anatomical locations of the planar surface of the foot. Matrix systems by contrast, consist of an array of small transducers arranged in rows and columns across the entire plantar planar surface. Due to their configuration, matrix systems can contain a

high number of sensors and are capable of capturing the complete PPD with a high degree of resolution. The advantages of discrete sensors over a matrix system include low cost, reduced power consumption, ease of manufacturing, increased durability, and minimal form factor [15–17,19]. Thus, discrete pressure sensors have been considered preferential sensor configuration for wearable field-appropriate PPMS for use in distance running [15]. Several studies have developed prototype systems for the quantification of running gait using a limited number of discrete pressure sensing elements located under bony landmarks on the plantar surface [62]. While these prototype systems show good promise, there is little research to guide the choice of sensor count or location [17,19]. These studies had good success reporting metrics such as GRF, and COP using highly reduced sensor counts [15,63] when combined with regression or machine learning methods. Research using sparse sensor layouts were shown to have moderate to low (6-8%) root mean squared error (RMSE) when used with a regression model to generate vGRF in walking and jogging [15]. However, limited research has actually quantified the effect of sensor count or position within a insole for the quantification of running gait [64]. It should be noted, however, that a discrete sensor system typically has fixed sensor locations and, thus, may only be appropriate for non-clinical foot types. Additionally, the use of discrete pressure sensors may lack critical spatial resolution in the PPD, potentially leading to errors in pressure measurements [18,61].

1.4.2 Spatial Resolution

The spatial resolution and dimensions of a pressure sensor should be based on the size of the structures being measured [61]. It has been advised that optimal pressure sensor size should have a maximal area of 5-6 mm^2 to avoid the underestimation of peak local pressure values due to the averaging effect of large sensors [61]. Therefore, it is recommended that discrete sensors area not exceed $5mm^2$ whenever possible. It should be noted that a wearable PPMS using a reduced

number of pressure sensing elements of this size will result in a lack of pressure measurement at all locations between pressure sensing elements [19]. This can lead to errors in pressure measurement as well as errors in pressure derived metrics such as COP [18]. Given that the complete PPD may be important for qualitative analysis of running gait and can be used as the basis for derivative biomechanical metrics, PPMS with reduced sensor counts may require some method of estimation [16,17,19] to recreate the complete PPD.

1.4.3 Sample rate

A sample rate of 100 Hz has been shown to be sufficient to accurately record temporal and kinetic metrics from an in-shoe plantar pressure measurement system in walking trials [65]. However accurate detection of foot contact events such as initial foot contact (IC) and terminal stance or toe off (TO) in runners would necessarily require a higher sample rate. Researchers investigating temporal events in running using plantar pressure measurement systems have used sample rates of 200 – 250 Hz for distance running and up to 2000 Hz for sprinting [1,12,66]. A minimum sample rate of 250 Hz with the ability for sample rate selection up to 1000 Hz would allow for system optimization depending on measurement needs and could greatly improve accuracy when determining peak values or temporal events such as foot contact events [66]. However, high sample rates may have a negative impact on battery life and possibly limit duration of use due to an increasingly large file size.

1.4.4 Pressure sensor response

Evaluation of wearable PPMS pressure sensor response characteristics is essential for ensuring accurate and reliable measurements from that system [8,56]. Typically, pressure sensor responses are characterized according to their linearity, hysteresis, drift, and creep [8,56,67].

Linearity describes the proportional response of a sensor to an applied load. If the electrical response of the sensor is proportional to increasing or decreasing load increments, the sensor is said to have a linear response. A high degree of linearity is advantageous over nonlinear response sensors as the sensor's response remains constant across all loads and does not loose resolution at low or high ranges [8]. Hysteresis describes the difference between the loading and unloading values of an output signal for a given input signal [56,67]. A sensor with high hysteresis will have a slow response time due to the sustained deformation of the sensor material impacting sensor accuracy. Drift describes the effect of pressure values increasing or decreasing over time [68] and creep describes the response of pressure values increasing at sustained loads [56]. Before use in research applications, wearable PPMS pressure sensor responses should be evaluated relative to research grade PPMS to ensure that they have similar levels of linearity, hysteresis, drift, and creep.

Beyond sensor response characteristics, the accuracy of pressure values after sustained use should also be assessed, particularly for resistive pressure sensors which have been shown to degrade quickly in running. For example, El-Kati et al., [57] reported a 40% error in pressure derived ground reaction forces after as little as five runs with the Tekscan® F-Scan™ system. The cyclic loading and bending of the pressure sensors during running can put substantial strain on the substrates of the matrix resistive sensors, rapidly degrading their response characteristics [8]. Additionally, in-shoe plantar pressure measurement systems must operate in environmental conditions where there are numerous mechanical, thermal and electrical factors that can negatively impact sensor output [8]. Future research is needed to determine the long-term effect of continued use on pressure measurement accuracy.

1.5 Summary

This chapter summarized and presented research, demonstrating the practical need for a field-appropriate wearable PPMS for research and sport applications in distance running. Based on the reviewed literature, it was clear that such a system could play a pivotal role by measuring relevant running metrics to reduce the risks of running related injuries and improve performances in distance running. Additionally, this technology could provide a much-needed tool for researchers allowing for measurement of running biomechanics in the natural training environment. Several measurement options were reviewed for their ability to act as a field-based running measurement system including 3D motion capture, IMUs, force platforms and pressure measurement systems. Of all the measurement modalities reviewed, only in-shoe plantar pressure measurement technology allows for the continuous measurement of running gait kinetic and kinematics in the natural training and competition environments. This chapter reviewed the many limitations of research grade in-shoe PPMS and reviewed several important design recommendations to address these limitations.

The following chapter will present validation research on a pressure insole system that has been developed to address the above-mentioned requirements as a potential wearable field-appropriate PPMS.

2. Characterization of the Kinetyx® SI Wireless Pressure-Measuring Insole during Benchtop Testing and Running Gait

2.1 Introduction:

Measurement of foot-ground interactions during running is critical to understanding and addressing the biomechanical factors related to overuse injuries [3,69,70] and improving performances [2,31]. Traditionally, standard laboratory-based measurement equipment such as in-ground force plates, or force-instrumented treadmills have been used to quantify foot-ground interactions during running. Increasingly, however, researchers have recognized the importance of measuring running foot-ground interactions outside of the laboratory in the natural training and competition environments [3,48]. Plantar pressure measurement systems (PPMS) offer a unique solution to researchers interested in measuring foot-ground interactions during running or walking, as well as for many different activities [36,39,46,71]. Unlike the standard laboratory tools mentioned previously, PPMS can be used both inside and outside of the laboratory, can continuously capture consecutive strides, and can record the distribution of pressures across the plantar surface of the foot [1,72]. Additionally, in-shoe PPMS have been shown to accurately capture important kinematic running gait metrics such as stance time, stride time, and stride rate [1,7,12,52,72,73]. Further, PPMS have shown promise to approximate kinetic characteristics of gait, such as path of center of pressure, and vertical ground reaction forces [48,52,59,71,74–77], although some research has shown inter-session force reliability is still inconsistent [57].

While PPMS show great potential for continuous running gait quantification, the design and form factor of most research-grade in-shoe PPMS, such as the industry-standard Tekscan® F-

scan™ system (Norwood, MA, USA) [13,57,78,79], are often bulky and can contain cumbersome components such as external cables, shoe-mounted pods, waist belts, and large external connectors. Although designed for accuracy, the form factor of such research-grade systems have been shown to interfere with normal running gait [13], limiting their utility and potentially reducing the validity of their data [7]. Additionally, such systems require setup and supervision by trained researchers and are therefore not viable for data collection during many practical and unsupervised use cases. Finally, research-grade PPMS can be expensive, and are thus not viable for broad-scale consumer use. The development of a cost-effective PPMS with an unobtrusive and field-appropriate form factor has many important applications across research, clinical practice, and sports performance [3].

Recently, a new generation of PPMS with completely integrated pressure-measuring technology is emerging [6,58,80,81]. These pressure-enabled 'smart insoles' are fully contained and can be used by simply replacing the existing sock liner of the shoe with the smart insole. This provides a significant improvement in form factor and design over traditional research-grade PPMS [6]. By employing a fully integrated design, smart insoles are capable of unobtrusive gait measurement that can be used across a broad range of research and consumer use applications with minimal impact on the wearer's natural gait. Additionally, due in part to their integrated form factor, smart insoles are able to be used broadly without researcher supervision [6,80]. One newly developed pressure-enabled smart insole is the Kinetyx® Sensory Insole™ (SI) (Kinetyx® Sciences, Calgary, CAN).

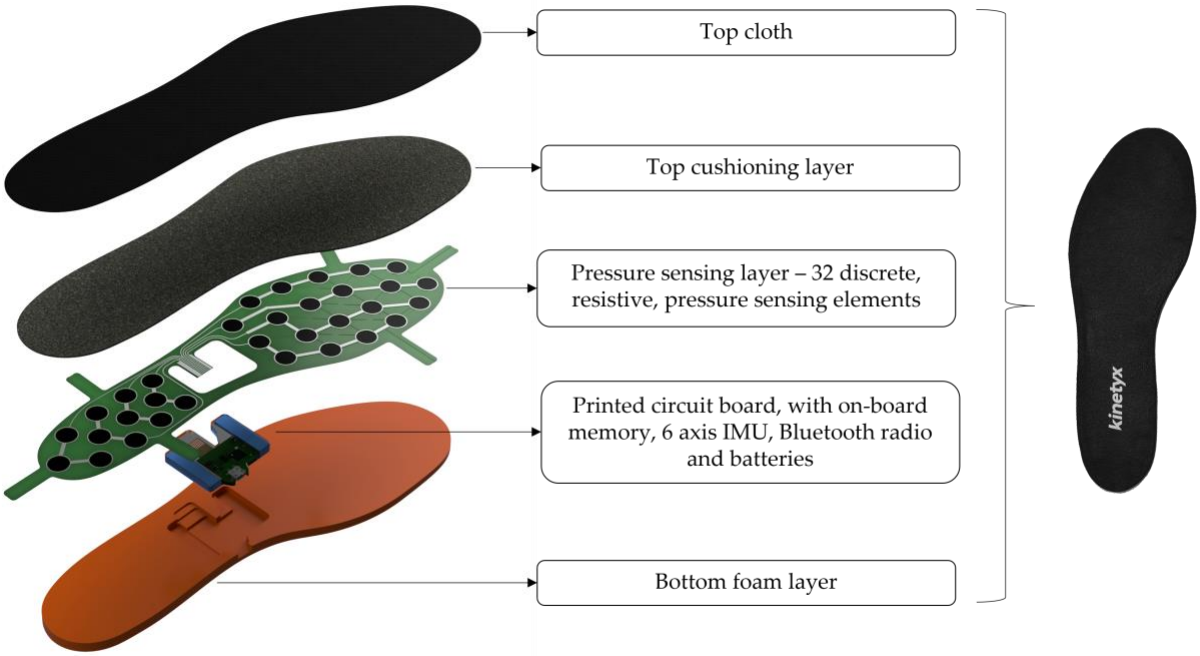

Figure 2-1 Expanded view of the Kinetyx® SI System displaying the main components of the system contained within the fully integrated design, including a pressure-sensing layer (green) which contains 32 resistive pressure-sensing elements distributed across the rearfoot and forefoot regions.

Similar to other smart insoles [58,75,80], the Kinetyx® SI employs a fully integrated design, including an integrated printed circuit board (PCB) with measurement electronics, and a pressure-sensing layer with 32 discrete resistive pressure-sensing elements (Figure *2-1*). Resistive pressure sensors are comprised of thin polymer films that exhibit a change in resistance with the application of pressure [8,82,83]. These sensors, with a thickness of only 0.2 mm, are widely used in alternate applications for their form factor, affordability, and versatility. Importantly, resistive pressure sensors are a more cost-effective method of measuring pressure over capacitive-style pressure sensors, which many of the research-grade PPMS employ. By employing resistive pressure sensors, smart insoles, such as the Kinetyx® SI, become cost-effective, and thus hold tremendous potential for researchers and consumers by enabling broad-scale field-appropriate use [82].

Despite its advantages, resistive pressure-sensing technology can vary widely in its accuracy and reliability [56,57,84]. Pressure sensor response characteristics such as drift, mean absolute error, and hysteresis can impact system accuracy both for pressure measurement and for derivative metrics such as ground reaction forces, center of pressure, and temporospatial gait metrics [56,57,68,74,85]. As such, resistive-based pressure-enabled smart insoles such as the Kinetyx® SI should be fully validated against lab quality equipment to properly characterize their performance and accuracy before use in research or consumer applications.

To that end, Giacomozzi [56] established benchtop testing procedures to assess the performance of PPMS. For example, using this protocol, Giacomozzi was able to evaluate five different PPMS, including the Tekscan® system, which was shown to be highly accurate relative to the other PPMS in benchtop testing. While this protocol has provided an important standardization of the methods used to characterize pressure-sensing technologies allowing for direct system-to-system comparisons [56], the applied loading rates of the sensors during standardized benchtop testing are far below those produced during running. Additionally, benchtop testing is executed without interaction with a human foot in situ and as such, may not properly capture the limitations of a given PPMS. For example, although the Tekscan® system performed well in the assessment by Giacomozzi [56], research on the same system by El Kati et al. [57] showed significant amounts of error in peak force measurement when used during sustained running. Thus, in order to fully characterize pressure-enabled smart insoles, the actual loading rates and conditions of running relative to gold standard gait biomechanics equipment is a necessary addition to any smart insole validation protocol [52,57,85]. Due its' improved form factor and fully integrated design, the SI system could offer an important new running sensor for researchers and clinicians, but it has yet to be evaluated relative to an industry-standard PPMS during benchtop testing and research-grade biomechanical devices during athletic activities. If pressure-enabled

smart insole systems can be determined as equivalent in response characteristics to laboratory-based systems, this can enable the potential to collect important mechanical data in situ.

Therefore, the purpose of this study was twofold. First, to assess the pressure sensor response characteristics of the Kinetyx® SI™ system alongside a validated research-grade PPMS (Tekscan® F-scan™; Figure *2-2*c) using an established PPMS benchtop validation protocol [56]. Second, to assess the pressure sensor response characteristics of the SI system during running across different speeds [52,86]. The results of this analysis will allow researchers and commercial users to understand the characteristics and limitations of the SI system and support ongoing evaluation and innovation of new smart insole and PPMS technologies.

Figure 2-2 Part 1 testing equipment : (a) linear force testing device with 30 mm diameter actuator disk and force plate used for the sinusoidal testing (b) pneumatic bladder pressure tester used for step test, static test, and reliability test (c) Tekscan® F-scan™ system. Part 2 testing equipment: (d) Bertec® force-instrumented treadmill

Materials and Methods

2.1.1 Part 1—Benchtop Tests

2.1.1.1 Benchtop Tests Data Collection

For the benchtop testing, the SI was tested alongside the sport version of the Tekscan® F-Scan™ insert. Each PPMS was new at the time of testing and used according to the manufacturer's specifications. The SI system comes pre-conditioned and calibrated; however, the F-Scan™ required conditioning, calibration, and equilibration before testing. A two-point calibration at 100

and 500 kPa was performed according to the manufacturer's specifications on the sport version of the F-Scan™ system. The specifications for each of the PPMS are listed in Table *2-1*.

Table 2-1 Research grade PPMS - Properties and listed specifications for the Kinetyx® and Tekscan® systems. Information on the Tekscan® system was taken from the Tekscan® F-Scan™ data sheet *[55]*. Information on the Kinetyx® SI system was supplied by the manufacturer upon request.

Plantar Pressure Measurement System Characteristics		
	Kinetyx® SI	Tekscan® F-Scan™
Technology	Resistive	Resistive
System weight—both sides (g)	130	862
Number of sensing elements	32	960
Max sample rate (Hz)	200	750
Resolution	12 bit	8-bit
Sensing range (kPa)	0–500	0–862
Insert Thickness (mm)	5 mm	0.2
Durability (uses)	Unknown	5–15

Two testing devices, similar to those employed by Giacomozzi [56] were utilized to assess the PPMSs; a pneumatic bladder pressure tester (PBPT, Figure *2-2*b) and a linear force testing device (LFTD; Figure 2a). The PBPT is a rigid structure with two parallel plates separated by a narrow gap where a PPMS insert is placed. An inflatable rubber membrane or bladder attached to the inside of the top plate can be inflated to apply uniform pressure across the entire surface of the PPMS. A digital pressure transducer (Greisinger Electronics GmbH, Germany) continuously measured pressure within the bladder throughout each trial. The LFTD consisted of an arbour press and a force plate (AMTI, Watertown, MA, USA; Figure *2-2*a). The force plate was secured to the base of the arbour press such that the arm of the arbour press was capable of applying an exact perpendicular load to the surface of the PPMS and the force plate simultaneously. All data was collected at 100 Hz using custom software (LabVIEW 2018 National Instruments, Austin, TX, USA). Four trials of each of the following four characterization tests were completed on two insoles from both the SI and F-Scan™ systems. All four trials of the benchtop tests were completed on the

same day and were performed at standard room temperature and humidity. Results from the four trials were averaged for each test.

The tests were:

Step Test: The PBPT was used to apply 100 kPa steps of static pressure from 0 to 500 kPa and back to 0 kPa to the entire sensing area of the PPMS (Figure *2-2* b). Each step had a minimum duration of 5 s and the PPMS were completely off-loaded for approximately 1 s after each step.

Sinusoidal Test: Using the LFTD, 10 sinusoidal pressure cycles ranging from 0–500 kPa were applied to each PPMS at approximately 1 Hz [56] (Figure *2-2*a). The percent hysteresis was averaged over the central eight cycles of each trial.

Static test: Using the PBPT, constant pressure of 300 kPa was applied to the entire sensing area of the PPMS for 120 s [87]. The pressure gradient was measured as the maximum change in pressure over the central 40 s of the loading period.

Reliability Test: The SI and F-Scan™ inserts were loaded according to the step test protocol on three consecutive days and assessed for instrument test re-test reliability [87].

2.1.2 Benchtop Tests Data Analysis

For the step test, the absolute and percentage root-mean-square error (RMSE), including their minimum, maximum, and mean values, along with Pearson's correlation coefficient (PCC) were calculated. For the sinusoidal test, percent hysteresis, PCC and RMSE were calculated. For the static test, absolute error and the rate of error (slope) were calculated. For the reliability test, mean pressure values reported at each step from the step test were compared using interclass correlation coefficients (ICC) (two ways mixed effects for absolute agreement). Direct comparisons (Student's *t*-test) were made between SI and F-Scan™ values from the step test,

sinusoidal test, and static test during the benchtop testing to determine if any statistical differences between the two PPMS existed on benchtop testing performance.

2.1.3 Part 2—Running

2.1.3.1 Running Data Collection

To assess the overall responsiveness of the SI sensors during running, summed pressure data were concurrently collected from the SI sensors (200 Hz) while participants ran on a force-instrumented treadmill (1000 Hz, Bertec®, Columbus, USA, Figure *2-2*d) [86]. All testing was conducted in the participants' own athletic footwear, which were fitted with a correctly sized SI system after the existing shoe's sock liners were removed. Each participant was instructed to perform 3 jumps at the start of each trial to create a manual sync event for post-hoc analysis. In total, 13 runners (8 male, 5 female) participants were recruited, aged 19–40 years (mean: 28 ± 5 years). Participant height ranged from 1.55 to 1.93 m (mean: 1.73 ± 0.10 m) and body mass ranged from 52.0 to 87.5 kg (mean: 66.6 ± 10.3 kg) [48]. All participants were free from injury at the time of testing, were familiar with treadmill running, and were given a 10 min self-selected warm-up. Each trial lasted for 60 s once the treadmill achieved steady state velocity. Each participant ran at 2.6, 3.0, 3.4 and 3.8 m/s with a self-selected rest interval between trials. These fixed speeds approximated a range of training and racing speeds used in previous studies of recreational runners [1,88,89]. Based on the results of previous research [57], the F-Scan™ system was deemed not suitable for running response evaluation. Thus, for this investigation only the SI sensors were assessed for responsiveness during running.

2.1.3.2 Running Data Analysis

The vertical ground reaction force (vGRF) data and the SI pressure data were both resampled to 100 Hz. The Kinetyx® SI pressure data was summed to create a sum of pressure signal (P_{sum}) [86]. Once resampled, data from the force-instrumented treadmill and the P_{sum} from the SI system were synchronized post-hoc using cross-correlation. Both signals were normalized 0–100% based on the maximum values for each trial. To enable the running data analysis, the vGRF and P_{sum} signals needed to be broken into the loading and unloading phases of each step. To do this, the vGRF data were filtered using a zero-lag low-pass 10 Hz Butterworth filter for signal processing and signal peak detection [90]. A 5% threshold was then used to determine signal onset and offset for each loading cycle [91]. Next, a peak detection algorithm was used on the filtered signals to determine the local maximum of each loading cycle (Figure *2-3*).

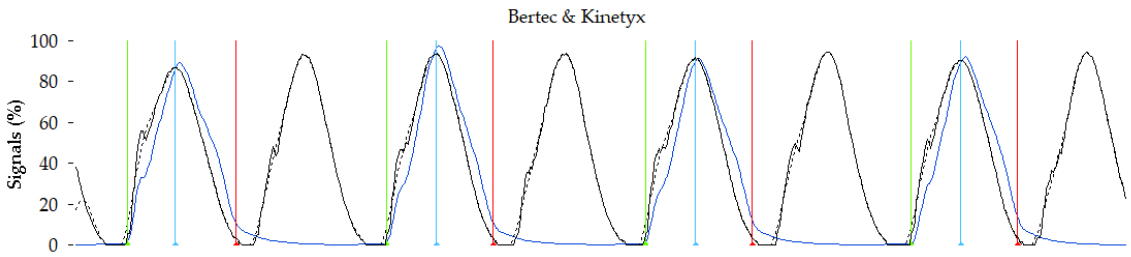

Figure 2-3 Normalized vGRF signals from the Bertec® force-instrumented treadmill (black) and the filtered version of this signal (black dashed). Normalized pressure sum signal from the Kinetyx® SI system (blue). Detection of signal onset (green), signal max (blue) and signal offset (red) for each loading cycle from a given foot from the Bertec vGRF data

For each trial, a mean loading and mean unloading trace was developed (Figure *2-4*). These mean signals were generated per trial and used to generate the following statistical measures. To assess the agreement between the SI and vGRF signal, Pearson's correlation coefficient (PCC), root mean squared error (RMSE), and percent hysteresis were computed per trial, similar to the sinusoidal trial in part 1 of this investigation. Repeated measured ANOVA were executed across speeds for each of the statistical measures.

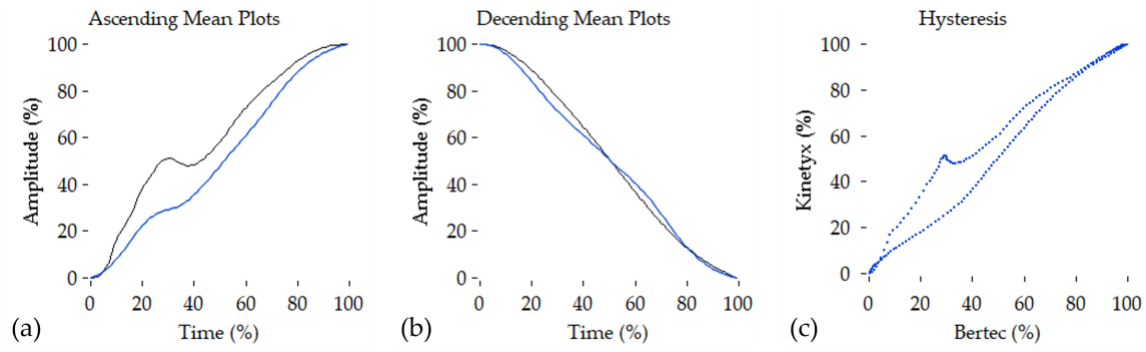

Figure 2-4Mean loading plots from the running data . (**a**) shows the mean normalized loading data from the ascending part of the signal from the Bertec (black) and SI (blue); (**b**) shows the mean normalized loading data from the descending part of the signal from the Bertec (black) and SI (blue); (**c**) shows the mean hysteresis plot of SI vs. Bertec

2.2 Results

2.2.1 Results Part 1:

The results from the step, static, sinusoidal, and reliability tests for the SI and F-Scan™ systems are summarized in Table *2-2*. The SI had similar linearity (Pearson's correlation coefficient, PCC = 0.86–0.97) and mean RMSE (9.17 ± 2.02) compared to the F-Scan™ (PCC = 0.87–0.92; RMSE = 15.96 ± 9.49) on the step test. The SI and F-Scan™ had comparable results for linearity and hysteresis on the sinusoidal test (PCC = 0.92–0.99; 5.04 ± 1.41) (PCC= 0.94–0.99; 6.15 ± 1.39), respectively. SI had statistically less mean RMSE (6.19 ± 1.38) than the F-Scan™ (8.66 ± 2.31) on the sinusoidal test and statistically less absolute error and slope (4.08 ± 3.26, 0.10 ± 0.08) than the F-Scan™ (16.38 ± 12.43, 0.41 ± 0.31) on the static test. The SI had comparable measures of reliability (interclass correlation coefficient, ICC = 0.97–1.00) to the F-Scan™ (ICC = 0.96–1.00).

Table 2-2 Benchtop testing results - Kinetyx® SI and Tekscan® F-Scan™ systems. Results are from tests evaluating both the absolute accuracy of the systems (Step Test, Sinusoidal Test) and for sensor response characteristics (Sinusoidal Test, Static Test) and for reliability (Test -ReTest Reliability). Significant differences between systems are shown in bold.

	Kinetyx®			**Tekscan®**		
PPMS	**SI 1**	**SI 2**	**SI avg.**	**F-Scan 1**	**F-Scan 2**	**F-Scan avg.**
Step Test (0–500 kPa)						
Linearity R^2 (range)	0.87–0.97	0.86–0.90	0.86–0.97	0.87–0.91	0.90–0.92	0.87–0.92
Mean RMSE (kPa)	10.72 ± 1.72	7.62 ± 0.32	9.17 ± 2.02	8.91 ± 4.47	23.01 ± 7.59	15.96 ± 9.49
MAX RMSE (kPa)	33.11 ± 5.61	19.85 ± 1.72	26.48 ± 8.06	17.66 ± 8.96	40.87 ± 13.04	29.27 ± 16.16
MIN RMSE (kPa)	1.85 ± 0.40	2.27 ± 0.82	2.06 ± 0.64	1.06 ± 0.39	0.69 ± 0.14	0.88 ± 0.34
Sinusoidal Test (0–500 kPa load cycling at ~1 Hz)						
Correlation R^2 (range)	0.98–0.99	0.92–0.98	0.92–0.99	0.97–0.99	0.94–0.99	0.94–0.99
RMSE (kPa)	5.33 ± 0.53	7.05 ± 1.49	***6.19 ± 1.38***	10.47 ± 1.74	6.86 ± 0.87	***8.66 ± 2.31***
Hysteresis (%)	5.34 ± 1.57	4.75 ± 1.39	5.04 ± 1.41	6.85 ± 1.45	5.45 ± 1.04	6.15 ± 1.39
Static Test (The central 40 sec. of a 120 sec. window held at 300 kPa)						
Total Error (kPa)	3.80 ± 4.34	4.37 ± 2.38	***4.08 ± 3.26***	26.98 ± 7.64	5.78 ± 1.63	***16.38 ± 12.43***
Slope (kPa/sec)	0.09 ± 0.11	0.11 ± 0.06	***0.10 ± 0.08***	0.67 ± 0.19	0.14 ± 0.04	***0.41 ± 0.31***
Test Re-Test Reliability (ICCs)						
ICC	0.995	0.998		0.988	0.997	
ICC (95%) (Lower)	0.973	0.989		0.669	0.957	
ICC (95%) (Upper)	0.999	1.000		0.999	1.000	
Day to Day Variability	10.02 ± 4.88	7.66 ± 2.95		16.92 ± 3.75	7.9 ± 3.32	

2.2.2 Results Part 2:

The results from the running tests are summarized in Table *2-3*. In total, 57 trials were analyzed for a total of 4031 foot-ground interactions. The SI pressure output had a near-perfect

linearity and low RMSE compared to the vGRF signal. The SI pressure output also had a mean hysteresis of 7.67% with a 28.47% maximum hysteresis.

Table 2-3 Running testing results
by subject or the Kinetyx® SI as compared to the vGRF data from the force-instrumented treadmill.

Participants	**1**	**2**	**3**	**4**	**5**	**6**	**7**	**8**	**9**	**10**	**11**	**12**	**13**
2.6 (m/s)													
RMSE (%)	11.9	6.7	15.0	8.6	5.1	13.0	7.9	12.2	9.0	9.8	11.1	9.7	9.0
R^2	0.97	1.00	0.96	0.99	0.99	0.98	0.99	0.96	0.97	0.99	0.98	0.99	0.99
Max Hysteresis (%)	26.7	15.6	44.2	15.8	11.3	35.9	21.2	35.5	20.6	25.6	32.8	19.8	31.8
Mean Hysteresis (%)	8.6	5.2	11.3	6.9	3.7	9.4	5.8	8.9	6.7	6.7	7.9	7.5	6.0
3.0 m/s													
RMSE (%)	12.9	7.6	13.6	9.3	7.5	13.1	7.5	14.1	8.6	10.3	11.7	10.3	9.1
R^2	0.96	0.99	0.95	0.99	0.99	0.98	0.99	0.91	0.97	0.98	0.98	0.98	0.99
Max Hysteresis (%)	30.0	17.5	45.7	17.7	16.7	35.7	20.5	43.2	19.6	27.1	37.6	23.5	33.0
Mean Hysteresis (%)	9.2	5.8	9.8	7.4	6.0	9.6	5.5	9.6	6.4	7.5	8.0	7.7	6.2
3.4 (m/s)													
RMSE (%)	12.4	13.7	9.4	7.0	13.8	7.1	15.0	8.6	8.9	10.6	12.4	9.8	12.4
R^2	0.96	0.95	0.99	0.99	0.97	0.98	0.85	0.95	0.97	0.97	0.99	0.98	0.95
Max Hysteresis (%)	30.5	42.2	20.4	17.2	36.3	17.8	44.9	22.7	26.5	34.8	24.9	34.8	32.9
Mean Hysteresis (%)	8.6	9.9	7.0	5.3	10.0	5.5	9.9	6.3	6.1	6.5	9.6	6.8	8.6
3.8 (m/s)													
RMSE (%)	13.3	13.7	8.4	6.9	15.1	6.5	14.6	8.5	12.6	11.8	11.2	12.4	10.8
R^2	0.95	0.94	0.99	0.99	0.96	0.97	0.75	0.95	0.94	0.99	0.97	0.96	0.98
Max Hysteresis (%)	32.6	42.6	19.5	18.8	41.3	21.1	42.9	24.6	39.3	25.5	40.6	30.0	27.0
Mean Hysteresis (%)	9.3	10.0	6.3	5.0	10.9	4.7	10.5	6.1	8.0	8.7	7.6	8.9	8.5

2.3 Discussion

Overall, this study has demonstrated that the SI system displayed a high level of accuracy and reliability when compared to an industry standard PPMS during standard benchtop testing. Additionally, when compared to a force-instrumented treadmill during running, the SI system pressure output showed strong correlation to the force measurement. However, during running there was notable hysteresis that may impact the generation of force-related gait metrics. Taken

together, these results support the use of this smart PPMS insole as a valid and reliable tool for field-based running assessment.

For the benchtop testing in this study, the methodology employed was chosen based on a previous study by Giacomozzi et al.[56]. During the series of benchtop tests, the SI system showed comparable results to the F-Scan™ during the step test and showed significantly less sinusoidal mean RMSE and static load error when compared to the F-Scan™ system. Further, both systems had near-perfect between-day reliability. It is important to note that there are differences between our results for the F-Scan™ system and those generated by Giacomozzi et al. [56]. In this study the linearity of the F-Scan™ system was lower than reported by Giacomozzi et al. [56]. During the step test and static test, the mean RMSE and error were similar but varied substantially between F-Scan™ sensors 1 and 2. During the sinusoidal test, the correlation and hysteresis were similar between the current study and Giacomozzi et al. [56], while the RMSE was much lower in this study. Some of the differences in the benchtop tests may be due to variability in sensors from the same manufacturer as well as potential differences in the measurement hardware between studies. While this study did not employ the exact testing equipment as Giacomozzi et al. [56] the PBPT was designed specifically for PPMS testing and the linear force testing used a research-grade force plate and a precision linear press. The results of the day-to-day reliability for both sensors in the present study, with high to near-perfect ICCs, would suggest that the variability of the specific sensors from the same manufacturer might be the cause for discrepancy between results of this study and that of Giacomozzi et al. [56] and not the testing equipment. The replication of most findings shows the repeatability and importance of conducting benchtop testing to evaluate PPMS based on the standards set out by Giacomozzi et al. [56]. While the results demonstrate comparable characterization of the SI system to an industry standard PPMS during benchtop tests, it is also important to understand the response of PPMS across a range of tasks such as running.

Although benchtop testing is important to characterize and compare pressure measurement systems, the testing parameters may be insufficient to assess PPMS that are to be used in highly dynamic loading activities such as running. The linearity of the SI insole compared to the force measurement was near-perfect, which is expected as pressure is the force divided by the area perpendicular to the applied force. This covariance supports the development of similar spatiotemporal gait metrics such as stride and stance timing and rate between pressure and force output [12,52,72,84]. However, the hysteresis findings, as seen across subjects in Table 3, demonstrate that there are differences in loading and unloading responses between the SI sensors and the force-instrumented treadmill. These differences in loading rates and the sensor responses are important to consider, as rate of force and pressure development during loading and unloading can impact the estimation of kinetic and kinematic metrics during gait. The loading rates during running are much higher than the loading rates of the benchtop sinusoidal test. This demonstrates the benefit of in situ testing such as running to properly characterize PPMS. Further, these results support the investigation of algorithms to transform the SI's pressure measurement into force output. While measures of peak ground reaction force could be established without complex methods, the ability of the SI sensor to display valid force outputs on a full range of ascending and descending values will require focused techniques to ensure accurate values. Future investigations will be important to establish the SI sensor against other PPMS such as the Novel® Loadsol™ that has demonstrated strong agreement against the Bertec® instrumented treadmill [52]. Further, in their study, Burns et al. [52] showed strong agreement between the Loadsol™ sensor and force measurement across different tasks. Comparisons such as those presented by Burns et al. [52] have great value for evaluating PPMS, and the SI sensor should be put through similar evaluations before being used in different tasks.

A limitation of this study design is that the PPMS being assessed are not being tested simultaneously in situ. For example, where multiple sensors are placed in the same shoe and measuring the same foot impact. While such tests would provide direct comparisons between systems, previous research has shown that there is an interference effect between in-shoe pressure insoles systems where the order in which they are placed within the shoe alters the pressure measurement of each system [74]. Another important limitation of this characterization is that the testing was conducted under constant (benchtop) or unknown (running) conditions of heat and humidity which have also been shown to affect resistive pressure sensors as are used in the SI system [92]. Further testing of the SI system under ranges of these conditions is warranted.

A limitation of the SI system is that it utilizes 32 discrete pressure-sensing elements and thus does not have complete coverage of all points of pressure application. In contrast, the F-Scan™ system utilizes a continuous array of 960 sensors and thus can capture all points of pressure application under the foot. The lack of complete coverage has implications for the calculation of contact area, which was not measured in this study [18]. Additionally, the lack of comparable spatial resolution of the SI system could have implications for subsequent biomechanical metric calculations, such as vertical ground reaction force estimation [15,18] and center of pressure, particularity at the extreme boundaries of the foot where coverage is potentially limited.

Despite these limitations, the overall form factor of the SI system has several advantages. At 65 g per insole, it is substantially lighter than the F-Scan™ system at 862 g. By simply replacing the running shoe's original sock liner, the SI system can potentially be worn without interfering with natural running gait. The F-Scan™ however, requires the participant to wear measurement hardware on their waist, including cables and large connectors mounted to the lateral aspects of their legs connecting the various components. PPMS with this form factor has been shown to interfere with natural running gait [13], potentially limiting the validity of gait measurements made

with the F-Scan™ system. It is important to note that at the time of testing, the most recent version of the F-Scan™ system was not available. It is possible that recent improvement in F-Scan sensor characteristics may support greater accessibility of this manufactured sensor for running-based assessment.

2.4 Conclusions

Overall, the SI PPMS performed similarly to or better than the F-Scan™ system during benchtop testing. Specifically, the SI displayed less mean RMSE during sinusoidal loading and less absolute error during static loading. Both the SI and F-Scan™ had near-perfect between-day reliability. During the running assessment, the SI pressure output had a near-perfect linearity and low RMSE compared to the force measurement from the Bertec® treadmill. However, the SI pressure output displayed a broad range of hysteresis which may have implications for the accurate quantification of kinetic gait measures during running.

These results highlight the need for future research to support further characterization of smart insoles such as the Kinetyx® SI during different athletic tasks. Additionally, this research highlights the need for an expanded standardized testing protocol that can be employed for the testing of smart insoles being used in dynamic activities such as running. Finally, this research evaluated the potential for resistive-based pressure measurement technology to provide a cost-effective alternative for use in smart insoles. Further development of smart insoles such as the SI may enable in situ running gait data collections to address biomechanical factors related to running related injuries and improve performances [3].

Given the viability of using discrete resistive sensor for a wearable PPMS, additional research is now needed to determine the optimal layout and estimation methods to determine the complete plantar pressure distribution. The following chapter presents this research.

3. Assessment of interpolation methods to reconstruct the complete plantar pressure distribution from sparse sensors during running

3.1 Introduction

In-shoe plantar pressure measurement systems (PPMS) are a valuable technology for the quantification of foot ground interactions during running gait. As opposed to traditional laboratory measurement tools such as in-ground force plates, in-shoe PPMS allow for the recording of consecutive steps, across a range of activities, and environments and provide important information on the distribution of forces across the plantar surface of the foot [3,6–8,36,46]. In running, accurate measurement of plantar pressure distributions (PPD) has been used successfully by researchers to calculate important biomechanical metrics such as the vertical ground reaction force (vGRF) [48,52,59,71,75,85,93–95] the trajectory of the center of pressure (COP) [49,51,76,96], the timing of foot contact events [1,12,53,65,97–99] and other derivative metrics used in clinical and athletic applications [100]. Beyond research applications, in-shoe plantar pressure data has been widely investigated for its potential at providing both real-time and summary-based feedback for injury prevention and management [3], and monitoring training in consumer running devices [6,101].

In research settings, commercial PPMS such as Pedar™ (Novel® Electronics Inc., GmbH, Munich, Germany), Medilogic (T&T medilogic Medizintechnik GmbH, Germany) and the F-Scan™ system (Tekscan® Inc., Boston, MA, USA) are widely used [84,102]. The Pedar™ system for example, employs a full array-based pressure insole with 99 capacitive sensors that cover the complete plantar surface [79]. Research on the Pedar™ system demonstrates it to have the highest

validity when compared against other research grade PPMS [56,84] during benchtop testing and it has been shown to perform well across a wide range of pressure values and tasks [84]. Designed for accuracy, the Pedar™ system, along with other research grade PPMS, have limited utility beyond laboratories due in-part to their high cost, memory and battery constraints [6,15,19], and highly encumbered form factors [13]. Further, such research grade PPMS can be complex to use and typically require calibration and operation by trained researchers [102]. Thus, despite the potential of plantar pressure measurement technology to play a transformative role in running performance monitoring [6], and injury monitoring [3], the currently available research grade PPMS do not offer viable solutions for these applications [6].

One method recommended by researchers for the design of a wearable PPMS which overcomes the design constraints associated with research grade systems is to use a reduced number of pressure sensing elements [16]. Using a reduced or *sparse* sensor layout has been proposed for consumer versions of PPMS as it could result in reduced power consumption (i.e. battery size and weight), reduced raw data files sizes [15], reduced production costs, improved durability and improved overall form factor [6,15,16,18,18]. Given that the human foot engages with both the ground and footwear through a limited series of anatomical contact points, a sparse sensor layout could be optimized to these locations [18,103]. For example, a recently validated consumer grade wearable running PPMS has been produced with 8 large pressure sensors placed under key plantar surface anatomical landmarks [20]. While sparse sensor layouts such as this have been investigated for their ability to directly measure the center of pressure [18,104–106] and vertical ground reaction forces; [15,59] they have not been investigated for their ability to measure the complete PPD in running which can provide important quantitative and qualitative information. Systems with sparse layouts have a substantial drawback over research grade PPMS with full pressure arrays, as they lack critical spatial resolution in the PPD. For example, a recent study by

Ciniglio et al. [18] evaluated the ability of a 16-sensor layout to measure PPD and derivative metrics. They found that the 16-sensor layout underestimated mean and peak pressure, vGRF, and contact area across all trials and tasks, regardless of insole size. One method employed to overcome restricted coverage with sparse layouts is to use large sensor areas [59,60]. While this method has been shown to be viable for the estimation of vGRF [60], large sensor areas result in local pressure underestimation due to the averaging effect of large sensors [17,107,108]. The effect of sensor size and resolution has been previously investigated and it has been proposed that for 90% accuracy in local peak pressure measurement requires as low as 5 mm spatial resolution [61]. In running, limited spatial resolution can lead to measurement errors since PPD during running involves high-frequency components and large pressure differentials [102,108]. Thus, optimal sparse sensor layouts still require the use of small (~5mm) sensor sizes with the consequence that measurement of plantar pressure at regions of the foot not covered by these sensors must be estimated. Depending on the estimation method chosen, estimation could yield substantial errors in the complete plantar pressure resolution [107,108] which in turn could lead to lower accuracy in any pressure derived metrics such as vGRF [109,110] and COP [76,109].

Given the relatively continuous contours of plantar surface anatomy [111,112], it may be possible to recreate the PPD by estimating the pressure applied between sparse sensor locations. Previous efforts to estimate the complete PPD from sparse sensor layouts has largely focused on walking data and employed either interpolation methods or machine learning/regression methods [16,17,19]. In these studies, the machine learning models generally out-performed the interpolation techniques [16] on PPD reconstruction. For example, Ostadabbas et al. [17]. found that sparse sensor layout with ten sensors had three times as much error when using Laplacian interpolation relative to their regression model, and five times as much error for linear and natural neighbor in walking data relative to their regression model. Similarly, Mun et al. [19] reported an accuracy

with correlation coefficients of 0.92 to 0.99 and root mean squared error values of approximately 8.0% for their machine learning model. However, the accuracy of these models may be limited to the activity and populations that they were trained on [19]. For example, Ostadabbas et al. [17] reported a 50% increase in estimated pressure error when participants walked at speeds greater than their model was trained under. A further complication with machine learning/regression models is that they may also transform the original pressure data derived from the sparse layout sensors [17]. Finally, machine learning models trained in research are often not made publicly available, so although the results are promising, data collection and training is required to employ these methods. By contrast, estimation techniques such as two-dimensional spatial interpolation are not bound by these limitations and could be used to reconstruct a spatially continuous PPD from a sparse number of sensors [16,113]. Standard 2D interpolation techniques include: bilinear interpolation, bicubic interpolation, and nearest neighbor [16,17]. However, it is currently unknown what the optimal interpolation method and sensor count would be to reconstruct the pressure array with minimal error during running. To date, no studies have evaluated the effect of sensor count, sensor placement, and interpolation method on the derivation of the complete PPD and derivative metrics during running. Additionally, no investigations have evaluated the effectiveness of PPD reconstruction techniques across several points of the running gait stance phase. Thus, the purpose of this investigation is to evaluate the effect of reduced sensor count and interpolation methods on the ability to derive the complete PPD during running across the stance phase. The results of this investigation could provide critical information for the development and design of a fully portable, consumer grade PPMS for use in running.

3.2 Materials and Methods

3.2.1 Subjects

A total of 18 (9 male, 9 female) participants were recruited aged 19 - 40 years (mean: 28 ± 5 years). Participant height ranged from 1.55 to 1.93 m (mean: 1.73 ± 0.10 m) and body mass ranged from 52.0 to 87.5 kg (mean: 66.6 ± 10.3 kg) [48]. All participants were free from injury at the time of testing and were familiar with treadmill running. The protocol and methodology were approved by the University of Calgary Conjoint Health Research Ethics Board (REB20-1734) and all participants provided written informed consent before participating.

3.2.2 Data collection

All participants wore their normal running footwear which spanned several brands. Prior to testing, each participant was fitted with the Pedar™ system (100 Hz, Novel®, Munich, DEU) where the sensors were placed within the participant's shoe on top of the existing insole. Each Pedar™ insert contains 99 pressure sensing elements and were sized for nearest fit to the participants shoe size. The Pedar™ system has a pressure sensing range of 15-600 kPa and has been shown to be valid under laboratory to have excellent pressure measurement accuracy[13,15]. Following a self-selected warm-up, participants ran on a treadmill (Bertec® Columbus, Ohio, USA) on level grade at 2.6 m/s (9.4km/h; 6:24 min/km), 3.0 m/s (10.8km/h; 5:33 min/km), 3.4m/s (12.2km/h; 4:54 min/km), and 3.8 m/s (13.7km/h; 4:23 min/km). In-shoe pressure data were collected for 75 s and were cropped for analysis from 25 s onward in the trial to ensure only steady-state running was used for the analysis.

3.2.3 Data analysis

All post processing and data analysis was completed using custom-written software (Python 3.6 https://www.python.org). For each trial, (Figure *3-1*) a standard threshold crossing algorithm using a 50N threshold was used on the vertical ground reaction force signal (vGRF) (Figure *3-1*) to determine the stance phase of the gait cycle [98]. Each stance phase (from initial-contact to toe-off) was then time normalized from 0 to 100 and a single mean stance phase was generated per trial (Figure *3-2*). From the mean stance, pressure data at: 10, 25, 50, 75, and 90% were indexed for further analysis. These were selected to provide points of analysis throughout the stance phase, including critical points at initial contact, midstance, and toe-off.

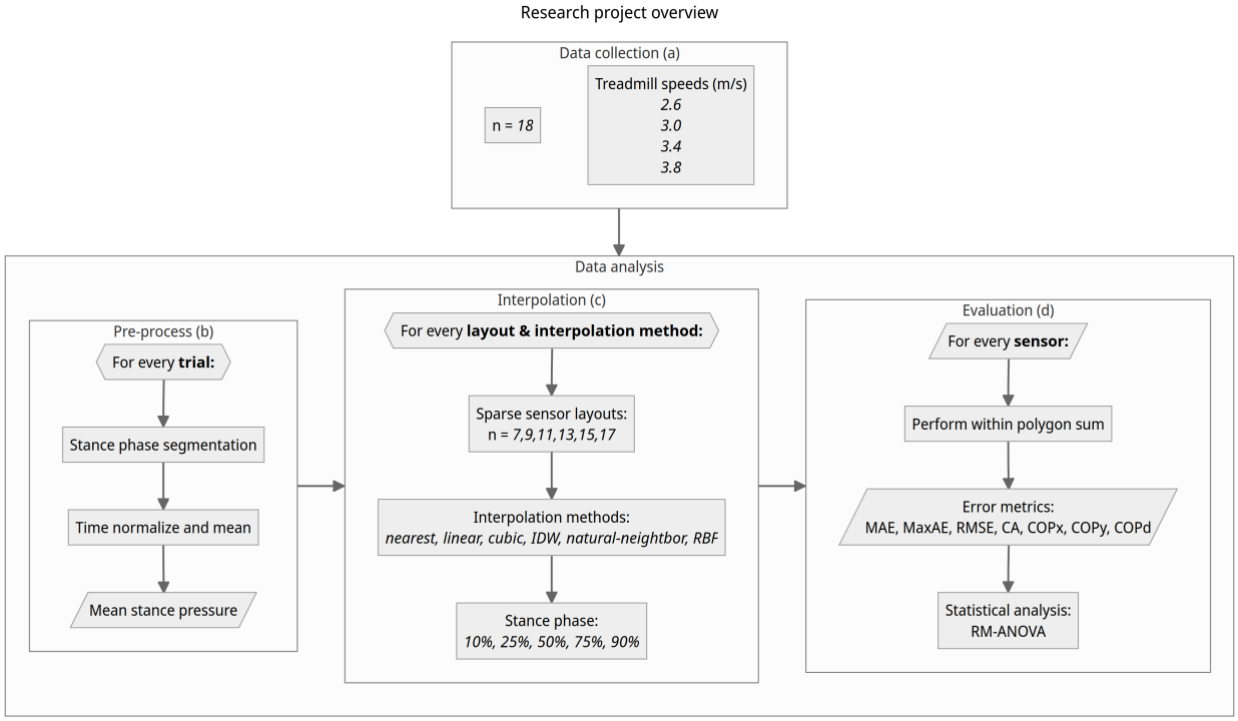

Figure 3-1 Overview of the data collection and data analysis methodology . (**a**) data collection protocol; (**b**) pre-processing methodology; **(c)** interpolation methodology; **(d)** evaluation methodology where MAE = mean absolute error (kPa), MaxAE, = maximum absolute error (kPa), RMSE = root mean squared error (kPa), CA = percentage of total contact area (%), COPx = absolute error in the center of pressure in the medial-lateral direction (mm), COPy = absolute error in the center of pressure in the anterior-posterior direction (mm), and COPdist = the absolute error center of pressure in the Euclidean distance (mm).

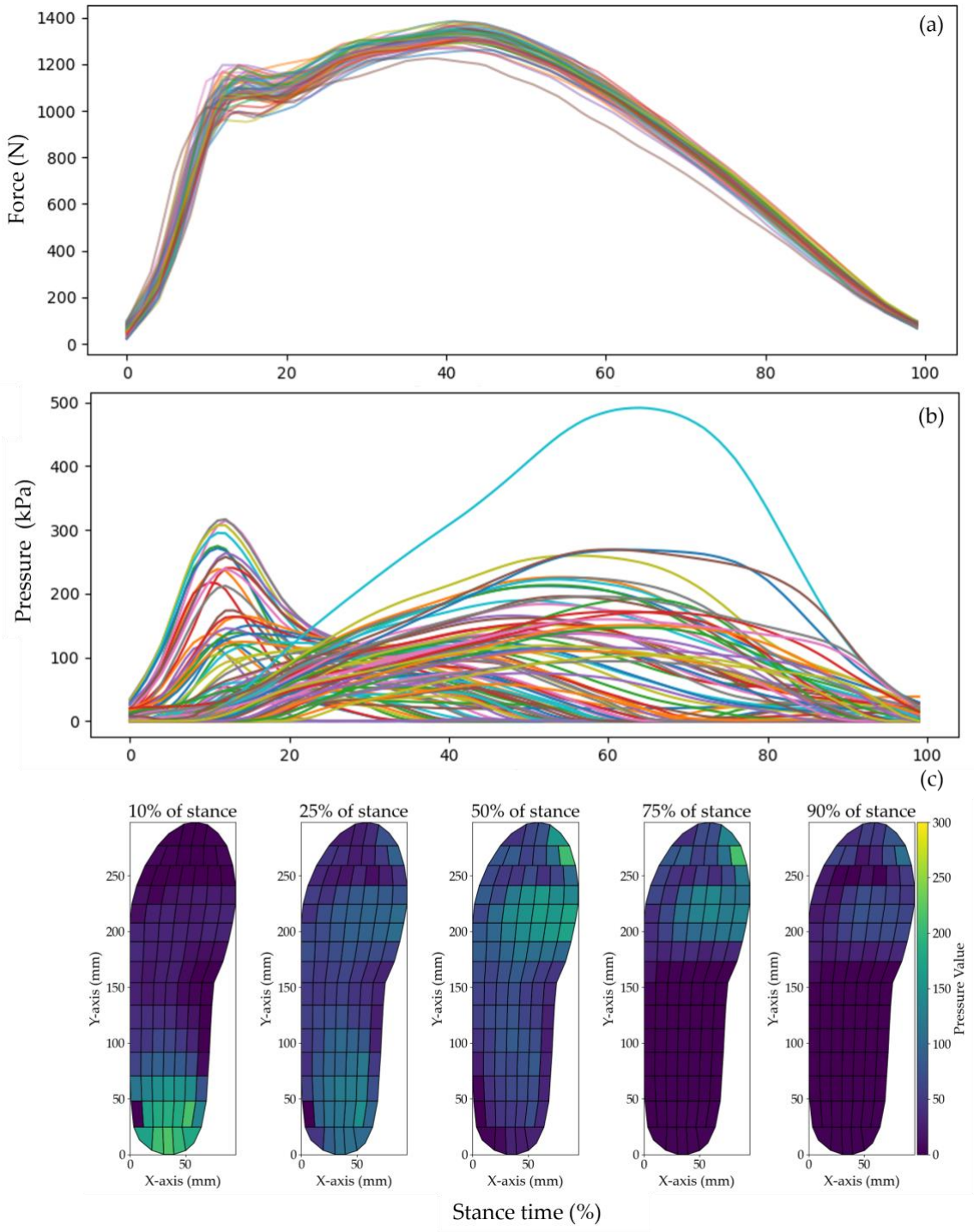

Figure 3-2 (a) Time normalized and stacked vertical ground reaction force (vGRF) signals. A threshold crossing with a threshold of 50 N was applied to the vGRF signal to determine initial foot contact and toe off events. The foot contact events were used to define the stance phase for each step across a given trial. Each stance phase was then time normalized and averaged to derive the mean pressure during stance for each trial. (b) Time normalized mean stance pressure data with all 99 pressure sensors. (c) Time normalized mean stance pressure data with all 99 pressure sensors at 10, 25, 50, 75, and 90% of stance.

Data analysis – sparse sensor layouts

The following sensor layouts presented by Fuchs et al. [15] were used to evaluate the different spatial interpolation methods as they represented similar locations to other studies that evaluated sparse sensor layouts in running [6,18,19]. Additionally, Fuchs et al. [15] demonstrated that the following 6 sparse sensor layouts (Figure *3-3*) used in their study, were able to estimate the vGRF in slow and fast jogging using a linear regression model with good levels (6 - 8%) of accuracy.

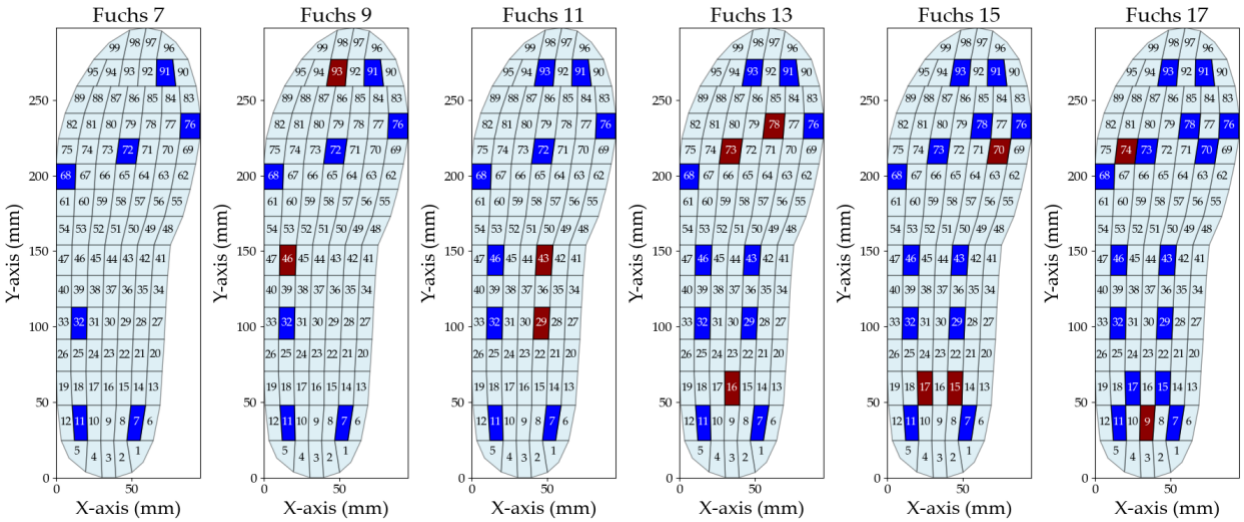

Figure 3-3 Sparse sensor layouts with increasing numbers of sensors [n = 7, 9, 11, 13, 15, 17] with location as reported by Fuchs et al. [1]. Blue sensors indicate the location of the selected sensors for a given layout and red sensors indicate the added sensors over the previous layout.

3.2.4 Data analysis – interpolation

The following 2D interpolation methods were applied to each sparse sensor layouts (Figure *3-4*) for each trial's mean stance data at each time step (10, 25, 50, 75, and 90%).

- **Nearest-neighbor interpolation (nearest)**: (SciPy -griddata) this method assigns the value of the nearest data point to the estimation point. [17].

- **Bilinear interpolation**: (SciPy – griddata) interpolation uses the values of the nearest points to estimate a value at a new point. It computes the weighted average of the nearest data points using barycentric coordinates [17].
- **Bicubic interpolation** (cubic) (SciPy -griddata) cubic interpolation fits a cubic polynomial to the nearest data points to estimate values. It provides a smoother result than bilinear interpolation but requires more computations.
- **Inverse distance weighting interpolation** (IDW): (custom) this method estimates values at new points based on the inverse of the distance to known data points. Closer data points have a greater influence on the estimation and the influence decreases as a power of the distance [114].
- **Natural-neighbor interpolation** (NN): (SciPy -griddata) this method is based on the Voronoi tessellation of data points and is considered useful for producing smooth surfaces from irregularly spaced data points [17].
- **Radial basis function interpolation** (RBF): (SciPy -rbf) RBF interpolation estimates grid values using a weighted sum of radially symmetric basis functions centered on data points using the Gaussian method [115].

All six of the above interpolations were computed using a combination of the sparse sensor centroid (x_n,y_n) locations and their corresponding pressure values and sensor boundary points. Given that the boundary points represented the perimeter of the pressure measuring area, they were assigned a pressure value of zero. As such, the area of the interpolation within the boundary points can be referred to as a 'convex hull' using the following definitions:

pressure data set:

$$(x_0, y_0, z_0), (x_1, y_1, z_1) \ldots . (x_n, y_n, z_n)$$

$$where:$$

$$x_i = medial\ lateral\ sensor\ centroid\ (mm)$$

$$y_i = anterior\ posterior\ sensor\ centroid (mm)$$

$$z_i = pressure\ value\ at\ that\ sensor\ location\ (kPa)$$

boundary data set:

$$(x_0, y_0, z_0), (x_1, y_1, z_1) \ldots . (x_n, y_n, z_n)$$

$$where:$$

$$x_i = medial\ lateral\ boundary\ coordinate\ (mm)$$

$$y_i = anterior\ posterior\ boundary\ coordinate (mm)$$

$$z_i = 0\ (kPa)$$

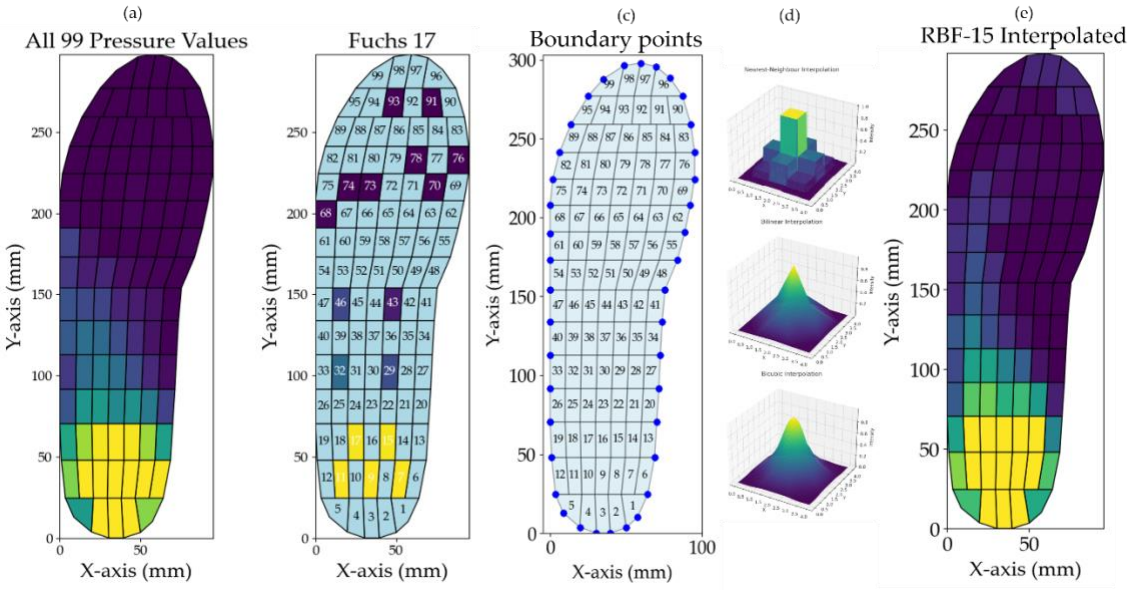

Figure 3-4 Illustration of the interpolation process starting with (a) the complete (n=99) reference pressure data at 10% of mean stance; (b) showing the same pressure data on the sparse (n=17) sensor layout; (c) the boundary points where pressure is assumed to be zero; (d) three of the 6 different spatial interpolation methods (top = nearest neighbour, middle = bilinear, bottom = bicubic); (e) the resultant interpolated pressure data from 17 sensor layout and bicubic interpolation.

3.2.5 Data analysis – error metrics

To evaluate the potential of each interpolation method and sensor layout to recreate the complete PPD, all six interpolation methods were applied to the mean pressure from each trial across each stance time step, using data from each of the six sparse sensor layouts (*interpolation method* x *sensor layout* x *stance phase*; herein referred to as *conditions*). The resultant interpolated pressure data from each condition, was then compared back to the reference pressure array to facilitate direct comparisons for pressure measurement accuracy. The following error metrics were calculated for each condition: mean absolute error (MAE), maximum absolute error (MaxAE), and root mean squared error (RMSE). In addition to the pressure error metrics, measures of contact area and center of pressure were also calculated. From these additional measures, error metrics were determined for each condition. These error metrics were: percentage of total contact area (CA), absolute error in the center of pressure in the medial-lateral direction (COPx AE) (Equation 1), absolute error in the center of pressure in the anterior-posterior direction (COPy AE) (Equation 1), and absolute error in COP distance (COPdist AE) (Equation 2).

Equation 1: center of pressure

$$COP_x = \frac{\sum_{i=1}^{n} P_i \cdot X_i}{\sum_{i=1}^{n} P_i} \quad COP_y = \frac{\sum_{i=1}^{n} P_i \cdot Y_i}{\sum_{i=1}^{n} P_i}$$

$$where:$$

$$(COP_x)\ represents\ the\ medial - lateral\ center\ of\ pressure$$

$$\left(COP_y\right)\ represents\ the\ anterior - posterior\ center\ of\ pressure$$

$$(P_i)\ is\ the\ pressure\ value\ of\ the\ (i)th\ sensor$$

$$(X_i)\ is\ the\ X\ coordinate\ of the\ (i)th\ sensor$$

$$(Y_i)\ is\ the\ Y\ coordinate\ of\ the (i)th\ sensor$$

$$(n)\ is\ the\ total\ number\ of\ sensors$$

Equation 2:center of pressure distance

$$COP_{\text{dist}} = \sqrt{(COPx_{\text{ref}} - COPx_{\text{int}})^2 + (COPy_{\text{ref}} - COPy_{\text{int}})^2}$$

$$where:$$

$$\left(COP_{x_{ref}}\right)\ represents\ the\ medial\ lateral\ center\ of\ pressure\ from\ the\ reference\ data$$

$$\left(COP_{y_{ref}}\right)\ represents\ the\ anterior\ posterior\ center\ of\ pressure\ from\ the\ reference\ data$$

$$\left(COP_{x_{int}}\right)\ represents\ the\ medial\ lateral\ center\ of\ pressure\ from\ the\ interpolated\ data$$

$$\left(COP_{y_{int}}\right)\ represents\ the\ anterior\ posterior\ center\ of\ pressure\ from\ the\ interpolated\ data$$

The error measures from each condition across all four speeds and all participants were combined for statistical analysis. To assess the differences between each interpolation method and sparse senor layout, a 6 (interpolation method) by six (sparse sensor layout) by five (stance phase) repeated measures ANOVAs (RMANOVAs) was performed for each error metric. A Holm correction was applied for post hoc tests where significant main effects and interaction effects were found. The significance level was set at $p < 0.05$. All statistical analysis was performed using JASP (Version 0.18, Amsterdam, The Netherlands) [116].

3.3 Results

3.3.1 Effect of sensor layout

The effect of sensor layout on the accuracy of the estimated PPD was evaluated across all error metrics (Figure *3-5*, Figure *3-6*).

A significant main effect ($p < .001$) for sensor layout was found for all error metrics. Post-hoc tests for layout on MAE found significant differences between all layouts with the 17-sensor layout performing the best. Post-hoc test for RMSE found significant differences between all layouts except for between 15 and 17 with the 17-sensor layout performing the best of all layouts. Post-hoc tests for layout on MaxAE found significant differences between all layouts except for between

9 and 11, 11 and 13, and 15 and 17 with the 15-sensor layout reporting the least MaxAE. Post-hoc tests for CA found significant differences between all layouts except for between 11 and 13, 11 and 17, and 15 and 17. Post-hoc tests for layout on COPx found significant differences between all layouts except 7 and 13 and 15 and 17 again with the 17 sensor layout reporting the least error. Post-hoc test for layout on COPy found significant differences between all layouts except for between 7 and 9, and 13 and 15, 13 and 17 and 15 and 17. Again, the 17-sensor layout had the least error on COPy. Post-hoc tests for layout on COPdist found significant differences between all layouts except for between 7 and 9, 11 and 13, 13 and 15 and 15 and 17 with the 17-sensor layout reporting the least error of all layouts.

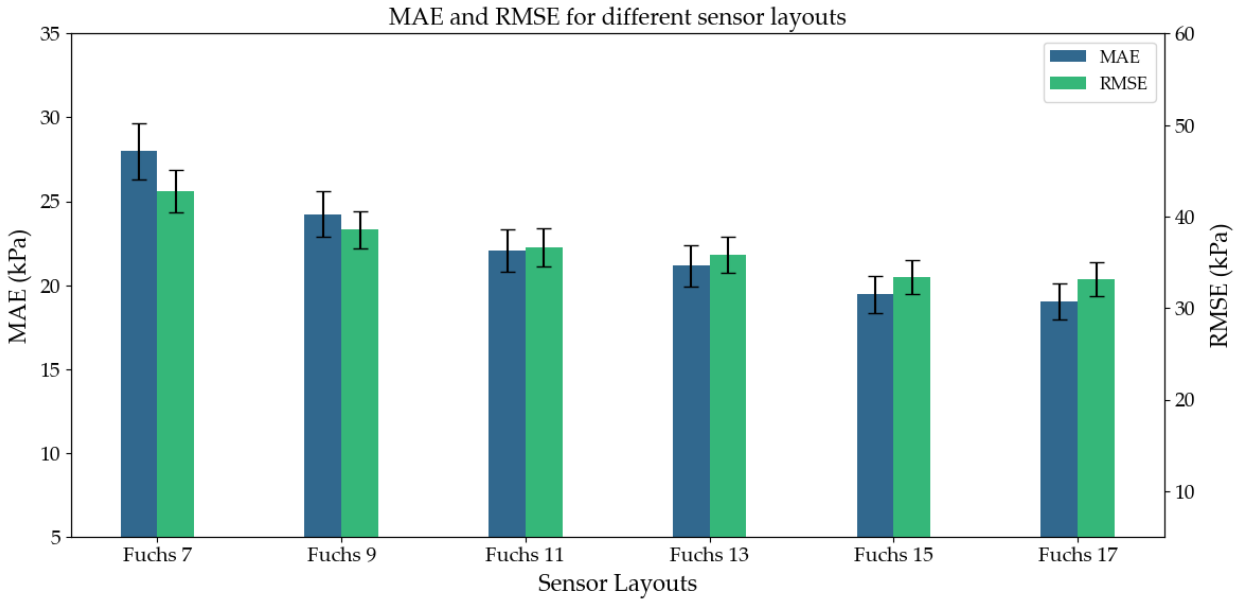

Figure 3-5 Error by layouts . Mean absolute error (MAE) and root mean squared error (RMSE) for all layouts. Interpolation methods and stance phases are consolidated. Fuchs 15 layout had the lowest MAE compared to all other layouts.

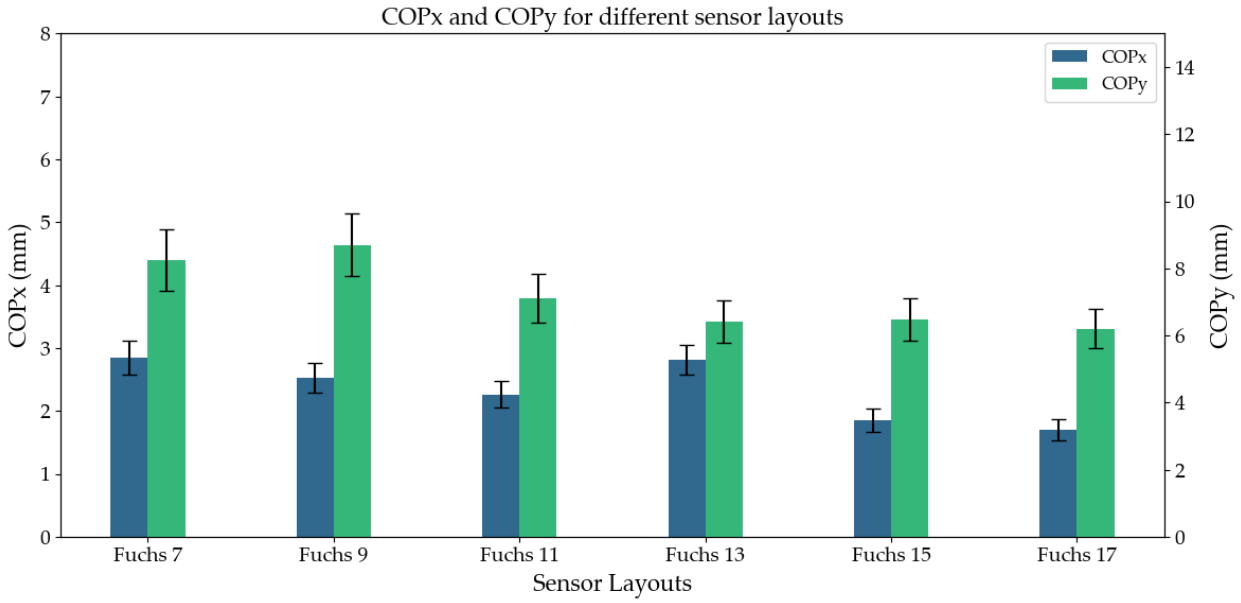

Figure 3-6 Center of pressure errors by layout . Medial-lateral center of pressure (COPx) and anterior-posterior center of pressure (COPy) for all layouts. A main effect ($p < .001$) was found for COPx and COPy for all layouts.

3.3.2 Effect of interpolation method

The effect of interpolation method on the accuracy of the estimated PPD was evaluated across all error metrics (Figure *3-7*, Figure *3-8*). A significant main effect ($p<.001$) for interpolation method was found for all error metrics. Post-hoc tests for interpolation methods on MAE found significant differences between all interpolation methods except for between bilinear and bicubic, bicubic and NN, and IDW and NN with RBF reporting the least MAE of all interpolation methods. For RMSE, post-hoc test found significant differences between all interpolation methods with RBF also reporting the least RMSE. For MaxAE, post-hoc tests found significant differences between all interpolation methods except between RBF and IDW with IDW reporting the least MaxAE. On measures of CA, post-hoc tests found significant differences between all interpolation methods with bilinear reporting the least difference in CA. Post-hoc tests for COPx found significant differences between all interpolation methods except for between bilinear and bicubic, bilinear and NN, bilinear and RBF, bicubic and NN, bicubic and RBF and NN and RBF with NN reporting the

least error in COPx. For COPy, significant differences were found between nearest and linear, nearest and IDW, bilinear and IDW, bicubic and IDW, IDW and NN, IDW and RBF with RBF reporting the least error. For COPdist, post-hoc tests revealed significant differences between all interpolation methods other than for bilinear and bicubic, bilinear and RBF, bicubic and NN, bicubic and RBF, and NN and RBF with bilinear also reporting the least error in COPdist.

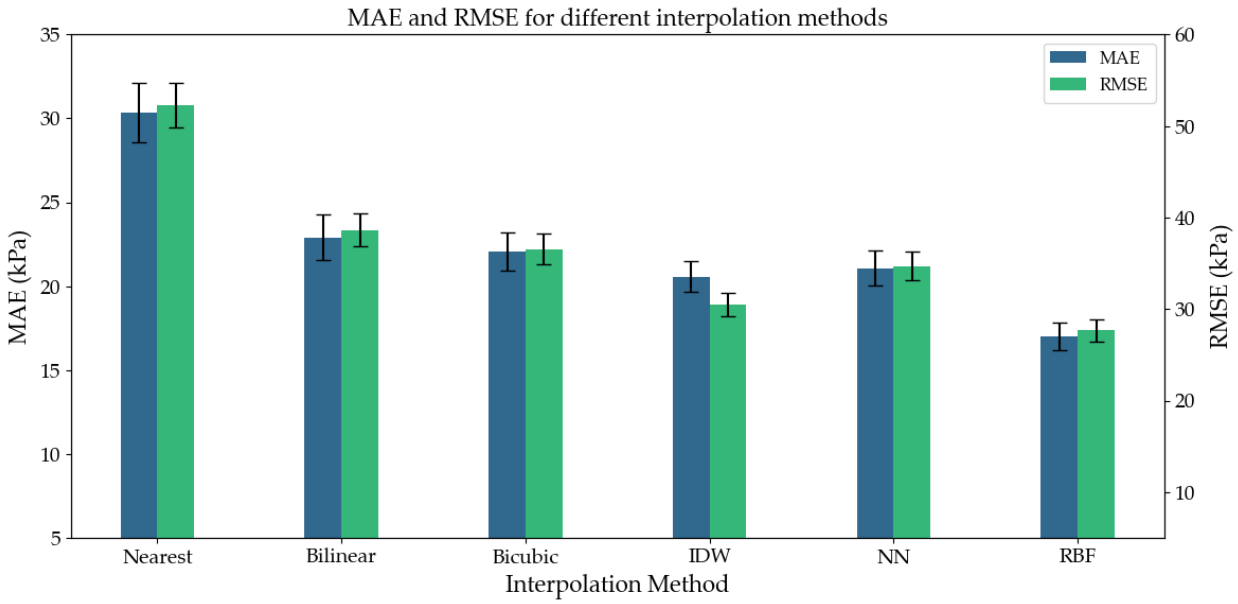

Figure 3-7 Error by interpolation method . Mean absolute error (MAE) and root mean squared error (RMSE) for all interpolation methods. Layouts and stance phases and are consolidated.

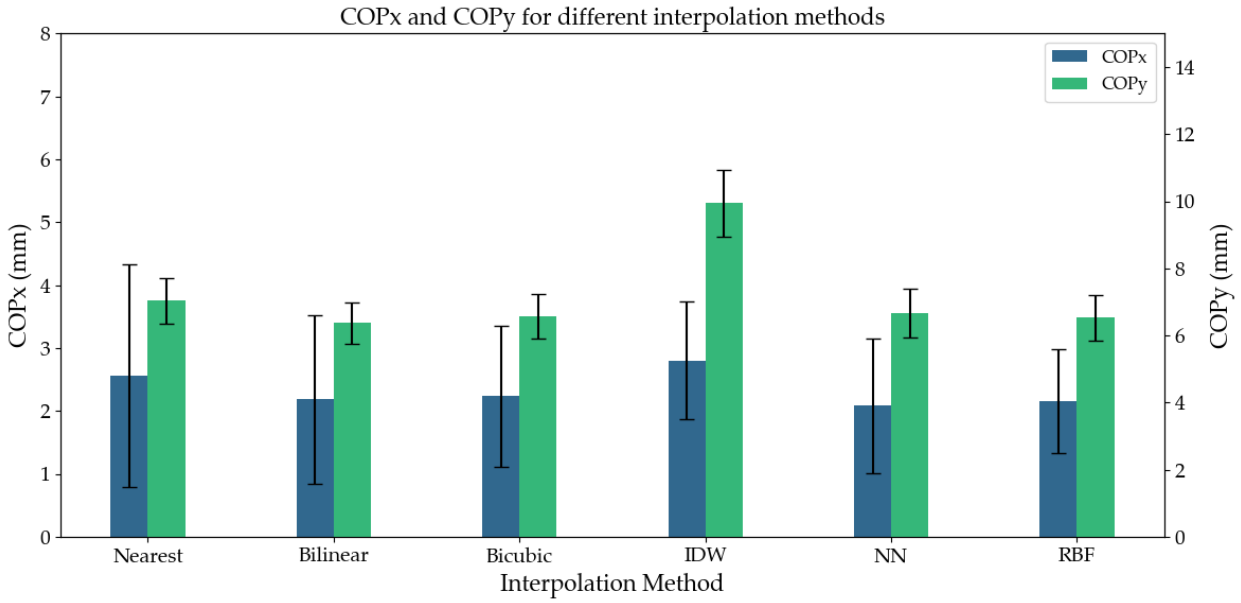

Figure 3-8 Center of pressure errors by interpolation method . Medial-lateral center of pressure (COPx) and anterior-posterior center of pressure (COPy) for all interpolation methods. A main effect ($p < .001$) was found for COPx and COPy between all interpolation methods.

3.3.3 Stance Phase

The effect of stance phase on the accuracy of the estimated PPD was also evaluated across all error metrics (Figure *3-9*, Figure *3-10*). A significant main effect ($p<.001$) for stance phase was found for all error metrics. Significant differences were found between all stance phases on measures of MAE and RMSE. Significant differences were found between all stance phases on measures of MaxAE except between 10% and 25%, and 50% and 75%. Significant differences were found between all stance phases on measures of COPx except between 10% and 50%, 10% and 75%, and 25% and 50%. Significant differences were found between all stance phases on measures of COPy except between 10% and 50%, 10% and 75%, and 25% and 50%. Significant differences were found between all stance phases on measures of COPdist except 10% and 50%.

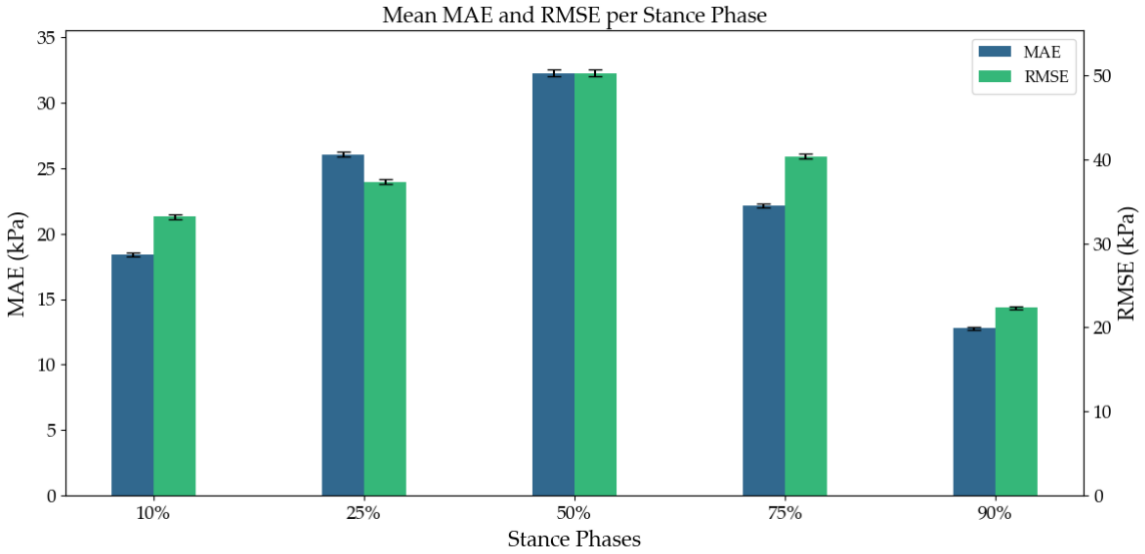

Figure 3-9 Error by stance phase . Mean absolute error (MAE) and root mean squared error (RMSE) for all interpolation methods. A main effect ($p < .001$) was found for MAE and RMSE between all stance phases.

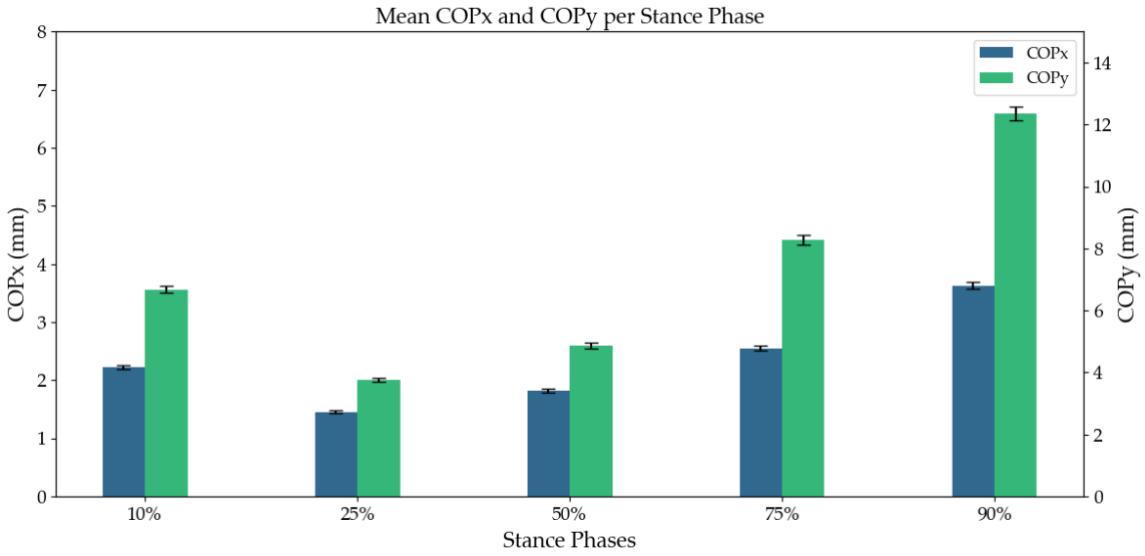

Figure 3-10 Center of pressure error by stance phase . Medial-lateral center of pressure (COPx) and anterior-posterior center of pressure (COPy) for all stance phases. A main effect ($p < .001$) was found for COPx and COPy between all stance phases.

3.3.4 Interaction effect of sensor layout, interpolation method and stance phase

Results revealed a significant interaction ($p<.001$) for sensor layout and interpolation method for all error metrics. Post-hoc tests for sensor layout and interpolation interaction on MAE revealed significant differences between numerous combinations of layouts and interpolation

methods. Importantly, the 15 sensors layout using the RBF interpolation method (RBF-15) had the lowest overall MAE (14.0 ± 0.6 kPa) across all speeds and stance phases. The RBF-15 combination of layout and interpolation method was significantly lower MAE than all other combinations, except for RBF with the 17-sensor layout (RBF-17). Post-hoc tests for RMSE revealed similar results as MAE. Significant differences were found across different combinations of interpolation methods and sensor counts. The RBF-15 also had significantly lower RMSE (23.9 ± 1.0 kPa) than all other combinations other than RBF-17 across all speeds and stance phases. Post-hoc tests for MaxAE again revealed significant differences across multiple different combinations of sensor count and interpolation methods. Similar to MAE and RMSE, the RBF-15 combination along with the IDW-15 combination had significantly lower MaxAE (103.9 ± 6.0 kPa and 103.9 ± 5.6 kPa respectively) than all other combinations. Post-hoc tests for sensor count and interpolation method on COPx revealed significant differences amongst several combinations. As with other error metrics, the RBF-15 had significantly lower (1.3 ± 0.1 mm) COPx mean absolute error than all other combinations other than RBF-17 and NN-17 combinations which reported the same COPx error. For COPy, post-hoc tests revealed the 17-sensor layout using bilinear interpolation (bilinear-17) had the lowest error of 5.2 ± 0.4 mm. The bilinear-17 was significantly lower than all other combinations other than linar-15, bicubic-15, bicubic-17, NN-15, NN17 and RBF-15. For COPdist, post-hoc tests found that the 17 sensor NN (17-NN) combination had the best performance and was significantly different than all other combinations other than RBF-15 and RBF-17. Post-hoc tests revealed that the 13-sensor bilinear (bilinear-13) combination has the best performance on percentage of total contact area 99.6 ± 1.1% and was significantly closer to 100% than all other combinations other than bilinear-15 and bilinear-17. Despite its superior performance on the pressure error metrics, the RBF-15 combination over reported contact area (108.2 ± 1.3) by over 8 %.

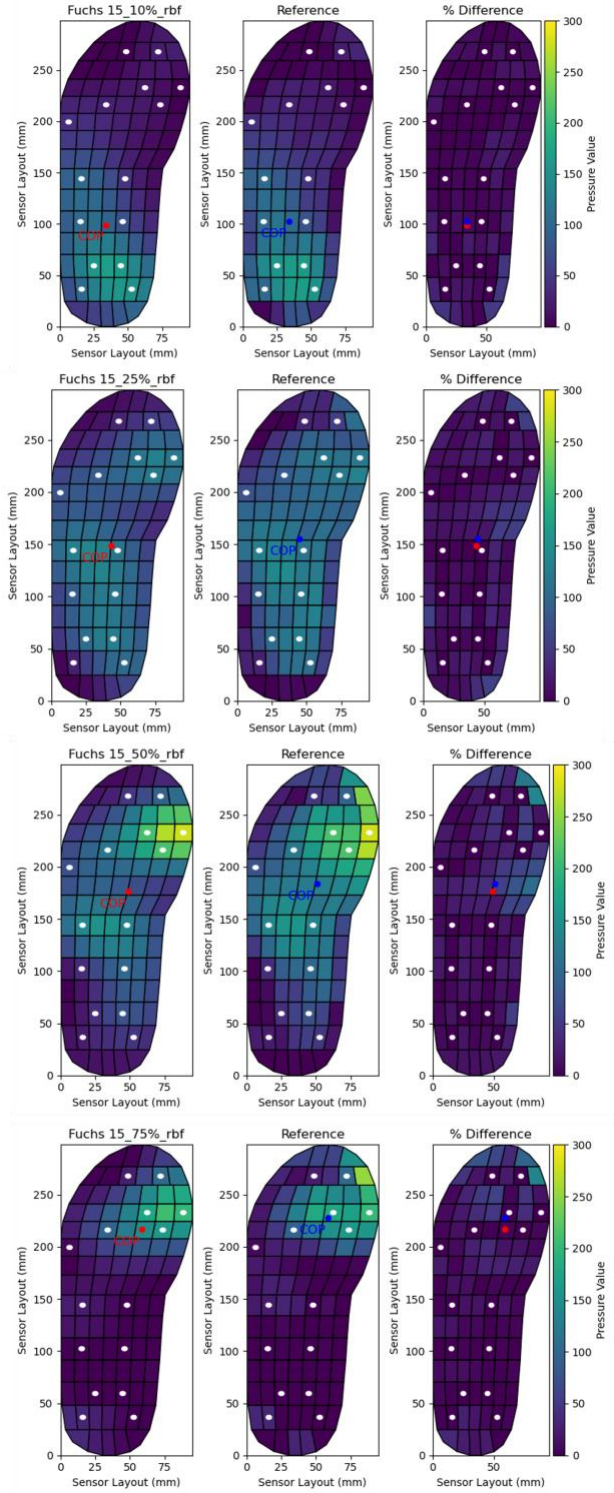

Figure 3-11 Pressure and center of pressure (COP) error plots at 10, 25, 50 and 75% of stance . White dots indicate sparse sensor locations for a given layout, red and blue dots show locations of the COP for the interpolated and reference pressure array respectively. (left) interpolated 15 sensor layout using radial basis function (RBF) at each

stance phase, (middle) reference (n=99) at each stance phase, and (right) error plot as the percent difference between the interpolated pressure array and the reference array.

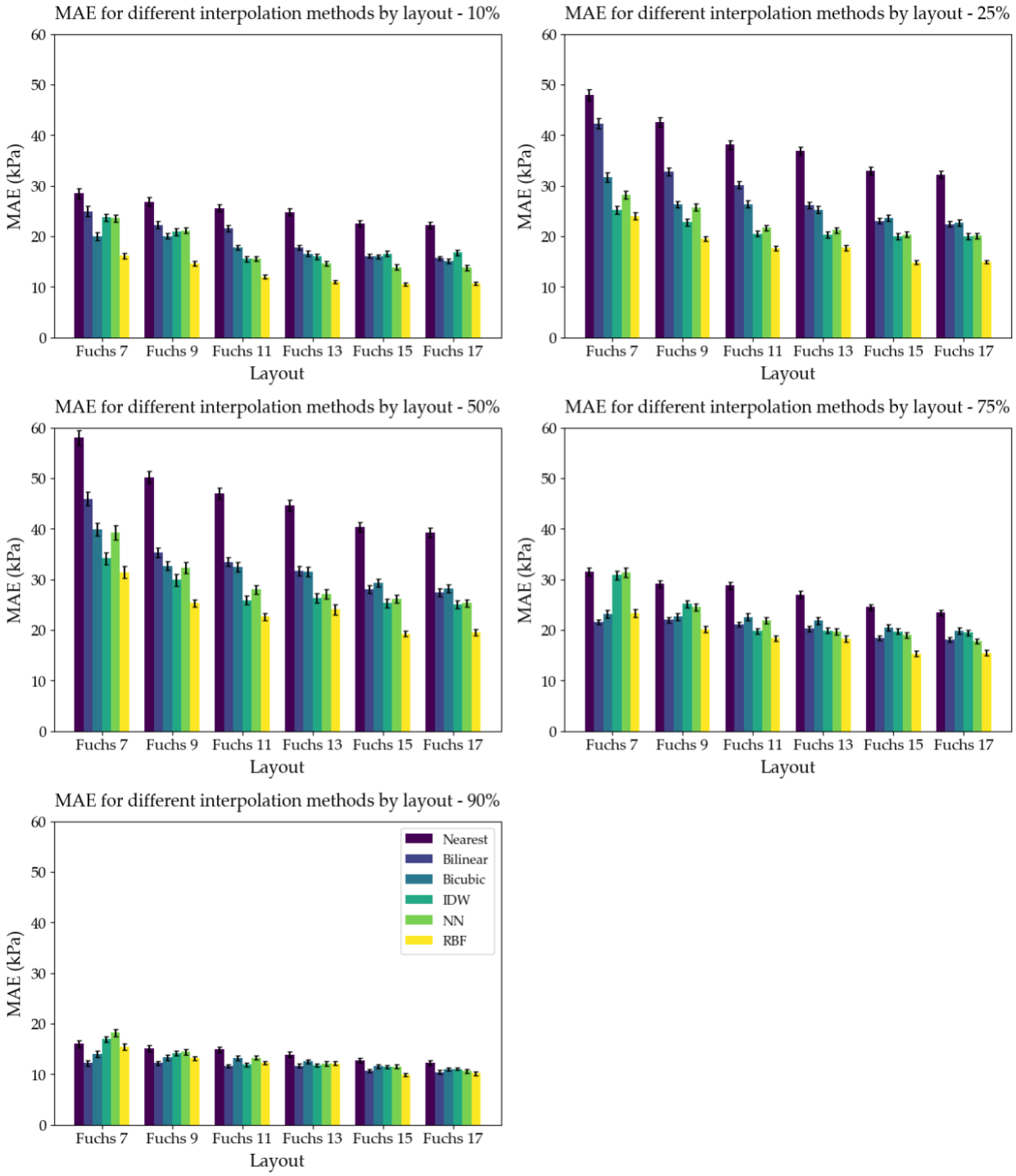

Figure 3-12 Mean absolute error (MAE) across different layouts and interpolation methods at each of the measured points in the stance phase.

Table 3-1 Mean absolute error (MAE) across different layouts and interpolation methods . Units are in kPa. Bolded values indicate the best performing interpolation method and layout for a given stance phase.

	Method	Fuchs 7	Fuchs 9	Fuchs 11	Fuchs 13	Fuchs 15	Fuchs 17
10%	nearest	28.5 (± 8.2)	26.9 (± 7.0)	25.6 (± 5.8)	24.8 (± 5.7)	22.5 (± 4.9)	22.2 (± 4.8)
	bilinear	25.0 (± 7.6)	22.3 (± 5.7)	21.6 (± 4.8)	17.8 (± 3.8)	16.1 (± 3.4)	15.7 (± 3.4)
	bicubic	20.0 (± 5.8)	20.0 (± 4.1)	17.8 (± 4.0)	16.6 (± 3.7)	16.0 (± 3.5)	15.1 (± 3.4)
	IDW	23.8 (± 5.7)	20.9 (± 5.0)	15.5 (± 4.3)	16.0 (± 4.0)	16.6 (± 4.0)	16.8 (± 4.3)
	NN	23.6 (± 5.4)	21.2 (± 4.7)	15.6 (± 3.8)	14.6 (± 4.0)	13.9 (± 4.1)	13.8 (± 4.2)
	RBF	16.2 (± 4.1)	14.6 (± 3.8)	12.0 (± 2.8)	11.0 (± 2.6)	**10.5 (± 2.3)**	10.7 (± 2.3)
25%	nearest	48.0 (± 8.9)	42.6 (± 7.4)	38.1 (± 6.6)	36.9 (± 6.3)	33.0 (± 5.6)	32.2 (± 5.6)
	bilinear	42.3 (± 8.4)	32.8 (± 6.2)	30.2 (± 5.3)	26.2 (± 5.2)	23.1 (± 4.4)	22.4 (± 4.4)
	bicubic	31.7 (± 7.2)	26.3 (± 4.7)	26.4 (± 5.8)	25.2 (± 5.5)	23.6 (± 5.0)	22.6 (± 4.9)
	IDW	25.2 (± 5.8)	22.8 (± 5.8)	20.5 (± 4.6)	20.3 (± 4.6)	20.0 (± 4.7)	20.0 (± 4.6)
	NN	28.2 (± 6.2)	25.7 (± 5.5)	21.7 (± 4.2)	21.2 (± 4.3)	20.4 (± 4.7)	20.1 (± 4.6)
	RBF	24.0 (± 5.5)	19.5 (± 3.8)	17.7 (± 3.6)	17.7 (± 4.5)	**14.8 (± 3.0)**	14.9 (± 2.9)
50%	nearest	58.0 (± 11.2)	50.2 (± 9.4)	47.0 (± 8.9)	44.7 (± 8.6)	40.4 (± 7.5)	39.2 (± 7.4)
	bilinear	46.0 (± 10.2)	35.3 (± 7.0)	33.5 (± 6.8)	31.6 (± 7.5)	28.0 (± 6.1)	27.3 (± 6.1)
	bicubic	39.8 (± 9.8)	32.7 (± 6.8)	32.5 (± 7.3)	31.5 (± 7.1)	29.3 (± 6.4)	28.2 (± 6.4)
	IDW	34.2 (± 9.5)	29.9 (± 9.1)	25.9 (± 7.0)	26.3 (± 7.4)	25.3 (± 6.4)	25.0 (± 6.3)
	NN	39.3 (± 10.9)	32.3 (± 8.2)	28.0 (± 6.5)	27.1 (± 7.5)	26.1 (± 6.3)	25.3 (± 6.0)
	RBF	31.4 (± 9.1)	25.4 (± 5.4)	22.6 (± 5.9)	24.0 (± 7.8)	**19.3 (± 4.7)**	19.5 (± 4.7)
75%	nearest	31.5 (± 6.3)	29.1 (± 5.8)	28.8 (± 5.7)	27.0 (± 5.3)	24.5 (± 4.6)	23.4 (± 4.4)
	bilinear	21.6 (± 3.9)	22.0 (± 4.1)	21.1 (± 3.9)	20.3 (± 4.3)	18.4 (± 3.3)	18.1 (± 3.3)
	bicubic	23.1 (± 6.3)	22.6 (± 5.5)	22.6 (± 5.6)	21.8 (± 5.1)	20.4 (± 5.0)	19.9 (± 5.1)
	IDW	30.9 (± 6.6)	25.2 (± 5.5)	19.8 (± 4.5)	19.9 (± 4.5)	19.8 (± 4.2)	19.5 (± 3.9)
	NN	31.4 (± 7.4)	24.6 (± 5.5)	21.9 (± 4.7)	19.6 (± 4.8)	19.0 (± 4.2)	17.7 (± 3.9)
	RBF	23.3 (± 6.3)	20.1 (± 4.8)	18.4 (± 4.2)	18.3 (± 4.9)	**15.3 (± 4.2)**	15.5 (± 4.7)
90%	nearest	16.0 (± 5.4)	15.1 (± 4.7)	14.9 (± 4.4)	13.9 (± 4.2)	12.7 (± 3.8)	12.2 (± 3.7)
	bilinear	12.2 (± 3.7)	12.2 (± 2.9)	11.7 (± 2.6)	11.7 (± 3.0)	10.7 (± 2.5)	10.4 (± 2.5)
	bicubic	14.0 (± 4.8)	13.3 (± 4.0)	13.2 (± 3.3)	12.5 (± 3.1)	11.6 (± 2.9)	11.0 (± 3.0)
	IDW	17.0 (± 4.2)	14.2 (± 3.6)	11.9 (± 2.9)	11.8 (± 2.4)	11.4 (± 2.4)	11.1 (± 2.1)
	NN	18.2 (± 5.7)	14.4 (± 4.2)	13.3 (± 3.4)	12.1 (± 3.1)	11.5 (± 2.9)	10.6 (± 2.7)
	FBF	15.4 (± 4.7)	13.1 (± 3.2)	12.2 (± 2.7)	12.1 (± 3.1)	**9.9 (± 2.7)**	10.1 (± 3.0)

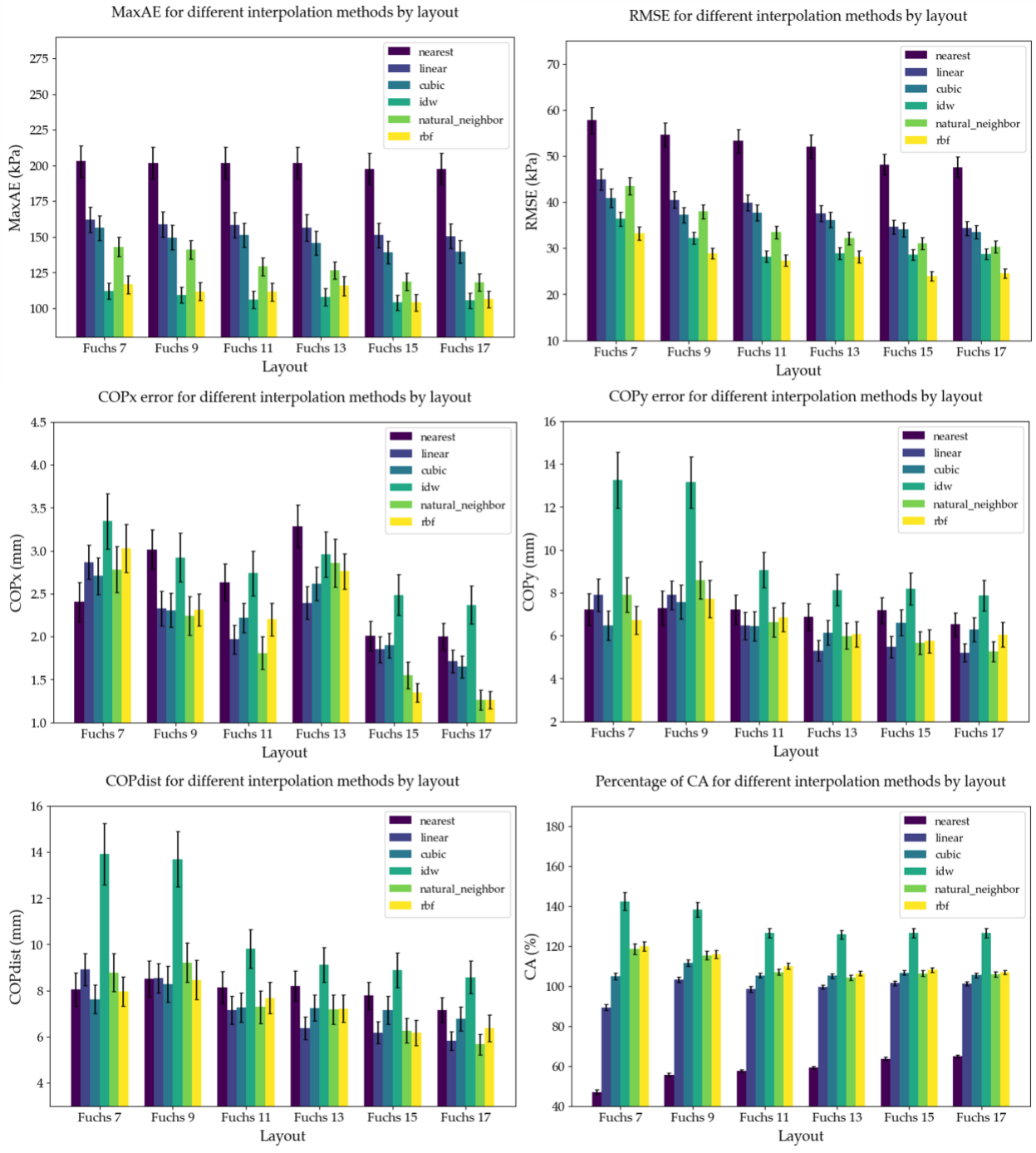

Figure 3-13 Error results by error metric (top-left) max absolute error (MaxAE), (top-right) root mean squared error (RMSE) (middle-left) medial-lateral center of pressure (COPx) error, (middle right) anterior-posterior center of pressure (COPy) error, (bottom-left) center of pressure distance from actual location, bottom-right percentage of actual contact area, across all layouts and interpolation methods For clarity, the stance phases are consolidated. Plots for each error metric across each stance phase can be found in Appendix B.

Table 3-2 Error metrics per layout and interpolation method . Best values for an error metric are in bold.

Method	Fuchs 7	Fuchs 9	Fuchs 11	Fuchs 13	Fuchs 15	Fuchs 17	Mean
				MAE (kPa)			
nearest	36.4 (± 2.4)	32.8 (± 2.0)	30.9 (± 1.8)	29.4 (± 1.7)	26.6 (± 1.5)	25.9 (± 1.5)	30.3 (± 0.6)
bilinear	29.4 (± 2.1)	24.9 (± 1.4)	23.6 (± 1.3)	21.5 (± 1.1)	19.3 (± 1.0)	18.8 (± 1.0)	22.9 (± 0.6)
bicubic	25.7 (± 1.5)	23.0 (± 1.1)	22.5 (± 1.1)	21.5 (± 1.1)	20.2 (± 1.0)	19.4 (± 1.0)	22.1 (± 0.5)
IDW	26.2 (± 1.1)	22.6 (± 1.0)	18.7 (± 0.9)	18.9 (± 0.9)	18.6 (± 0.8)	18.5 (± 0.8)	20.6 (± 0.4)
NN	28.1 (± 1.3)	23.6 (± 1.0)	20.1 (± 0.9)	18.9 (± 0.9)	18.2 (± 0.9)	17.5 (± 0.9)	21.1 (± 0.4)
RBF	22.0 (± 1.0)	18.5 (± 0.8)	16.6 (± 0.7)	16.6 (± 0.8)	**14.0 (± 0.6)**	14.1 (± 0.6)	**17.0 (± 0.3)**
Mean	28.0 (± 0.7)	24.2 (± 0.5)	22.1 (± 0.5)	21.1 (± 0.5)	19.5 (± 0.4)	**19.0 (± 0.4)**	
				MaxAE (kPa)			
nearest	203.0 (± 11.5)	201.7 (± 11.6)	201.7 (± 11.6)	201.7 (± 11.6)	197.7 (± 11.5)	197.7 (± 11.5)	200.6 (± 3.5)
bilinear	162.1 (± 9.3)	158.7 (± 9.4)	158.3 (± 9.5)	156.4 (± 9.5)	151.0 (± 9.0)	150.4 (± 9.0)	156.2 (± 3.8)
bicubic	156.2 (± 8.8)	149.5 (± 8.9)	151.1 (± 8.8)	145.6 (± 8.7)	139.0 (± 8.1)	139.5 (± 8.1)	146.8 (± 3.5)
IDW	112.1 (± 5.8)	109.1 (± 5.8)	106.1 (± 6.2)	107.7 (± 6.3)	103.9 (± 5.6)	105.3 (± 5.6)	**107.4 (± 2.4)**
NN	142.9 (± 7.1)	141.0 (± 6.9)	129.1 (± 6.6)	126.5 (± 6.4)	118.7 (± 6.3)	118.2 (± 6.2)	129.4 (± 2.7)
RBF	116.6 (± 6.5)	111.6 (± 6.5)	111.4 (± 6.7)	115.6 (± 7.0)	103.9 (± 6.0)	106.3 (± 6.0)	110.9 (± 2.6)
Mean	148.8 (± 3.4)	145.3 (± 3.4)	143.0 (± 3.5)	142.3 (± 3.5)	**135.7 (± 3.3)**	136.2 (± 3.3)	
				RMSE (kPa)			
nearest	57.7 (± 3.0)	54.6 (± 2.7)	53.3 (± 2.6)	52.1 (± 2.6)	48.1 (± 2.4)	47.6 (± 2.3)	52.2 (± 1.1)
bilinear	45.0 (± 2.4)	40.5 (± 1.9)	39.9 (± 1.8)	37.5 (± 1.8)	34.6 (± 1.6)	34.3 (± 1.6)	38.6 (± 0.8)
bicubic	40.8 (± 2.1)	37.2 (± 1.7)	37.7 (± 1.8)	36.1 (± 1.7)	34.1 (± 1.6)	33.5 (± 1.5)	36.6 (± 0.7)
IDW	36.3 (± 1.6)	32.2 (± 1.4)	28.2 (± 1.3)	28.9 (± 1.3)	28.6 (± 1.2)	28.7 (± 1.3)	30.5 (± 0.6)
NN	43.5 (± 1.9)	37.9 (± 1.5)	33.5 (± 1.4)	32.2 (± 1.4)	31.0 (± 1.4)	30.3 (± 1.3)	34.7 (± 0.6)
RBF	33.2 (± 1.5)	28.9 (± 1.2)	27.4 (± 1.2)	28.1 (± 1.3)	**23.9 (± 1.0)**	24.6 (± 1.0)	**27.7 (± 0.5)**
Mean	42.8 (± 0.9)	38.6 (± 0.7)	36.7 (± 0.7)	35.8 (± 0.7)	33.4 (± 0.7)	**33.2 (± 0.6)**	
				COPx (mm)			
nearest	2.4 (± 0.2)	3.0 (± 0.2)	2.6 (± 0.2)	3.3 (± 0.3)	2.0 (± 0.2)	2.0 (± 0.2)	2.6 (± 0.1)
bilinear	2.9 (± 0.2)	2.3 (± 0.2)	2.0 (± 0.2)	2.4 (± 0.2)	1.8 (± 0.2)	1.7 (± 0.1)	2.2 (± 0.1)
bicubic	2.7 (± 0.2)	2.3 (± 0.2)	2.2 (± 0.2)	2.6 (± 0.2)	1.9 (± 0.2)	1.6 (± 0.1)	2.2 (± 0.1)
IDW	3.3 (± 0.3)	2.9 (± 0.3)	2.7 (± 0.3)	3.0 (± 0.3)	2.5 (± 0.2)	2.4 (± 0.2)	2.8 (± 0.1)
NN	2.8 (± 0.3)	2.2 (± 0.2)	1.8 (± 0.2)	2.9 (± 0.3)	1.5 (± 0.2)	**1.3 (± 0.1)**	**2.1 (± 0.1)**
RBF	3.0 (± 0.3)	2.3 (± 0.2)	2.2 (± 0.2)	2.8 (± 0.2)	**1.3 (± 0.1)**	**1.3 (± 0.1)**	2.2 (± 0.1)
Mean	2.9 (± 0.1)	2.5 (± 0.1)	2.2 (± 0.1)	2.8 (± 0.1)	1.8 (± 0.1)	**1.7 (± 0.1)**	
				COPy(mm)			
nearest	7.2 (± 0.8)	7.3 (± 0.9)	7.2 (± 0.7)	6.9 (± 0.7)	7.2 (± 0.6)	6.5 (± 0.6)	7.1 (± 0.3)
bilinear	7.9 (± 0.8)	7.9 (± 0.7)	6.5 (± 0.7)	5.3 (± 0.5)	5.5 (± 0.5)	**5.2 (± 0.4)**	**6.4 (± 0.3)**
bicubic	6.5 (± 0.7)	7.6 (± 0.8)	6.4 (± 0.7)	6.1 (± 0.6)	6.6 (± 0.6)	6.3 (± 0.6)	6.6 (± 0.3)
IDW	13.3 (± 1.4)	13.2 (± 1.2)	9.1 (± 0.9)	8.1 (± 0.8)	8.2 (± 0.8)	7.9 (± 0.8)	10.0 (± 0.4)
NN	7.9 (± 0.9)	8.6 (± 0.9)	6.6 (± 0.7)	6.0 (± 0.6)	5.7 (± 0.5)	5.3 (± 0.5)	6.7 (± 0.3)
RBF	6.7 (± 0.7)	7.7 (± 0.9)	6.9 (± 0.7)	6.1 (± 0.6)	5.7 (± 0.6)	6.0 (± 0.6)	6.5 (± 0.3)
Mean	8.3 (± 0.4)	8.7 (± 0.4)	7.1 (± 0.3)	6.4 (± 0.3)	6.5 (± 0.2)	**6.2 (± 0.2)**	
				COPdist (mm)			
nearest	8.1 (± 0.7)	8.5 (± 0.8)	8.1 (± 0.7)	8.2 (± 0.7)	7.8 (± 0.6)	7.2 (± 0.5)	8.0 (± 0.3)
bilinear	8.9 (± 0.7)	8.5 (± 0.7)	7.1 (± 0.6)	6.4 (± 0.5)	6.2 (± 0.5)	5.8 (± 0.4)	**7.1 (± 0.2)**
bicubic	7.6 (± 0.6)	8.3 (± 0.8)	7.3 (± 0.7)	7.2 (± 0.6)	7.2 (± 0.6)	6.8 (± 0.5)	7.4 (± 0.3)
IDW	13.9 (± 1.4)	13.7 (± 1.2)	9.8 (± 0.9)	9.1 (± 0.8)	8.9 (± 0.8)	8.6 (± 0.7)	10.7 (± 0.4)
NN	8.8 (± 0.9)	9.2 (± 0.9)	7.3 (± 0.7)	7.2 (± 0.7)	6.3 (± 0.6)	5.7 (± 0.5)	7.4 (± 0.3)
RBF	8.0 (± 0.7)	8.5 (± 0.9)	7.7 (± 0.7)	7.2 (± 0.6)	6.2 (± 0.6)	6.4 (± 0.6)	7.3 (± 0.3)
	9.2 (± 0.4)	9.5 (± 0.4)	7.9 (± 0.3)	7.6 (± 0.3)	7.1 (± 0.3)	**6.8 (± 0.2)**	
				CA (%)			
nearest	47.0 (± 1.2)	55.5 (± 1.1)	57.5 (± 0.8)	59.2 (± 0.8)	63.7 (± 0.8)	64.9 (± 0.8)	57.97(±0.93)
bilinear	89.4 (± 1.6)	103.2 (± 1.5)	98.4 (± 1.4)	**99.6 (± 1.1)**	101.5 (± 1.1)	101.2 (± 1.1)	**98.9(±1.3)**
bicubic	104.9 (± 1.7)	111.7 (± 1.7)	105.3 (± 1.3)	105.2 (± 1.2)	106.7 (± 1.3)	105.5 (± 1.2)	106.6(±1.4)

IDW	142.4 (± 4.7)	138.3 (± 4.0)	126.5 (± 2.4)	125.8 (± 2.4)	126.5 (± 2.5)	126.5 (± 2.5)	131.0(±3.2)
NN	118.6 (± 2.8)	115.3 (± 2.3)	107.0 (± 1.6)	104.2 (± 1.4)	106.4 (± 1.4)	105.9 (± 1.4)	109.6(±1.9)
RBF	119.8 (± 2.5)	115.9 (± 2.0)	110.0 (± 1.6)	106.4 (± 1.2)	108.2 (± 1.3)	106.8 (± 1.1)	111.2(±1.7)
Mean	103.7 (± 1.1)	106.6 (± 0.9)	100.8 (± 0.6)	**100.1 (± 0.6)**	102.2 (± 0.6)	101.8(±1.5)	

3.4 Discussion

This study was the first of its kind to evaluate the estimation of PPD from sparse sensor in running across different speeds and at key points in the stance phase. Error metrics for pressure (MAE, MaxAE, RMSE, and CA) along with error metrics for COP (COPx, COPy and COPdist) were calculated to assess the effect of different interpolation methods and sensor counts on estimated PPD and derivative COP measures during treadmill running. Statistical analysis found significant main effects for layouts, interpolation methods and stance phases. With respects to sensor layout, the 17-sensor layout was found to be the best performing on measures of MAE, RMSE, COPx, COPy, and COPdist, whereas the 15-sensor layout was the best performing on MaxAE. However, for all error metrics, statistical analysis revealed non-significant differences between the 15 and 17 sensor layout performances. With respects to interpolation methods for the estimation of PPD, the Gausian radial basis function (RBF) had significantly better performance on MAE, and RMSE than all other methods. The IDW interpolation method had the best performance on MaxAE however, there was no significant difference in performance between IDW and RBF. Thus, for the estimation of the complete PPD, the RBF method was found to perform better than all other methods evaluated in this investigation. On measures of COP, the bilinear interpolation method had the best performance on COPy, COPdist and CA and RBF had the best performance for COPx. However, no significant differences were found between the bilinear and RBF interpolation methods across all measures of COP. Thus, for the estimation of COP, both the RBF and the bilinear interpolation methods were shown to be superior to all other methods tested in this investigation.

Taken together, the 15-sensor layout (RBF-15) has the best overall performance on pressure estimation for MAE, MaxAE, and RMSE and was able to reconstruct the complete PPD with only 14.0 ± 0.6 kPa of overall MAE across all stance phases. Additionally, the RBF-15 had the lowest MAE at each point in the stance phase (Table *3-1*). Although RBF-15 showed better performance over sparse sensor layouts with lower sensor counts, there were minor and non-significant differences between RBF-15 and RBF-17 sensor layout on measures of MAE, RMSE, and MaxAE. These results indicate that given the reduction in total sensor count by two sensors, the RBF-15 superior combination of layout and interpolation method for the systems recreating the complete PPD in running. For the estimation of center of pressure, the bilinear-17 combination had similar or better performance than other combinations with as little as 1.3 (± 0.1) mm in COPx, and 5.2 (±0.4) mm in COPy. NN-17 has the best performance for COPdist with 5.2 (± 0.4) mm position error. However, there was no significant difference between bilinear-17 and RBF-15 on COPx, COPy and COPdist. Given these finding, for PPD estimation from sparse sensors and derivative COP estimation, the RBF-15 was found to be the optimal combination.

With respect to stance phase, significant differences were found for all error metrics. Pressure estimation metrics of MAE and RMSE found significant differences on all stance phases with the highest pressure measurement errors occurring at 50% stance (Figure *3-9*). This is due to the highest pressures typically occurring at mid stance. Other researches investigating PPD estimation methods have similarity observed an increase in PPD estimation error as pressure values increase [16,17]. In contrast, for measures of COP, the highest errors occurred near toe off at 90% of stance. Given these differences, these results are important information for the evaluation of PPD estimation methods. Future researchers should evaluate estimation method accuracy throughout the stance phase with an emphasis at mid-stance, initial-contact, and toe off where the PPD estimation and COP location determination may be the most challenging.

To our knowledge, this was the first investigation to use the RBF method for the reconstruction of the PPD from sparse sensors. This method has been used in image data reconstruction [115] but its success with pressure data in running warrants further investigation. It is also worth noting that the IDW interpolation method slightly outperformed RBF for every layout except 7 on MaxAE. This result was surprising given the success of the RBF method over all other interpolation methods on MAE and RMSE. One possible explanation for these results is that unlike the RBF method, the IDW method estimates values at new locations based on the inverse of the distance to the sparse data points, thus, closer pressure data points have a greater influence on the estimation values. For localized regions of high pressure, such as the heel, the IDW method may do a better job of estimating adjacent pressure values.

Notably, the maximum pressure absolute error (MaxAE) remained high across all layouts and interpolation methods. Observationally, many of the maximum absolute pressure errors were located between the outermost sparse sensor locations and the insole boundary especially in the toe and heel regions (Figure *3-11*). In this sensor-insole boundary region, the interpolation methods appear to struggle to estimate pressure values. This is likely because the insole boundary points (Figure *3-4*) were assigned a pressure value of zero prior to the interpolations and interpolation functions are either under or over estimating pressures to fit their function to the zero-pressure value. Differences in plantar surface anatomy may also complicate boundary sensor estimations especially in narrower sensor distribution areas like the rear-foot. The use of alternate interpolation methods or regression models may be better able to predict pressure values within the boundary region. Alternatively, different non-zero pressure values could be assigned to the insole boundary points prior to interpolation to improve accuracy. Additionally, the location of max pressure errors could be used to inform sensor placements in future designs where additional sensors are permitted.

Few researchers have investigated re-creating the entire PPD from sparse layouts. The majority of published research in the area has focused on walking data and using machine learning methods for the estimation. Mun et al. [19] used a machine learning approach (LSTM) to estimate the complete PPD from a 9-sensor layout. Although they found an 8% relative RMSE, several key differences are worth referencing. Firstly, in their investigation, the assessment of their model's accuracy was done using regression (correlation coefficients) and relative RMSE which was only calculated for whole foot regions. Thus, no information was provided on maximum estimated pressure errors relative to the reference system. Additionally, given that the activity in their research was walking, the range of pressure values that the model needed to account for were significantly smaller than in running. Research by Ostadabbas et al. [17] demonstrated that using a ten-sensor layout, the PPD estimation error was three to five times as high for conventional interpolation methods such as bilinear and natural neighbor than using their principal component analysis (PCA) derived model. These results were even greater when the sensor count reach as low as 7. Their results showed a clear improved performance improvement using a knowledge-based regression model over "blind" interpolation techniques [17]. Farnoosh at al. [16] demonstrated that their machine learning model outperformed interpolation techniques even with sensor counts as low as four reporting a RMSE of 6.7 kPa per sensing cell.

Although these results appear promising, caution should be taken when using machine learning approaches for PPD estimation. For example, Ostadabbas et al. [17] reported as much as 50% error in PPD estimation when participants walked at speeds faster than their model was train with. An additional complication of a machine learning approach is that the machine learning algorithm would need to be trained in lab, likely on a treadmill to record a sufficient number of steps over various speeds and grades. However, known pressure differences are present between treadmill and overground running [4] limiting the validity of the pressure values generated in

overground running conditions. Further, the machine learning or regression models, are often not made publicly available, requiring develops of wearable PPMS to train their own models. Finally, such machine learning models may have low generalizability unless they been trained using data from across a variety of running speeds, surfaces, and footwear.

By contrast, interpolation functions may offer an advantage over machine learning or regression methods. For example, machine learning models may transform the input pressure data, however, interpolation methods guarantee that the generated PPD passes through all the data points from the sparse pressure data, which ensures a higher degree of fidelity to the actual measurement conditions [17]. Lastly, interpolating functions exhibit a high degree of flexibility to approximate a diverse array of functions, making them potentially more versatile and adaptable method for reproducing the PPD across a variety of conditions.

This research has several limitations. Firstly, the complexity of this study design (6 layouts x 6 interpolation methods, x 5 stance phases X 4 speeds) produced a very large number of factors. To reduce complexity of the analysis, the error metrics from all speeds were considered together rather than being completed per speed. Future research evaluating PPD estimation from a single layout should evaluate the accuracy of the desired PPD estimation method across a broad range of speeds and grades. A further important limitation of this research is that the foot types in this investigation were all non-clinical and thus, the ability of the interpolation methods to perform with clinical or abnormal foot types can't be assumed. Finally, although other researchers have investigated estimation of PPD from sparse layouts, differences in how these estimated methods were evaluated have limited direct comparisons of our results to other research results. This problem is not just limited to research of PPD. In a recent (2022) systematic review of running wearables by Mason et al. [7] the lack of consistency amongst wearables reporting running gait metrics and validation error metrics was key finding of their review.

The Pedar™ sensors used in this investigation are capacitive and likely represent optimal pressure sensor performance, however, capacitive sensors have been noted for their high production cost so a viable, consumer systems would likely need to be built using an inexpensive alternative pressure sensor technology such as resistive [18]. Research-grade resistive PPMS have been shown to degrade quickly with use, and may perform sub-optimally over time, which in turn would directly affect the accuracy of the estimated PPD [57]. Thus, in addition to performing testing using resistive sensors with similar layouts, evaluation of the PPD accuracy over several days of use should also be considered.

Based on the results of this research, any future investigation examining the accuracy of PPD estimation should report MaxAE at multiple points across the stance phase. Additionally, future investigations should focus on methods to address the maximal pressure errors in the boundary pressure sensors and to properly characterize the region between the outmost sensors and the boundary points. One method to address these errors could be to experiment with the shifting of the rear-foot and toe sensor locations. Alternatively, using different interpolation methods within the sensor envelope vs. outside the sensor envelope may improve performance.

Given the reported success of machine learning based PPD estimation methods, a direct comparison between a machine learning approach and the RBF interpolation method would be warranted [17]. For example, future research might investigate using the sparse sensor layouts used in this investigation and training a machine learning model using methods such as LSTM [19] to see if such a model would outperform the RBF interpolation method. Additionally, future work should also investigate the accuracy of the RBF-15 method to determine vGRF and compare those results to the Fuchs' vGRF estimation results. Although Fuchs et al. [15] was able to re-produce vGRF with a good degree of accuracy, their method was still depended on the use of regression coefficients. If the PPD generated using the RBF-15 combination can produce similar or better

performance than the regression model used by Fuchs, it could increase the utility of the RBF-15 method. Finally, layouts and interpolation combinations such as RBF-15 that have shown good performance should be further tested on different grades, running surface conditions, and footwear types.

Given the value for real-time qualitative and quantitative feedback on plantar pressure future research should also evaluate the capacity of the RBF interpolation method to run in real-time environments.

Importantly, this investigation evaluated the effect of sensor count on PPD estimation using proscribed layouts with increasing sensor counts ranging from 7-17 however, the effect of sparse sensor placement within the insole was not investigated. Although, the location of the pressure sensors within an insole could have a large impact on the accuracy of a given estimation method [61], evaluation of the effect of sensor placement within an insole on PPD estimation is computationally demanding task given the theoretical number of possible combinations. Further, each possible combination can only be evaluated in conjunction with the use of a given estimation method. By constraining the analysis using masking areas machine learning methods such a Random Forrest Regressor, or PCA could be employed to look at the corresponding elements within the full pressure data that most predict the complete PPD.

3.5 Conclusions

The results of this research indicated that the Gaussian RBF method using a 15-sensor layout had the optimal combination for pressure estimation and performance. This research along with previous research by Fuchs et al. [15] have shown that the 15-sensor layout can sufficiently provide pressure data for the accurate estimation of vGRF, COP, and PPD in running. However, large maximal pressure differences were still found between estimated PPD and the reference

pressure data, across all interpolation methods and sensor counts. Future research should investigate improvements to PPD estimation methods for this region. Thus, it is recommended that for applications where accurate maximal pressures are important, more sensor density in the heel and toe regions are required to minimize pressure measurement errors.

Given the success of a sparse sensor layout to reproduce the PPD using interpolation methods, future research should investigate their ability to accurately calculate gait metrics as compared to research grade systems which starts with accurate detection of foot contact events. However, the detection of foot contact events may be highly dependent on the algorithm chosen.

4. Evaluation of Different Pressure-Based Foot Contact Event Detection Algorithms across Different Slopes and Speeds

4.1 Introduction

Recent advancements in running wearable technologies have enabled continuous monitoring of running mechanics in field-based settings. Accurate running wearables could provide an essential tool for evaluating injuries and providing measurements that can be utilized to improve performances [2,7,117]. The quantification of running gait with wearable technology requires accurate identification of foot contact events (FCEs), such as initial foot contact (IC) and toe-off (TO). FCEs are important landmarks in the running gait cycle that allow for the determination of temporal metrics, such as stride rate (SR), ground contact time (GCT), and swing time (ST). Further, FCEs are needed to correctly segment phases of the gait cycle and allow appropriate kinematic and kinetic comparisons between strides, limbs, and across cohorts [118,119]. The accurate detection of FCEs in wearable devices is dependent on both the properties of the sensors being used and the algorithm used to process the sensor signals [1,66,120]. However, before wearable running sensors can be used to quantify running gait, the accuracy of such technologies should be assessed relative to laboratory-grade measurement systems.

The current laboratory-based method of determining FCEs employed by gait researchers is through the use of vertical ground reaction force (vGRF), and is typically measured using in-ground force plates or force measuring treadmills [65,66,118,121–123]. The standard approach for FCE identification from measured force is to determine when the force has risen above (IC) and fallen below (TO) a specific force threshold (ex. 20 N) [66,122]. While this is a standard and simple

approach, the detection of FCEs in running from vGRF requires the use of specialized lab-based equipment. Consequentially, there is limited research on runners in their normal training or competition environments [1,118]. To address these limitations researchers have investigated different wearable sensors for their ability to accurately detect FCEs during running, including the use of accelerometers, gyroscopes, force sensing resistors (FSRs), and in-shoe plantar pressure measurement systems (PPMSs) [1,7,97,120,123]. Among these technologies, in-shoe PPMSs have the unique advantage of providing both kinematic and kinetic running gait data, including the path of the center of pressure and the distribution of forces under the foot. Additionally, PPMSs have been shown to be more accurate in the detection of FCEs when compared against inertial sensors in walking trials [97]. While good agreement has been shown in the detection of FCEs between PPMSs and those determined from lab-based vGRF in walking trials [65,97,118], few researchers have investigated the accuracy of in-shoe PPMSs in the detection of FCEs during running [7,52,123]. As running has faster loading rates and shorter contact times compared to walking, this presents a different set of constraints and challenges for the development of pressure-based running wearable technology [120]. Additionally, running presents a broad range of use-case conditions, such as surface, grade, speed, and individual differences in foot strike patterns, all of which may impact the ability of a wearable to accurately determine FCEs [124]. Moreover, the potential changing properties of a PPMS, such as drift, creep, or hysteresis, which can occur over extended duration use [52,56,57,85], could further impact a given FCE detection algorithm's functionality and accuracy. Taken together, these considerations have required researchers investigating the use of pressure-based sensors to quantify running gait to employ different algorithms in an effort to approximate the accuracy of the standard force plate or force treadmill approaches more closely. For example, early research by Hausdorff et al. [65] evaluated an algorithm for the detection of running FCEs using inexpensive FSR data which were shown to be highly accurate for IC detection

(mean 0 ms ± 3 ms,) and TO detection (mean −1 ms ± 8 ms) when compared to an in-ground force plate. However, their algorithm processed uncalibrated (voltage) sensor data which have a nonlinear response and may not function similarly on calibrated (linear) pressure sensor data. Additionally, their algorithm was only tested on level grade running and thus, may not be appropriate for use in a running wearable which could be used across a broad range of conditions. More recently, Mann et al. [1] conducted an investigation evaluating the accuracy of a custom in-shoe pressure insole system. Mann et al. [1] employed a FCE detection algorithm similar to Hausdorff et al. [65]. However, their testing was similarly only conducted on level grades at self-selected speeds (2.78–3.33 m/s). Harle et al. [120] evaluated custom built hardware and algorithms to detect FCEs from in-shoe pressure data during sprinting. Their algorithm employed a different method than Hausdorff et al. [65] and was shown to be accurate for the detection of FCEs in sprinting. However, their algorithm was not tested at recreational running paces, or on different grades, and so may not be appropriate for a running wearable device. While these present interesting and valuable approaches by researchers there are also many other event detection algorithms from other signal processing methods that may support the appropriate determination of FCEs using PPMSs. For example, Zhou and Zang [125] developed a novel signal onset detection method, that could be employed when detecting FCEs from in-shoe pressure data where signal onsets may not be as abrupt as force signals.

The evaluation of multiple FCE methods may help advance the development of pressure-based running wearables. Despite this, there are no investigations to date, that evaluate the accuracy of different algorithms used to determine FCEs during running when measured from PPMSs. Additionally, there are, to date, no investigations that have evaluated the accuracy of different pressure based FCE algorithms, across different running speeds and grades. Thus, the purpose of this study was to (a) evaluate the accuracy of different pressure based FCE detection algorithms

across different running speeds and grades to (b) evaluate which foot contact event detection algorithm has the best agreement with a gold standard method.

4.2 Materials and Methods

4.2.1 Participants and Protocol

A total of 18 (9 male, 9 female) participants were recruited aged 19–40 years (mean: 28 ± 5 years). Participant height ranged from 1.55 to 1.93 m (mean: 1.73 ± 0.10 m) and body mass ranged from 52.0 to 87.5 kg (mean: 66.6 ± 10.3 kg) [48]. All participants were free from injury at the time of testing and were familiar with treadmill running. The protocol and methodology were approved by the University of Calgary human research ethics committee and all participants provided written informed consent before participating. All participants wore their normal running footwear which spanned several brands. Prior to testing, each participant was fitted with the Pedar™ system (100 Hz, Novel®, Munich, DEU) where the sensors were placed within the participant's shoe on top of the existing insole (Figure 1). Each Pedar™ insert contains 99 pressure sensing elements. The Pedar™ system has a pressure sensing range of 15–600 kPa and has been shown to be valid under laboratory conditions at estimating vGRF [47,79], and to have excellent pressure measurement accuracy [56,85].

Figure 4-1 Novel® Pedar™ pressure insole system . (a) Complete system (b) Pedar™ insole positioned within an insole (taken from https://www.novel.de/products/pedar/ accessed on 15 January 2023).

Following a self-selected warm-up, participants ran on a force-instrumented treadmill (2400 Hz, Bertec®, Columbus, OH, USA) while vGRF and plantar pressure were simultaneously recorded. Subjects ran on level ground at 2.6 m/s (9.4 km/h; 6:24 min/km), 3.0 m/s (10.8 km/h; 5:33 min/km), 3.4 m/s (12.2 km/h; 4:54 min/km), and 3.8 m/s (13.7 km/h; 4:23 min/km), six degrees inclined at 2.6, 2.8, and 3.0 m/s, and six degrees declined at 2.6, 2.8, 3.0, and 3.4 m/s. Data were collected for 75 s. At the start of each trial, subjects were asked to perform a stationary stance on the treadmill belt followed by three consecutive two-foot jumps. The jumps were used during post hoc analysis to synchronize data from the two systems. Following the jumps, the belt speed was increased to the selected running speed for a given trial. Data were cropped for analysis from 25 s onward in the trial to ensure only steady state running was collected.

4.2.2 Post-Hoc Data Processing

All post-hoc data processing (Figure *4-2*) was performed using custom software (LabVIEW™ 2018 National Instruments™, Austin, TX, USA). To facilitate direct comparisons

between FCEs determined from the reference vGRF signal and FCEs determined from in-shoe pressure data, both the force and pressure signals were resampled to 1000 Hz [73,120]. The vGRF data were then filtered using a zero-lag, 50 Hz, fourth order, low-pass Butterworth filter. To increase the generalizability of the results of this investigation, a single pressure sum signal which comprised a sum of all 99 pressure sensors was generated [86]. The sum of pressures (P_{sum}) was selected for application on the FCE algorithms, as it constituted a simplified signal that could be easily generated from any PPMS regardless of its configuration (array or discrete) or pressure sensor count [1,65,120]. Additionally, P_{sum} was selected as a signal which is potentially less susceptible to differences in foot strike patterns, and one that closely approximated vGRF signals in profile [86,120]. Thus, for this investigation, the FCEs, as measured from the plantar pressure data, were derived from the P_{sum} signal. Next, the vGRF and the P_{sum} data were temporally aligned based on the synchronizing jumps using cross-correlation [48]. P_{sum} was then normalized [0–100] based on the maximal value within each trial [120]. Finally, the data were cropped to the 50 s period for each trial.

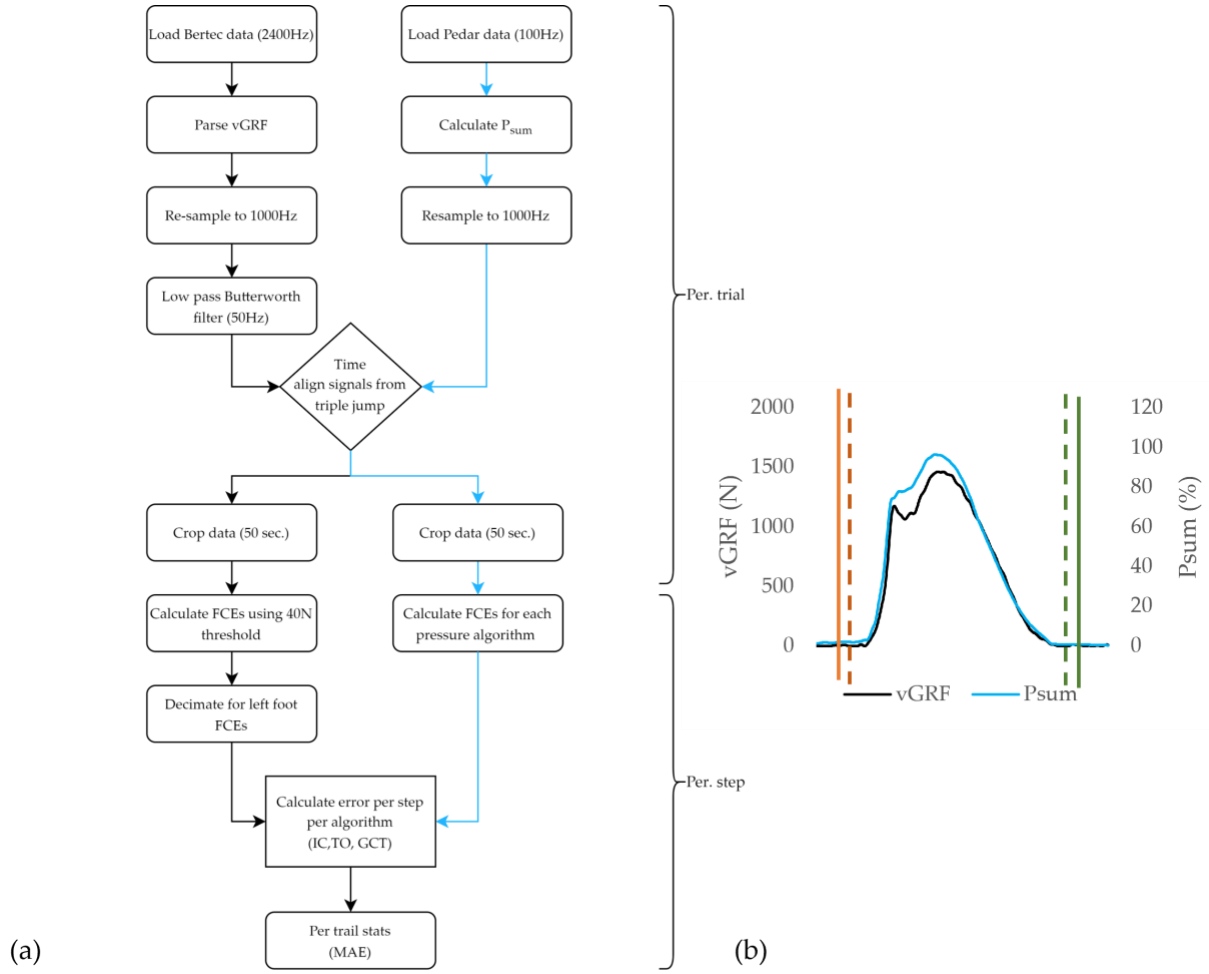

Figure 4-2 (a) Data processing (N = 18) flowchart detailing the processing of the reference vGRF data from the force instrumented treadmill (black) and Psum data from the PPMSs (blue) for each trial and for each stance within a given trial. (b) Single stance with overlayed vGRF signal (black) and P_{sum} (blue). Overlayed reference of vGRF initial foot contact events (red dashed) and reference vGRF toe off events (green dashed) FCEs, as determined using the P_{sum} signal using a given FCE algorithm (solid orange for initial foot contact and solid green for toe off).

4.2.3 Reference FCE Detection

For each trial, IC and TO event locations were derived from the vGRF signal from the force instrumented treadmill, to provide 'gold-standard' reference dataset by which the different FCE detection algorithms were evaluated (Figure *4-2*). A standard threshold crossing method [73,126] was used for FCE detection, with a 40 N threshold for all trials (Figure *4-3*). The 40 N threshold value was determined through iterative testing, to be the lowest threshold to correctly identify FCEs across all speeds, treadmill grades, and participants, where signal artifacts, such as noise due to

belt/platform vibration, and shear loading on positive and negative grades were not impacting FCE detection [73,126]. Although other researchers have employed thresholds ranging from 10–50 Ns on force instrumented treadmills for FCE detection, due to the inclines used in this protocol, and the belt vibrations, 40 N was deemed to be the lowest threshold value that could be used across all grades, speeds, and participants without needing to apply additional filtering to the vGRF signal which has been shown to impact the timing of FCE detection [66,73,90].

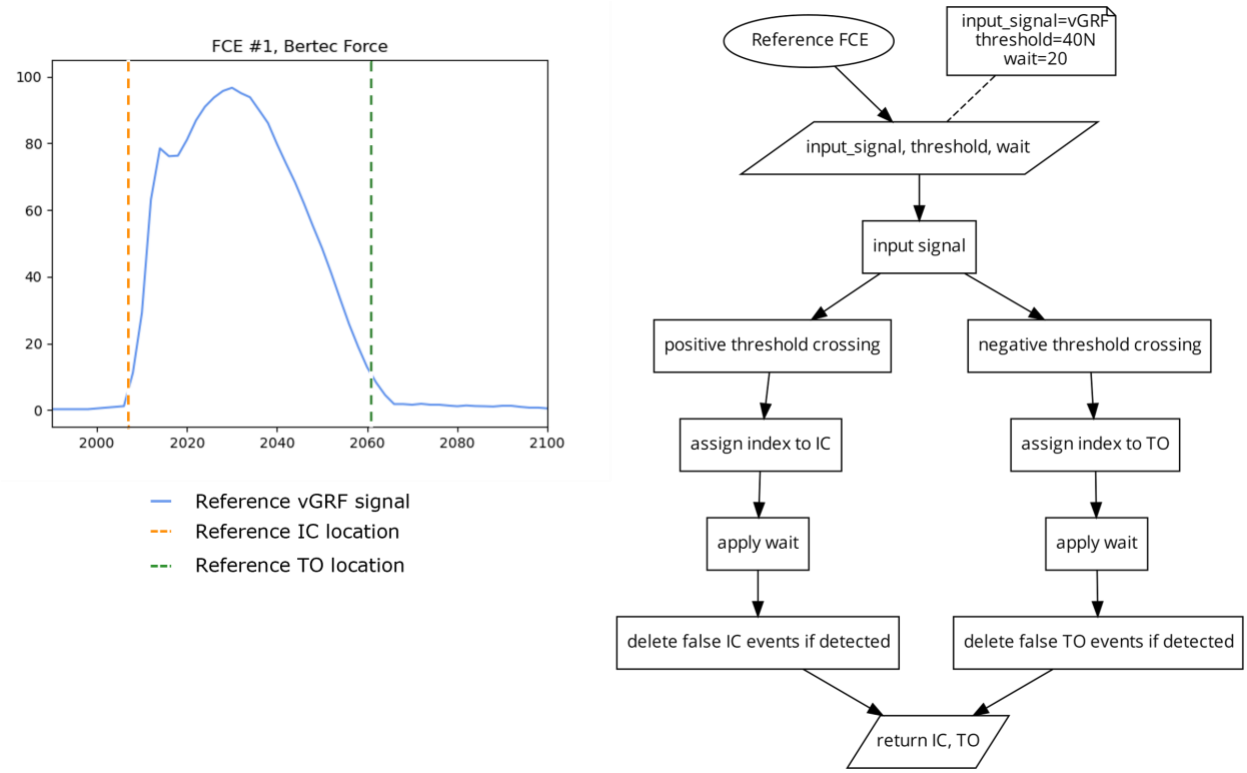

Figure 4-3 FCE-1 – reference system. Plot (left) displaying a single stride and location of the reference IC and TO events (dashed vertical), as determined by a standard threshold crossing algorithm (right) using a 40 N threshold on the vGRF signal.

4.2.4 Pressure Based FCE Detection

The following seven different algorithms were applied to the P_{sum} signal (Appendix A) for the link to a repository containing a custom Python (version 3.6) implementation of each FCE

algorithm). Wherever appropriate, the specific parameters used in each of the following algorithms were taken directly from the literature. Otherwise, parameters were iteratively modified and tested until the greatest number of FCEs were successfully detected. Additionally, for each algorithm, a 'wait' period was used, such that any FCE detected in the following 20 samples after the first detected IC or TO were removed to eliminate false positives (see Appendix A for addition details on the wait function).

FCE Algorithm 1 (FCE1) - Threshold Crossing

This algorithm (Figure *4-4*) identifies the indices where the input signal crosses a threshold in an ascending direction and checks to see if the following 20 indices remain above the threshold to find the locations of IC. This has the advantage of eliminating false positives in noisy data where the widths of peaks are typically much shorter in cycle length than the dominant signal [118]. The algorithm also identifies the indices where the signal crosses the same threshold value, in the descending direction, and then checks to see if the following 20 indices were also below the threshold to find the location of TO. For this investigation, a threshold of 10% of the maximum signal was used. This threshold was also determined using iterative testing where the 10% threshold was chosen as the lowest possible threshold for both IC and TO that generated the greatest number of correct FCE detections across all participants and conditions.

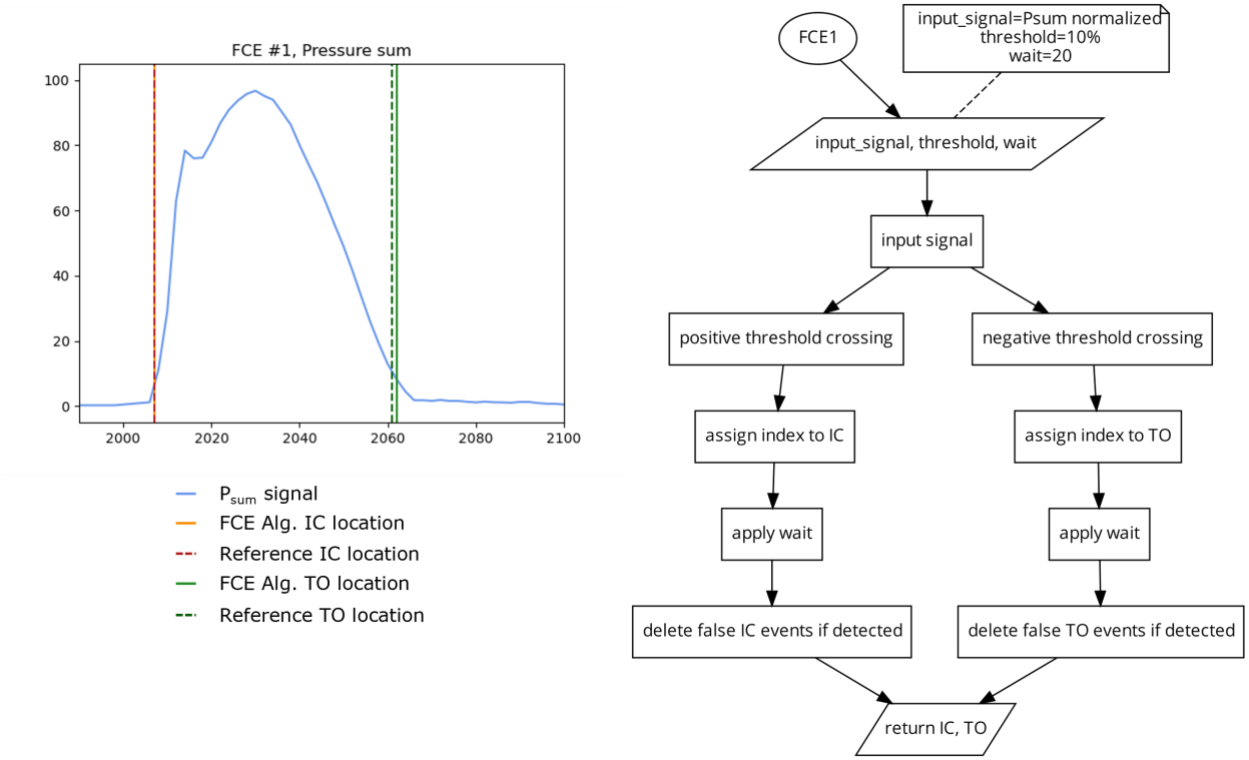

Figure 4-4 FCE-1 Plot (left) displaying a single stride and the location of the reference FCEs (dashed vertical lines) and the FCEs (solid vertical) determined by the FCE1 algorithm (right) using a 10% of the max-imum signal threshold on the Psum signal.

Algorithm 2 (FCE2) 2 Different Thresholds

This algorithm (Figure *4-5*) uses the same method as FCE1, but uses different thresholds for IC detection and TO detection. This algorithm was included in this investigation to assess if using different static thresholds for IC and TO can account for the potential differences in pressure onset and offset slopes present in some FSR and PPMS signals [120]. Due to the fast rate of signal onset in running, the detection of IC is less sensitive to the selected threshold value. However, near toe off, pressure signals can have a much slower rate of offloading and thus the chosen threshold could have a greater impact on TO detection. While lower thresholds should increase the accuracy of the algorithm, too low of a threshold could leave the algorithm susceptible to changes in signal, such as drift [68], or residual pressure present during the swing phase. For this investigation, the

IC threshold was set at 5% of the maximum signal and the TO threshold was set to 10% of the maximum signal (Figure *4-5*). The thresholds of 5 and 10% were selected in a similar manner, as described for FCE1.

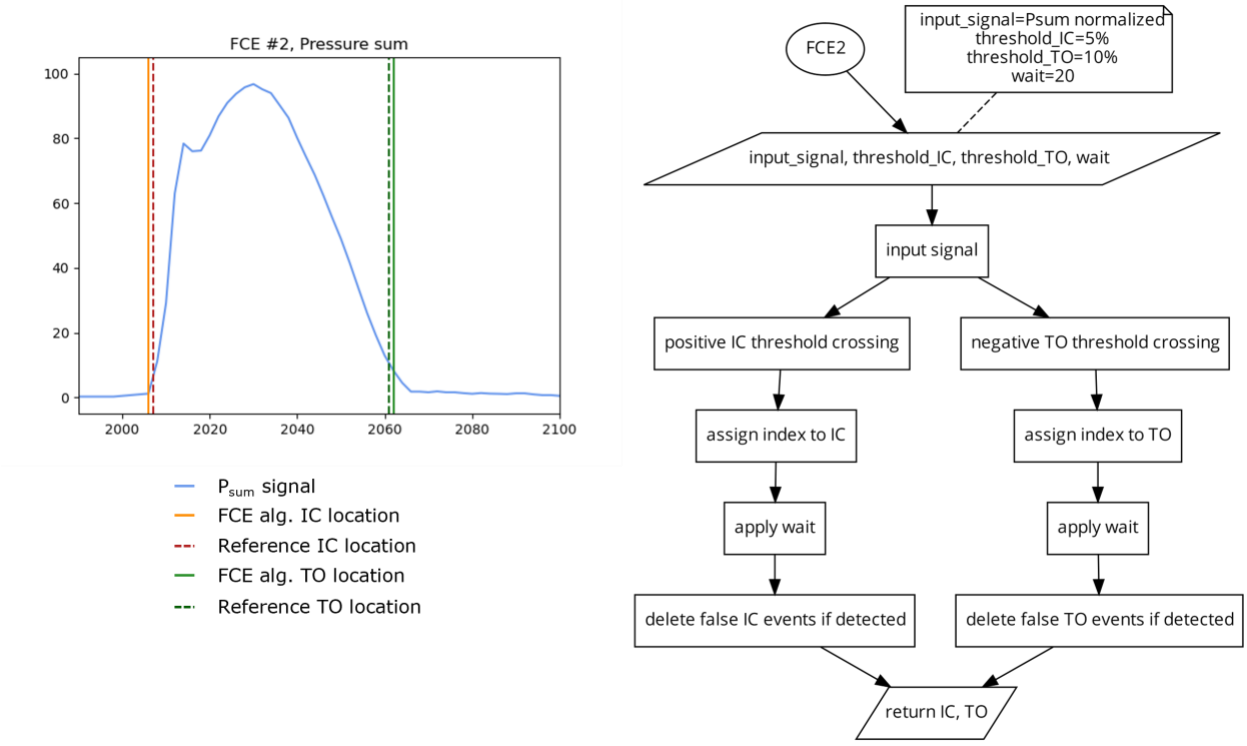

Figure 4-5 FCE-2 Plot (left) displaying a single stride and the location of the reference FCEs (dashed vertical) and the FCEs (solid vertical) determined by the FCE2 algorithm (right) using a 5% of the maximum signal threshold for IC and a 10% of the maximum signal threshold for TO.

Algorithm 3 (FCE3) 2 Peak Derivative

This algorithm (Figure 4-6 FCE-3) takes the first derivative of the P_{sum} signal [97]. The signal derivative is then filtered at 12 Hz using a zero-lag low-pass Butterworth filter. A peak detect function is applied on the signal derivative to find the locations of the signal peaks which are then assigned to the locations of IC. The peak detect function is then applied to the inverse of the signal derivative to determine the locations of the negative peaks as the locations of TO.

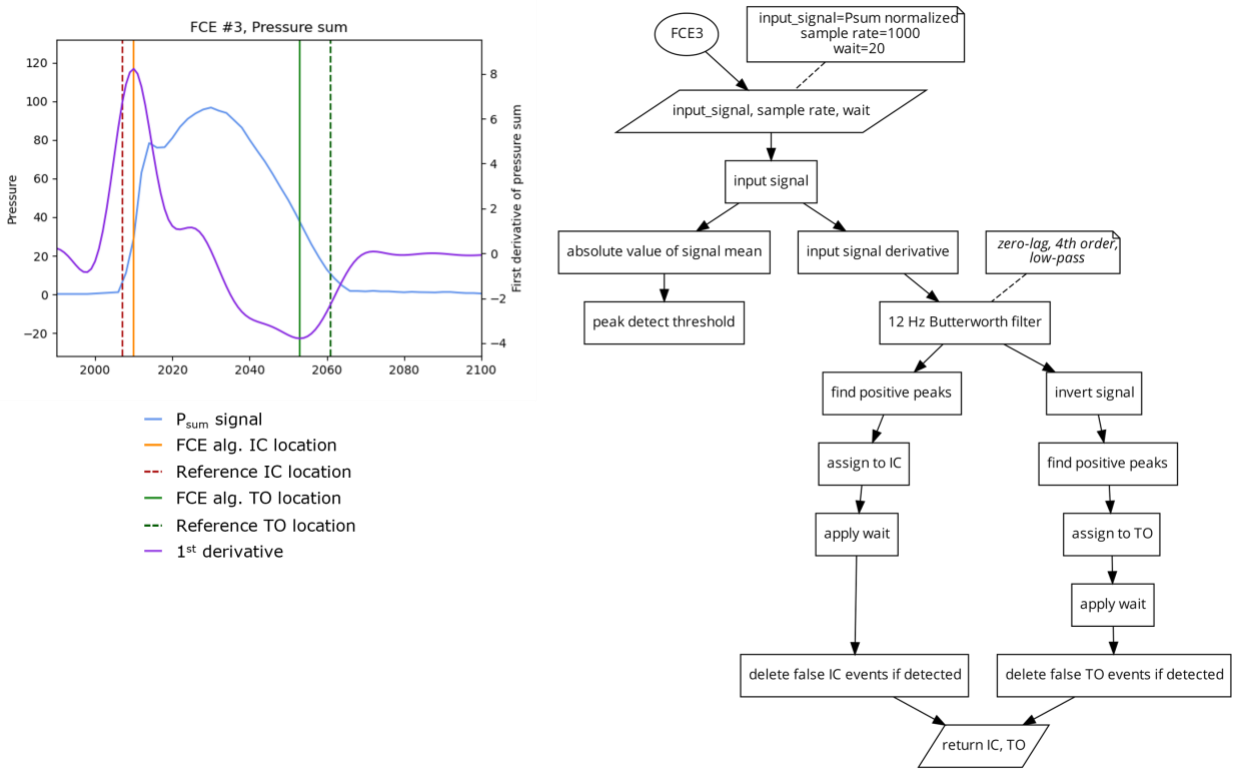

Figure 4-6 FCE-3 Plot (left) displaying a single stride and the location of the reference FCEs (dashed vertical) and the FCEs (solid vertical), as determined by the FCE3 algorithm (right).

Algorithm 4 (FCE4) 2 Slope Extension Method

To find the location of IC, this algorithm generates a linear function based on the magnitude and location of the maximal positive slope (the positive peak of the first derivative) of the signal and finds the time intercept where the pressure signal would be zero. To find the location of TO, this algorithm (Figure 4-7 FCE-4) generates a second linear function based on the magnitude and location of the maximal negative slope (the negative peak of the first derivative) and finds the time-intercept where pressure would be zero. This algorithm does not rely on static values and is responsive to different rates of signal onset and offset, which may increase the reliability of this algorithm when used in PPMS with drifting signals.

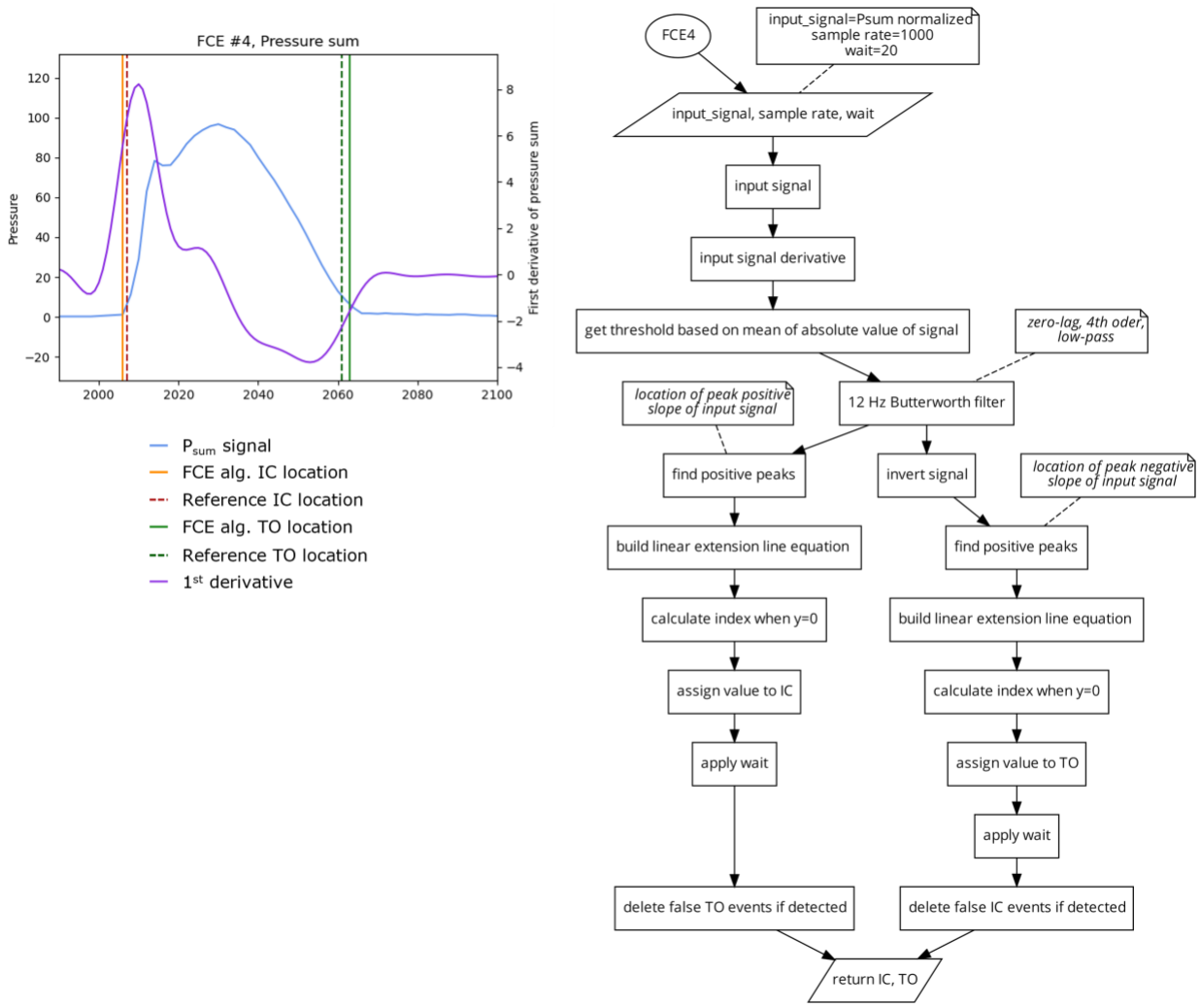

Figure 4-7 FCE-4 Plot (left) displaying a single stride and the location of the reference FCEs (dashed vertical) and the FCEs (solid vertical), as determined by the FCE4 algorithm (right).

Algorithm 5 (FCE5) 2 Low-Frequency Unity

This algorithm (Figure 4-8 FCE-5) uses a fourth order, 2 Hz, zero lag, low-pass Butterworth filter to generate a highly smoothed sinusoidal version of the P_{sum} signal. A peak detect is then used to find the locations of the peaks and valleys of the smoothed signal. The original P_{sum} signal is then broken into segments of ascending (from valley to peak) and descending (from peak to valley) based on the locations of the peaks and valleys of the 2 Hz filtered signal. A unity line (which is a linear ramp of values going from the start of each segment to the end) is generated. Then the

absolute difference between the original signal and its unity line is calculated and the location of the maximal difference is determined to be the location of IC from the ascending segments and TO for the descending segments [125]. Similar to FCE4, this algorithm also does not rely on static values, potentially increasing its reliability regardless of running technique, surface, or grade.

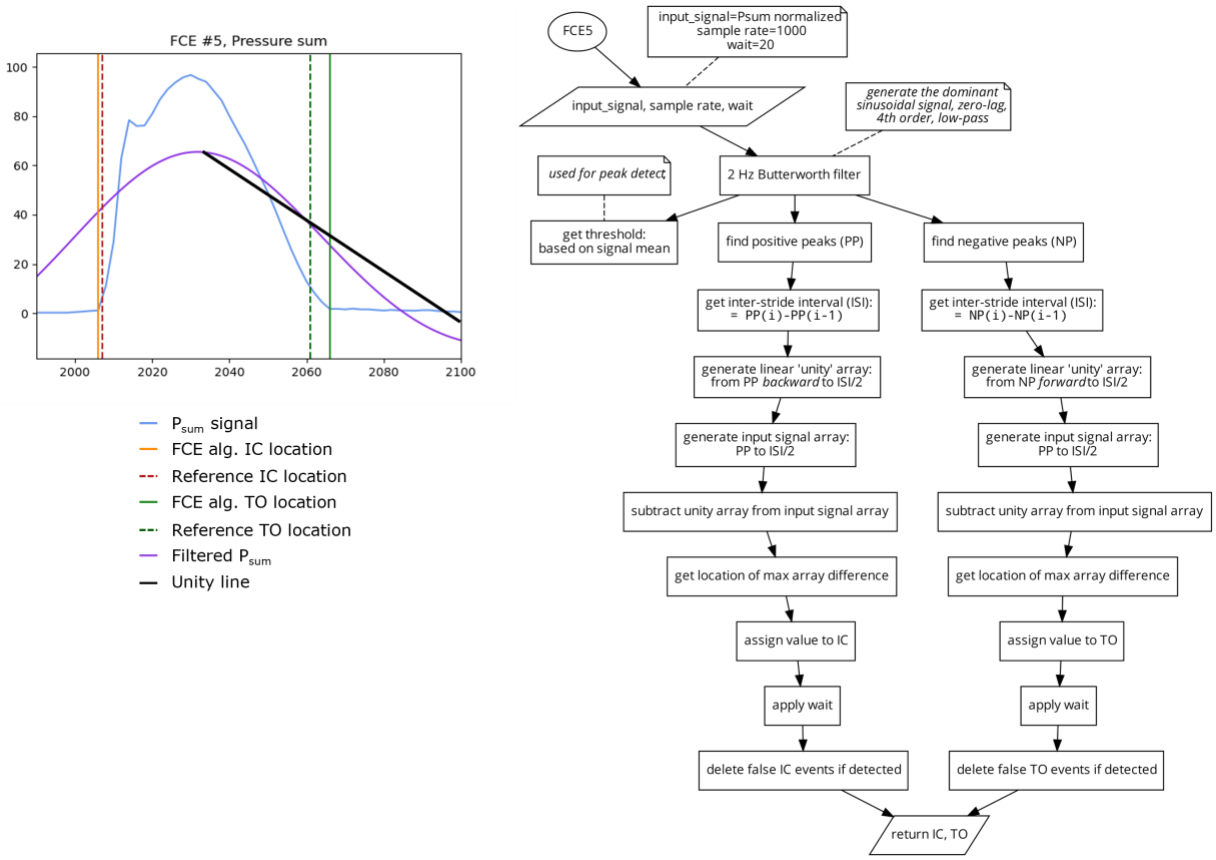

Figure 4-8 FCE-5 Plot (left) displaying a single stride and the location of the reference FCEs (dashed vertical) and the FCEs (solid vertical), as determined by the FCE5 algorithm (right).

Algorithm 6 (FCE6) 2 Harle et al.

This algorithm (Figure 4-9 FCE-6) is based on the method of foot contact event detection presented by Harle et al. [120]. A rough estimate of IC and FO events is first found using a threshold crossing (FCE1) with a threshold of 50% of P_{sum} maximum signal. This provides a late estimate of IC and an early estimate of TO locations. Following this, the first derivative of the input signal is

generated. Next, a fine estimate of IC is found using a search window from the derivative signal that is 10 samples backwards from the rough IC location. The algorithm then searches within that window for the last index with a value less than 0.3, as the fine estimate of IC. A fine estimate of TO, is similarly created using a refined search window from the inverse of the derivative signal which has 10 samples going forward from the coarse estimate TO event. The algorithm then searches this window for the first value that goes below 0.3 of the derivative signal as the fine estimate of TO.

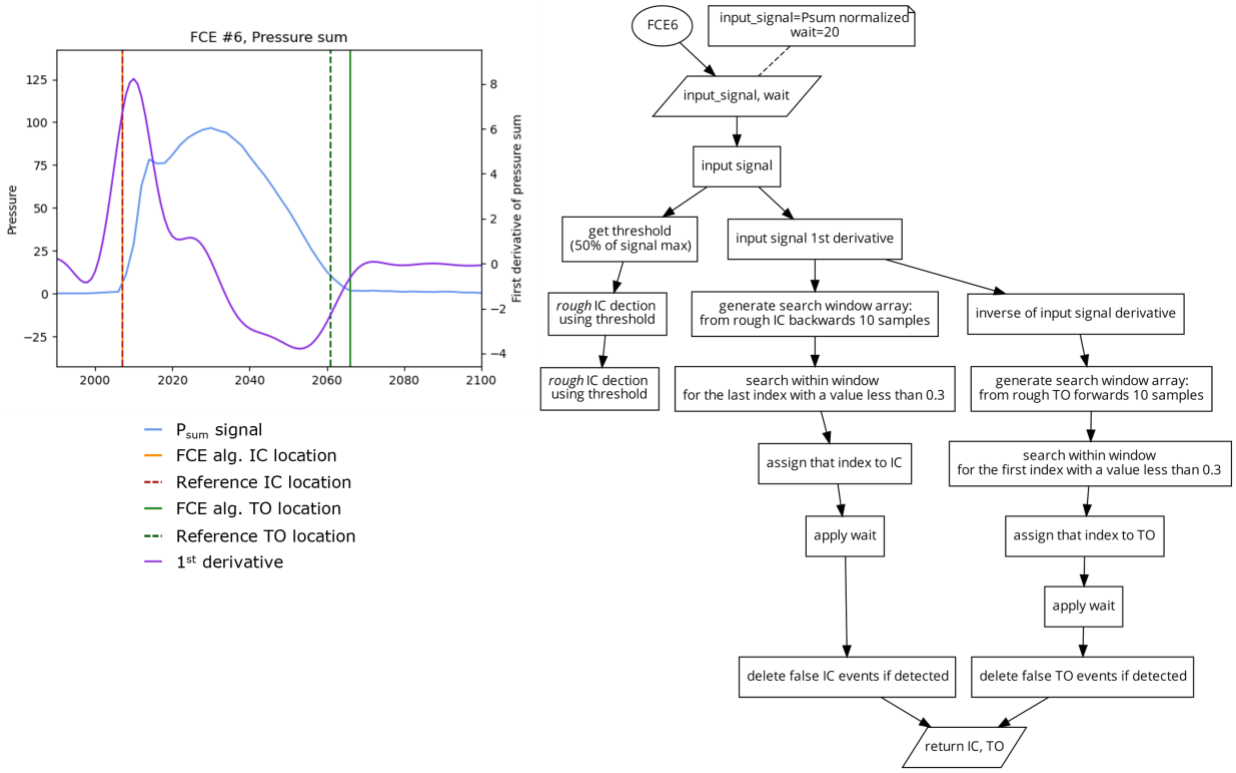

Figure 4-9 FCE-6 Plot (left) displaying a single stride and the location of the reference FCEs (dashed vertical) and the FCEs (solid vertical), as determined by the FCE6 algorithm (right).

Algorithm 7 (FCE7) 2 Mann et al. & Hausdorff et al.

This algorithm (Figure 4-7 FCE-4) is based on the method of foot contact event detection presented by Mann et al. and Hausdorff et al. [1,65]. First, a coarse estimate of IC and TO are determined using the FCE1 algorithm using a threshold based on the mean of P_{sum} signal. The first derivative of the P_{sum} signal is then filtered using a fourth order, 12 Hz, zero lag, low-pass Butterworth filter. Similar to the method presented in FCE6, a search window from the derivative signal that is 30 samples backwards from the rough IC location is generated. IC is defined as the time point within the search window when the first-grade derivative diverged from the zero line but remained below 1. Similar to IC, TO was determined using a search window from the derivative signal that is 30 samples forwards from the rough TO location. Within this search window, TO was defined as the time point when the first-grade derivative converged from a negative value of 1 towards the zero line.

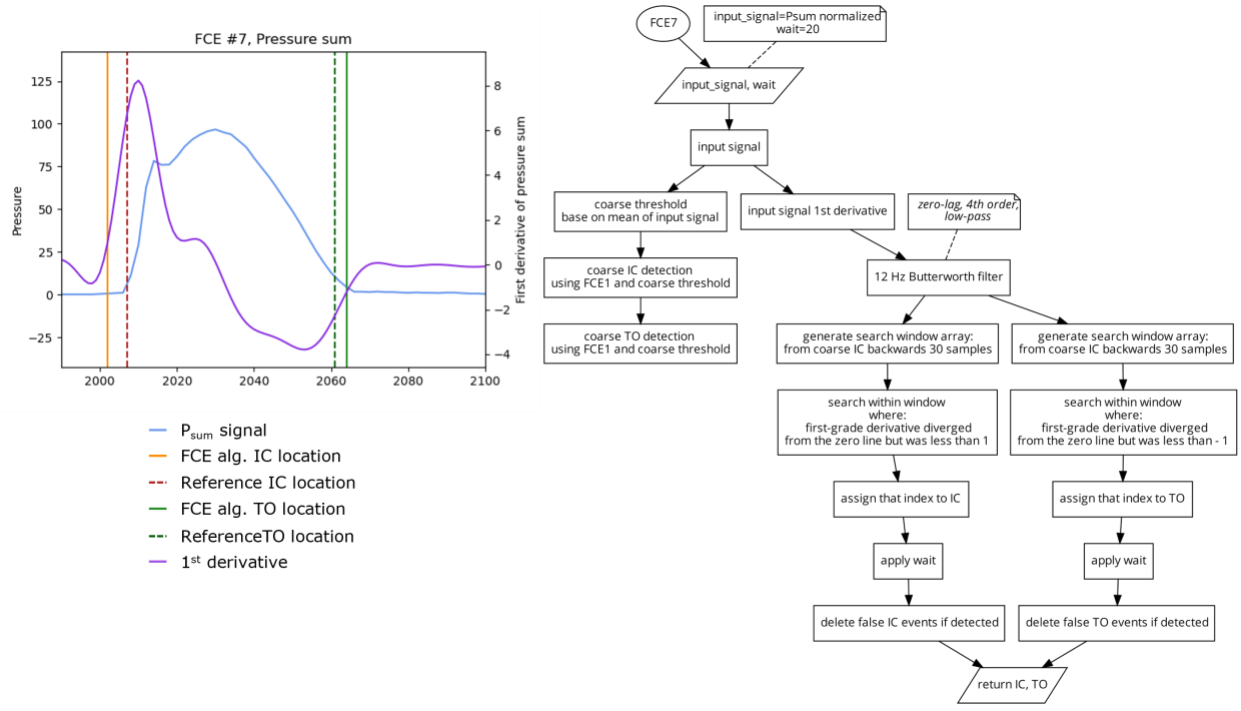

Figure 4-10 FCE-7 Plot (left) displaying a single stride and the location of the reference FCEs (dashed vertical) and the FCEs (solid vertical), as determined by the FCE7 algorithm (right).

4.2.5 Data Analyses and Statistics

Each of the 7 FCE algorithms were used to determine locations of IC and TO events for every step in every trial. Additionally, for each set of FCEs detected, the stance time (GCT) was also calculated as the time (ms) between a given IC and its successive TO event. Error values were then taken as the absolute value of the difference between the vGRF based IC, TO, and GCT values and those determined from each of the pressure based FCE detection algorithms.

For each trial, the mean absolute error (MAE) was calculated between the foot contact events, as detected by the reference vGRF signal and the FCE detected by each of the pressure based FCE algorithms. All statistical analyses were completed using JASP™ version 0.16.4. The statistical significance was accepted as $p < 0.05$.

4.2.6 Algorithms across speed (level grade)

To assess the differences between each algorithm across speeds (2.6, 3.0, 3.4, and 3.8 m/s), a 4 (speed) by 7 (algorithms) repeated measures ANOVA was performed on the MAE for IC, TO, and GCT. Tukey's HSD post-hoc tests were used in the case of significant main effects and interactions. For safety reasons, the fastest running speed (3.8 m/s) was only completed on level treadmill grades. Thus, for the algorithm by speed part of the investigation, only level grade data were used.

4.2.7 Algorithms across speed, across grades

To assess the differences between each algorithm across speeds and grades, a 2 (speed) by 3 (grades) repeated measures ANOVA was performed on the MAE for IC, TO, and GCT. Only 2 speeds were run across all 3 grades and therefore the analysis was limited to only 2.6 and 3.0 m/s. Tukey's HSD post hoc tests were used in the case of significant main effects and interactions.

4.3 Results

The IC, TO, and GCT determined using a 40 N threshold on the vGRF data were used as the reference criterion against which each pressure based FCE algorithm was assessed. Absolute differences from the reference criterion value were calculated and the mean values for each trial termed mean absolute error (MAE) measured in milliseconds. Descriptive statistics for each algorithm for IC, TO, and GCT are summarized in Table *4-1*.

Table 4-1 Error metrics for foot contact event algorithms . Mean and standard deviations of the mean absolute error (MAE) (ms) for initial-contact (IC), foot-off (FO), and ground contact time (GCT) determined for each algorithm across all speeds (2.6, 3.0, 3.4, and 3.8 m/s) on a level grade. *, †, ‡ indicates where significant differences were found.

		Initial Foot Contact (IC)	Toe Off (TO)	Stance Time (GCT)
Speeds	**Algorithms**	**Mean MAE ± SD (ms)**	**Mean MAE ± SD (ms)**	**Mean MAE ± SD (ms)**
2.6	FCE1	0.7 ± 0.3 *	1.3 ± 0.9 *	7 ± 5
	FCE2	1.3 ± 2.0	1.3 ± 0.9	12 ± 11
	FCE3	3.7 ± 0.9 †	15.9 ± 4.5 †‡	94 ± 24 *
	FCE4	1.3 ± 0.8	2.4 ± 0.9	12 ± 8
	FCE5	1.5 ± 0.5	3.7 ± 1.4	26 ± 8
	FCE6	1.4 ± 0.6	3.4 ± 1.2	24 ± 7
	FCE7	5.1 ± 0.5 ‡	2.9 ± 1.1	41 ± 7 †
3.0	FCE1	1.0 ± 1.1 *	1.7 ± 1.4 *	8 ± 5
	FCE2	1.2 ± 1.2	1.7 ± 1.4	10 ± 6
	FCE3	3.7 ± 1.4 †	12.4 ± 5.5 †	79 ± 25 *
	FCE4	1.5 ± 0.8	2.1 ± 1.6	13 ± 6
	FCE5	1.5 ± 0.8	4.1 ± 2	26 ± 10
	FCE6	1.4 ± 0.6	3.5 ± 1.4	22 ± 6
	FCE7	5.0 ± 1.2 ‡	3.7 ± 1.7	43 ± 9†
3.4	FCE1	1.0 ± 1.1 *	1.7 ± 1.4 *	8 ± 5
	FCE2	1.2 ± 1.2	1.7 ± 1.4	10 ± 6
	FCE3	3.7 ± 1.4 †	12.4 ± 5.5 †	79 ± 25 *
	FCE4	1.5 ± 0.8	2.1 ± 1.6	13 ± 6
	FCE5	1.5 ± 0.8	4.1 ± 2	26 ± 10
	FCE6	1.4 ± 0.6	3.5 ± 1.4	22 ± 6
	FCE7	5.0 ± 1.2 ‡	3.7 ± 1.7	43 ± 9 †
3.8	FCE1	1.0 ± 0.9 *	2.5 ± 3.3 *	10 ± 8
	FCE2	1.3 ± 0.8	2.5 ± 3.3	12 ± 7
	FCE3	3.1 ± 1.0 †	10.7 ± 4.6 †	66 ± 22 *
	FCE4	1.6 ± 0.8	2.3 ± 2.2	16 ± 8
	FCE5	1.6 ± 0.7	3.3 ± 2.9	23 ± 12
	FCE6	1.6 ± 1.0	3.2 ± 2.7	20 ± 11
	FCE7	5.7 ± 0.8 ‡	3.4 ± 2.3	45 ± 12 †

4.3.1 Algorithms across speeds (level grade)

For the IC MAE, there was a significant main effect for algorithm (Figure *4-11*). Post hoc revealed that FCE3 and FCE7 had a significantly greater MAE than all the other algorithms. Additionally, FCE1 had a significantly smaller MAE than all the other algorithms. For the TO

MAE, there was a significant main effect for algorithm and a speed by algorithm interaction. Post hoc tests revealed that FCE3 had a significantly greater MAE than all other algorithms and FCE1 had a significantly smaller MAE than FCE3 and FCE7. Additionally, FCE3 at 2.6 m/s had a significantly larger MAE than FCE3 at all other speeds. For the GCT MAE, there was a significant main effect for algorithm and a speed by algorithm interaction. Post hoc revealed that FCE3 was significantly different than all other algorithms and FCE3 was different across all speeds, with the lower speeds having a greater error. Furthermore, algorithm FCE7 was different than all other algorithms but not different across speeds.

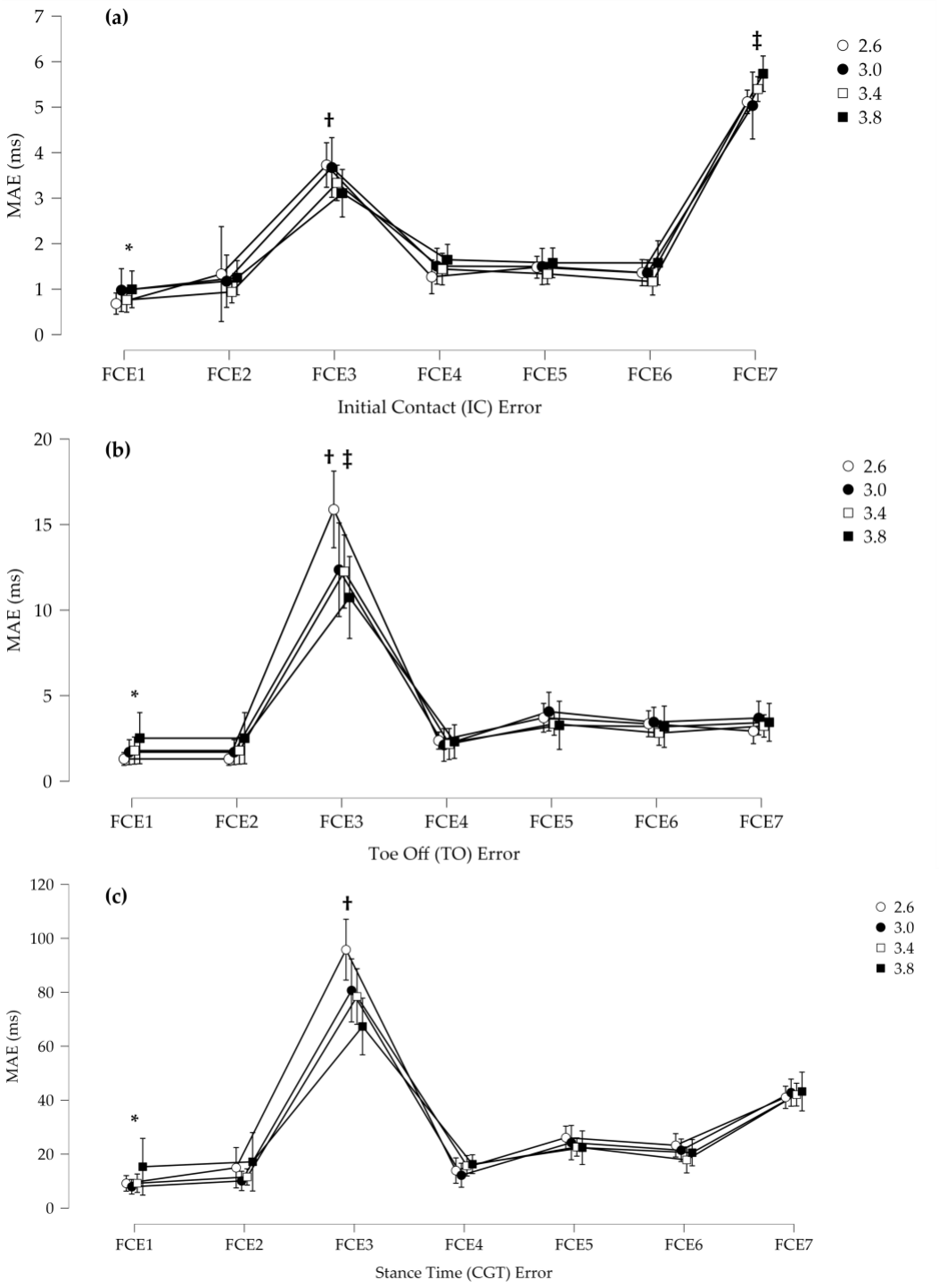

Figure 4-11 Error metric results (a) Mean absolute error (MAE) for the detection of initial foot contact (IC). * FCE1 was significantly smaller than all other algorithms, † FCE3 was significantly higher than all others except FCE7, and ‡ FCE7 was significantly higher than all other FCE algorithms. (b) MAE for the detection of toe off (TO). * FCE1 had significantly smaller than FCE3 and FCE7, † FCE3 was significantly higher than all other algorithms, and ‡ FCE3 was significantly higher at 2.6 m/s than all other speeds. (c) MAE for stance time (GCT). * FCE3 was significantly higher than all other algorithms by speed, and † FCE7 was significantly higher except for FCE3 than all other algorithms. Error bars represent standard deviations.

4.3.2 Algorithm across speed and across grades

For the IC MAE, there was a significant main effect for grade and significant speed by grade and grade by algorithm interactions (Figure *4-12*). Post hoc revealed that for grade, downhill and level are different than uphill. Post-hoc revealed that for grade by algorithm interaction for FCE3 and FCE4, downhill and level were different than uphill. For the TO MAE, there was a significant main effect for algorithm and a speed by algorithm interaction. Post hoc revealed that all other algorithms were different from FCE3 and FCE7. There were no other differences. For GCT, there was a significant main effect for algorithms and no other interactions. Post hoc revealed that algorithms FCE1, FCE2, and FCE4 were significantly lower than all other algorithms. Furthermore, algorithm FCE3 had a significantly higher MAE than all other algorithms.

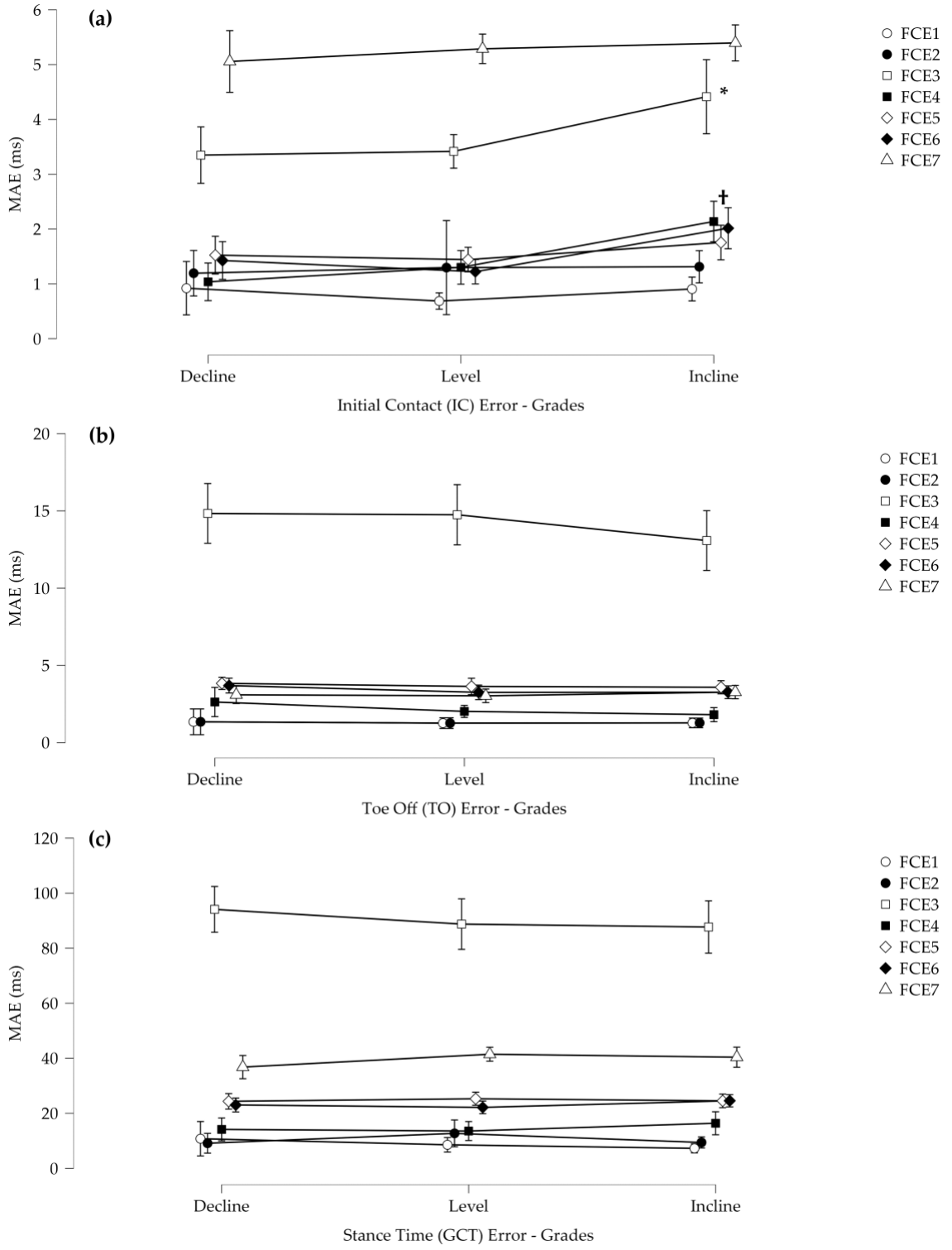

Figure 4-12 Error metric results – grade (a) Mean absolute error (MAE) for the initial foot contact events (IC) across all grades (* FCE3 was significantly higher on inclines than all other grades, and † indicates that FCE4 showed as significantly higher on inclines than at all other grades. (b) Mean absolute error (MAE) for the toe off events (TO) across all grades (c) Mean absolute error (MAE) for stance time (GCT) across all grades. Error bars represent standard deviations.

4.4 Discussion

This is the first study to compare different algorithms used to determine FCEs from PPMSs against a gold-standard instrumented treadmill during running on different grades. Overall, the results suggest that while many algorithms performed well against the standard vGRF FCE approach, and were consistent across speeds and grades, some common algorithms performed poorly against the standard and were speed and grade dependent. These results support the use of a few valid and reliable PPMS FCE algorithms that may be useful in research and smart sensor applications.

When vGRF is not available for gait research, foot switch sensors, technologically similar in principle to PPMSs, have been used as a proxy for determining FCEs [90]. Indeed, these types of pressure sensors have been the standard against which kinematic FCE algorithms are compared, across different running speeds, grades, and foot strike styles [127]. This demonstrates the importance of ensuring that the most accurate PPMS FCE algorithm can be established, not only for smart sensor applications, but also as a tool for running research. To ensure that their foot switch technology and algorithm was valid for comparison of different kinematic-based FCE algorithms, Alvim et al. [90] performed a small pilot study with two male subjects walking and running at different speeds. Alvim et al. [90] compared footswitch-derived FCEs to a force platform using the technique presented by Hausdorff et al. [65] (FCE7 in this study). During the running assessment, they found approximately ±10 ms error for IC and a ±18 ms error for FO for rearfoot strike pattern and approximately ±40 ms error for IC and TO in the midfoot strike pattern which caused them to exclude midfoot strikes from their comparison. In the present study, this same algorithm (FCE7) was one of the poorest performing algorithms and had between 25 ms MAE for IC and 20 ms MAE for TO, which together result in approximately 40 ms MAE in GCT. While the present study did

not quantify foot strike pattern, these findings are consistent with the pilot study by Alvim et al. [90] and suggest that other algorithms may be more suitable alternatives to the one developed by Hausdorff et al. as standard FCE PPMS algorithms when force plates are not available.

In the present study, when comparing each algorithm across speeds on level ground, a few algorithms were identified as poor performers against the reference. The peak derivative algorithm (FCE3) had the highest MAE for IC, TO, and GCT time. Further, FCE3 was dependent on speed with a worse performance at lower speeds. The Hausdorff and Mann algorithm (FCE7) had a higher MAE at IC than all other FCE algorithms. This resulted in FCE3 and FCE7 performing the worst on the GCT MAE. FCE3 uses the peak positive derivative to determine IC and the peak negative derivative to determine FO. Based on the nature of rising and falling signals, such as the force or pressure during walking and running, it is expected that the peak positive slope (derivate) would occur later than an onset of force or pressure and a peak negative slope (derivate) would occur before the complete removal of force or pressure. Therefore, it is not surprising that FCE3 performed as it did. Additionally, the speed dependent response for this algorithm is also expected. For example, as speeds increase and the rate of force/pressure development and removal increases, the time between the initial increase and decrease in pressure and the positive and negative peak derivatives diminishes. This could explain the improved response of the peak derivative as speed increases. It is important to mention that while FCE3 performed poorly compared to the other algorithms at determining TO and IC events, the peak derivative signal is an important basis for other FCE algorithms tested in this study (FCE 4,6,7), as it can reliably determine the peak rising and falling slope. How the peak derivative signal is used within each algorithm can therefore determine the overall algorithm accuracy, as this can result in poor (FCE 7) or good (FCE 4,6) algorithm performance.

There were a few well performing FCE algorithms in this study, as FCE 1, 2, 4, 5, and 6 all performed well with a low GCT MAE error (10 ms [FCE1] to 20 ms [FCE6]). Interestingly, two of the top performing FCE algorithms were FCE1 and FCE2, which are simple threshold-based algorithms. This result replicates the finding of Hanlon et al. [97] when comparing FSR to force during walking. These two algorithms were consistent across speeds and grades and FCE1 had the least MAE for IC. This result may be related to the fact that the PPMS sensor used in this study is a calibrated capacitive PPMS, as opposed to uncalibrated piezoresistive sensors, such as the footswitch technology. These different types of pressure sensor technologies have different characteristic responses which may require different algorithms for accurate FCE detection [56]. For example, the specific device used in this study has been shown to have high validity compared to a force instrumented treadmill for aspects, such as loading rate, which could support comparable IC detection using similar thresholding techniques [86]. Other PPMS devices may have different characteristic linearity and hysteresis in both static and dynamic conditions, which may change how different FCE algorithms perform with different PPMS sensor makes and types [56]. Additionally, another important consideration is that the algorithms in this study were applied to a pressure sum of all the plantar pressure data. As different PPMSs have different sensing areas and number of active sensors, it would be valuable to compare FCE algorithms applied to discrete or summed pressure data. Taken together, PPMS FCE comparisons may need to be reassessed and determined specifically for the intended PPMS technology.

An important consideration for determining the suitability of an FCE algorithm for smart sensor deployment in running applications is how an algorithm performs across different speeds and grades. In this investigation, it was found that there was a difference across grades for the IC MAE, such that decline and level had a lower MAE than incline for FCE3 and FCE4. As described above, FCE3 is solely based on the peak derivative. In this specific case, the peak derivative on the

ascending limb of the pressure occurred later than the rise in force. As the incline on the treadmill may modify the direction of the resultant force, this may result in a decreased vGRF and a longer delay between the force threshold and the peak derivative of pressure. This is also corroborated by the similar result for grade observed in FCE4 which relies upon both the magnitude and timing of the peak derivative slope. As the MAE is also greater in the incline for FCE4, this would suggest a decreased slope consistent with a potentially modified vGRF. Interestingly, there were no other differences across grades and speeds for TO or GCT supporting robust performance of all algorithms. It should also be notes that the treadmill speeds used in this investigation do not include the typical training and competition speeds of elite distance runners [128]. Consequently, additional algorithm testing may be necessary before the results of this investigation can be extended to this athlete population.

When evaluating the algorithms in this study it is important to consider their potential application within wearable sensor technology. An important factor related to this is the processing requirements for accurate determination of FCEs. As the simplest processing intensive algorithms, the threshold-based FCE1 and FCE2, are rather appealing, however important technical limitations in wearable sensor technology may limit their use. For example, FCE1 and FCE2 rely on static values. However, if extensive sensor creep happens throughout a trial, which is common in some PPMS systems [56,85], or over the lifetime of the sensor, then algorithms, such as FCE1 and FCE2, may likely result in unreliable values. Additionally, as PPMS signals are not immune to erroneous data or spikes that can result in false positives for IC or TO event detection, it is common that filtering may be required as a first step in processing. However, the amount of smoothing can potentially negatively impact FCE detection accuracy and may modify the thresholds chosen within specific algorithms [66]. Additionally, filtering may not be viable in embedded environments where processing power and power consumption are heavily constrained.

4.5 Conclusions

This study evaluated the accuracy of different pressure based FCE detection, when compared to a standard laboratory-based method using vGRF from a force instrumented treadmill during running. A few valid and reliable PPMS FCE algorithms, such as simple threshold crossing, have been shown to be valid across various speeds and grades. Such methods may be useful in research and in the validation of smart sensor applications. Despite their accuracy, caution should be used when employing such algorithms in other pressure based wearables due to their known sensor properties, such as drift and hysteresis [56,129], and future research should be employed to evaluate the algorithms in their intended technology application under varied conditions and constraints.

5. Summary and Conclusions

5.1 Summary

This chapter provides a summary of preceding research studies focused on the evaluation and application of wearable pressure sensing technology in running. The research completed for this dissertation covered three main topics: the validation and characterization of a protype wearable PPMS, the evaluation of sensor layout and interpolation methods for plantar pressure distribution from sparse sensors, and the assessment of algorithms for foot contact event detection across varying conditions. Insights drawn from these research projects aim to enhance our understanding and guide the development of wearable pressure sensing technology for use in field-based running gait biomechanics.

Chapter 2 presented research that evaluated a fully integrated wearable PPMS (SI), demonstrating its high level of accuracy and reliability when compared against a research-grade in-shoe PPMS (F-Scan™). Benchtop testing revealed that the SI system performed comparably, and in some cases superiorly, to the industry-standard F-Scan™ system, exhibiting less error during sinusoidal loading and less absolute error during static loading. Both systems demonstrated near-perfect between-day reliability, underscoring the consistency of these PPMS. The SI system's pressure output showed a high degree of linearity and low error when compared to the force measurements obtained from the Bertec® treadmill during treadmill running. However, the presence of hysteresis in the SI's pressure output warrants attention, as it may influence the accurate quantification of kinetic gait measures.

The study identified certain limitations to be taken into consideration when interpreting the findings. Due to durability concerns, only the SI PPMS was tested during treadmill running. Further, the testing protocol evaluated the PPMS on a limited number of pressure cycles and did

not evaluate the systems across the number of cycles typically seen in distance running sessions, which are known to impact the performance of resistive pressure sensors.

Despite certain limitations, including the SI system's use of discrete pressure-sensing elements and reduced coverage compared to the F-Scan's ™ matrix pressure array, the SI system's lightweight and unobtrusive form factor presents a significant advantage. Its fully integrated form factor can be seamlessly integrated into runners' footwear, allowing for unencumbered, natural gait, enabling accurate and valid running gait assessments. Additionally, the findings highlight the potential of resistive-based pressure measurement technology as a cost-effective alternative for wearable PPMS designs. This research demonstrated the potential of a fully integrated wearable PPMS as a reliable and valid tool for running gait assessments, paving the way for future research and developments in wearable PPMS technology.

Chapter 3 presented research evaluating the accuracy of different interpolation methods on their ability to derive the complete plantar pressure distribution (PPD) during running from a sparse sensor layout. The Gaussian radial basis function (RBF) method, with a 15-sensor layout (RBF-15), emerged as the optimal combination sensor layout and interpolation method for PPD estimation, with superior performance in terms of pressure estimation error and center of pressure measure error. The RBF-15 combination not only excelled in reconstructing the complete PPD with a minimal overall MAE but also consistently demonstrated the lowest MAE at each point in the stance phase. Despite its success, the study acknowledged challenges, particularly in accurately representing maximum pressure values. Maximal pressure absolute errors remained high across all layouts and interpolation methods, with errors predominantly located between the outermost sparse sensor locations and the insole boundary, especially in the toe and heel regions. Future research is needed to improve PPD estimation methods, particularly for boundary regions. Additionally, future research is needed to further quantify the effects of sparse sensor placement for its effect on the

determination of maximal pressures. The study's results, in conjunction with previous research by Fuchs et al., [15] affirm that a 15-sensor layout is adequate for accurate estimation of vertical ground reaction forces, center of pressure, and PPD in running.

Chapter 4 presented research evaluating different foot contact event (FCE) detection algorithms using plantar pressure-measuring insoles against a gold-standard instrumented treadmill across various running grades. This was the first investigation to evaluate different FCE detection algorithms for use in in-shoe PPMS. As the detection of FCE are the basis for the determination of many critical gait metrics, the accuracy of the method is paramount. This study aligns with previous research that has identified the critical need for accurate PPMS FCE algorithms for both smart sensor applications and running research.

Of the seven different algorithms evaluated, some algorithms demonstrated poor performance compared to the reference, especially at lower speeds. The peak derivative algorithm (FCE3) and the Hausdorff [65] and Mann [1] algorithm (FCE7) were identified as the poorest performers, with higher mean absolute error (MAE) in contact time (GCT), initial foot contact (IC), and toe off (TO) events. Algorithms FCE 1, 2, 4, 5, and 6 all showed promising results, with low MAE across various conditions. In particular, the most accurate FCE methods were the threshold-based algorithms FCE1 and FCE2. However, the performance of these algorithms could vary significantly depending on the PPMS technology they are used with, and requirements (such as real-time vs. post-hoc). The selection of a given FCE algorithm should be tailored to the specific technology used, considering the characteristics of the PPMS sensors.

The study successfully evaluated the accuracy of various pressure-based FCE detection algorithms against a standard laboratory method using vertical ground reaction force from a force instrumented treadmill during running. Certain algorithms, particularly simple threshold crossing methods, proved to be valid and reliable across different speeds and grades. However, alternate

algorithms presented in this study may perform more reliably within their intended technological application, considering the known sensor properties such as drift and hysteresis that may become present during sustained use. Before applying these algorithms to other pressure-based wearables, future research should be conducted to validate the algorithms.

5.2 Limitations

Across the three research projects reviewed, several limitations inherent to wearable pressure sensing technology have been identified. The discrete nature of the pressure-sensing elements, and their inability to cover the entirety of the foot's plantar surface, can lead to inaccuracies in capturing precise pressure distribution, especially during dynamic activities like running. Additionally, the studies point out challenges related to hysteresis, sensor drift, and the impact of environmental conditions on pressure sensor performance. The calibration and validation of these systems against gold-standard instruments remains a critical step and additional research is needed to assess the accuracy of calibrations after sustained use. The current state of technology also exhibits limitations in accurately capturing maximal pressure points, particularly at the boundaries of the sensor layout, which can be crucial for specific biomechanical analysis or measurement applications such as footwear design.

One of the pivotal challenges in the realm of wearable pressure sensing technology, especially in running, is ensuring the durability and sustained accuracy of the pressure sensors over the product's lifespan. Running, by its nature, subjects sensors to millions of loading cycles, each contributing to the gradual wear and tear of the system. The repetitive impact, flexing, and cyclic loading can lead to sensor degradation, potentially compromising the accuracy and reliability of the data collected. Over time, this wear and tear can result in sensor drift, or component level hardware failures. This is particularly problematic in long-term studies or during extended training

sessions where consistent and accurate data is paramount. Importantly, most research grade, and wearable in-shoe PPMS do not provide a warning if pressure values have deviated from normal leading to the collection of potentially error prone data.

The durability of pressure sensors is derived from their material properties and designs and the number of highly durable, yet inexpensive pressure sensing materials is extremely limited. Most pressure sensors utilized in wearable technology are either resistive or capacitive, each with their own set of challenges when it comes to long-term use. Resistive sensors, while generally more affordable, can suffer from quicker degradation due to their reliance on the deformation of their sensing elements.

Addressing these issues is crucial for the advancement of wearable pressure sensing technology in running and a significant effort from researchers and engineering is needed to develop thin, inexpensive pressure sensors that can withstand the rigors of repetitive running cycles while maintaining accuracy. Additionally, there is a need for robust calibration and validation protocols that can account for the potential changes in sensor performance over time, ensuring that the data remains reliable throughout the lifespan of the product.

5.3 Future Directions

By enabling field-based quantification of running gait, researchers can turn their attention to activities and sports that previously were inaccessible. One such application is in the rapidly growing sport of trail running. The unique demands and biomechanics of trail running, with its uneven terrain, rapid changes in elevation, and varied running surfaces, present a new opportunity to employ wearable pressure sensing technology. Future developments could focus on enhancing sensor resilience and accuracy under these challenging conditions, potentially integrating

additional sensory inputs like accelerometry to provide a more comprehensive understanding of foot-ground interactions in this and other activities.

Moving beyond the current capabilities of pressure measurement, the integration of sensors capable of measuring shear, or 3D forces would mark a significant advancement. This addition would enable a more complete analysis of running mechanics, providing valuable insights into aspects like traction, and anterior-posterior forces during running. Developing lightweight, durable, and precise sensors capable of shear or 3D force measurement will be a crucial next step in the evolution of wearable PPMS.

Harnessing the data from wearable pressure sensors to directly calculate running power could improve performance monitoring and training optimization in running-based sports. This would entail developing algorithms capable of translating pressure data into power output, considering factors like running speed, grade, and individual runner characteristics. Ensuring the accuracy and reliability of these calculations will be paramount, as will the need for user-friendly interfaces to convey this information to athletes in real-time.

The application of advanced machine learning methods holds great promise for modeling and monitoring injury-prone gait patterns, predicting the risk of injury, and guiding interventions for injury prevention [130]. Future research could focus on developing and validating machine learning models using large datasets of pressure data from diverse runner populations, across various running conditions. Incorporating additional data types, such as kinematic and kinetic data, could further refine these models. The ultimate goal would be to create real-time monitoring systems that can provide immediate feedback to runners, helping them to adjust their gait in real-time and minimize their injury risk.

5.4 Conclusions

Wearable pressure sensing technology has emerged as a pivotal tool in the biomechanical analysis of running, enabling invaluable insights into foot-ground interactions and gait patterns, across a broad range of conditions and environments. The research projects presented here, demonstrate the capability of these systems to provide accurate and reliable pressure data during running in form factors suitable for field-based applications. However, the development process is far from complete, and numerous challenges for long-term durability and accuracy imposed by dynamic activities such as running remain.

Looking ahead, research in wearable pressure sensing technology stands to make significant advances in running and other running-based sports, providing a greater understanding of biomechanics in the athletes' natural training and competition environments. Hardware and materials advancements may open the possibilities of durable sensors for shear or even 3D force measurements. Additionally, advancement in machine learning methods may play a pivotal role, offering the potential for real-time injury prevention, personalized gait analysis, and new methods in running biomechanics.

In conclusion, while wearable pressure sensing technology has already made a substantial impact on the field of sports biomechanics and running analysis, its full potential is yet to be realized. Continued innovation, rigorous validation, and commitment to accuracy and reliability will ensure that this technology continues to evolve, benefiting athletes, coaches, and researchers worldwide for many years.

6. References

1. Mann, R.; Malisoux, L.; Brunner, R.; Gette, P.; Urhausen, A.; Statham, A.; Meijer, K.; Theisen, D. Reliability and Validity of Pressure and Temporal Parameters Recorded Using a Pressure-Sensitive Insole during Running. *Gait Posture* **2014**, *39*, 455–459, doi:10.1016/j.gaitpost.2013.08.026.

2. Moore, I.S. Is There an Economical Running Technique? A Review of Modifiable Biomechanical Factors Affecting Running Economy. *Sports Med.* **2016**, *46*, 793–807, doi:10.1007/s40279-016-0474-4.

3. Mann, R.; Malisoux, L.; Urhausen, A.; Meijer, K.; Theisen, D. Plantar Pressure Measurements and Running-Related Injury: A Systematic Review of Methods and Possible Associations. *Gait Posture* **2016**, *47*, 1–9, doi:10.1016/j.gaitpost.2016.03.016.

4. García-Pérez, J.A.; Pérez-Soriano, P.; Llana, S.; Martínez-Nova, A.; Sánchez-Zuriaga, D. Effect of Overground vs Treadmill Running on Plantar Pressure: Influence of Fatigue. *Gait Posture* **2013**, *38*, 929–933, doi:10.1016/j.gaitpost.2013.04.026.

5. Van Hooren, B.; Fuller, J.T.; Buckley, J.D.; Miller, J.R.; Sewell, K.; Rao, G.; Barton, C.; Bishop, C.; Willy, R.W. Is Motorized Treadmill Running Biomechanically Comparable to Overground Running? A Systematic Review and Meta-Analysis of Cross-Over Studies. *Sports Med.* **2020**, *50*, 785–813, doi:10.1007/s40279-019-01237-z.

6. Almuteb, I.; Hua, R.; Wang, Y. Smart Insoles Review (2008-2021): Applications, Potentials, and Future. *Smart Health* **2022**, *25*, 100301, doi:10.1016/j.smhl.2022.100301.

7. Mason, R.; Pearson, L.T.; Barry, G.; Young, F.; Lennon, O.; Godfrey, A.; Stuart, S. Wearables for Running Gait Analysis: A Systematic Review. *Sports Med.* **2022**, doi:10.1007/s40279-022-01760-6.

8. Abdul Razak; Zayegh, A.; Begg, R.K.; Wahab, Y. Foot Plantar Pressure Measurement System: A Review. *Sensors* **2012**, *12*, 9884–9912, doi:10.3390/s120709884.

9. Burns, G.T.; Zendler, J.D.; Zernicke, R.F. WIRELESS INSOLES TO MEASURE GROUND REACTION FORCES: STEP-BY- STEP VALIDITY IN HOPPING, WALKING, AND RUNNING. **2017**.

10. Hasegawa, H.; Yamauchi, T.; Kraemer, W.J. Foot Strike Patterns of Runners at the 15-Km Point during an Elite-Level Half Marathon. *J. Strength Cond. Res.* **2007**, *21*, 888.

11. Clark, K.P.; Ryan, L.J.; Weyand, P.G. A General Relationship Links Gait Mechanics and Running Ground Reaction Forces. *J. Exp. Biol.* **2017**, jeb.138057, doi:10.1242/jeb.138057.

12. Harle, R.; Taherian, S.; Pias, M.; Coulouris, G.; Hopper, A.; Cameron, J.; Lasenby, J.; Kuntze, G.; Bezodis, I.; Irwin, G.; et al. Towards Real-Time Profiling of Sprints Using Wearable Pressure Sensors. *Comput. Commun.* **2012**, *35*, 650–660.

13. Kong, P.W.; De Heer, H. Wearing the F-Scan Mobile in-Shoe Pressure Measurement System Alters Gait Characteristics during Running. *Gait Posture* **2009**, *29*, 143–145, doi:10.1016/j.gaitpost.2008.05.018.

14. Larson, P.; Higgins, E.; Kaminski, J.; Decker, T.; Preble, J.; Lyons, D.; McIntyre, K.; Normile, A. Foot Strike Patterns of Recreational and Sub-Elite Runners in a Long-Distance Road Race. *J. Sports Sci.* **2011**, *29*, 1665–1673, doi:10.1080/02640414.2011.610347.

15. Fuchs, P.X.; Hsieh, C.-H.; Chen, W.-H.; Tang, Y.-S.; Fiolo, N.J.; Shiang, T.-Y. Sensor Number in Simplified Insole Layouts and the Validity of Ground Reaction Forces during Locomotion. *Sports Biomech.* **2022**, 1–14, doi:10.1080/14763141.2022.2057354.

16. Farnoosh, A.; Ostadabbas, S.; Nourani, M. Spatially-Continuous Plantar Pressure Reconstruction Using Compressive Sensing. In Proceedings of the Machine Learning for Healthcare Conference; PMLR, 2017; pp. 13–24.

17. Ostadabbas, S.; Nourani, M.; Saeed, A.; Yousefi, R.; Pompeo, M. A Knowledge-Based Modeling for Plantar Pressure Image Reconstruction. *IEEE Trans. Biomed. Eng.* **2014**, *61*, 2538–2549, doi:10.1109/TBME.2014.2322993.

18. Ciniglio, A.; Guiotto, A.; Spolaor, F.; Sawacha, Z. The Design and Simulation of a 16-Sensors Plantar Pressure Insole Layout for Different Applications: From Sports to Clinics, a Pilot Study. *Sensors* **2021**, *21*, 1450, doi:10.3390/s21041450.

19. Mun, F.; Choi, A. Deep Learning Approach to Estimate Foot Pressure Distribution in Walking with Application for a Cost-Effective Insole System. *J. NeuroEngineering Rehabil.* **2022**, *19*, 4, doi:10.1186/s12984-022-00987-8.

20. Van Hooren, B.; Willems, P.; Plasqui, G.; Meijer, K. The Accuracy of Commercially Available Instrumented Insoles (ARION) for Measuring Spatiotemporal Running Metrics. *Scand. J. Med. Sci. Sports* **2023**, *33*, 1703–1715, doi:10.1111/sms.14424.

21. Strohrmann, C.; Rossi, M.; Arnrich, B.; Troster, G. A Data-Driven Approach to Kinematic Analysis in Running Using Wearable Technology. In Proceedings of the 2012 Ninth International Conference on Wearable and Implantable Body Sensor Networks; IEEE: London, United Kingdom, May 2012; pp. 118–123.

22. van Gent, R.N.; Siem, D.; van Middelkoop, M.; van Os, A.G.; Bierma-Zeinstra, S.M.A.; Koes, B.W.; Taunton, J.E. Incidence and Determinants of Lower Extremity Running Injuries in Long Distance Runners: A Systematic Review * COMMENTARY. *Br. J. Sports Med.* **2007**, *41*, 469–480, doi:10.1136/bjsm.2006.033548.

23. Toresdahl, B.; McElheny, K.; Metzl, J.; Kinderknecht, J.; Quijano, B.; Ammerman, B.; Fontana, M.A. Factors Associated with Injuries in First-Time Marathon Runners from the New York City Marathon. *Phys. Sportsmed.* **2022**, *50*, 227–232, doi:10.1080/00913847.2021.1907257.

24. Willy, R.W. Innovations and Pitfalls in the Use of Wearable Devices in the Prevention and Rehabilitation of Running Related Injuries. *Phys. Ther. Sport* **2018**, *29*, 26–33, doi:10.1016/j.ptsp.2017.10.003.

25. Napier, C.; MacLean, C.L.; Maurer, J.; Taunton, J.E.; Hunt, M.A. Kinematic Correlates of Kinetic Outcomes Associated With Running-Related Injury. *J. Appl. Biomech.* **2019**, *35*, 123–130, doi:10.1123/jab.2018-0203.

26. Napier, C.; Cochrane, C.K.; Taunton, J.E.; Hunt, M.A. Gait Modifications to Change Lower Extremity Gait Biomechanics in Runners: A Systematic Review. *Br. J. Sports Med.* **2015**, *49*, 1382–1388, doi:10.1136/bjsports-2014-094393.

27. Elstub, L.J.; Nurse, C.A.; Grohowski, L.M.; Volgyesi, P.; Wolf, D.N.; Zelik, K.E. Tibial Bone Forces Can Be Monitored Using Shoe-Worn Wearable Sensors during Running. *J. Sports Sci.* **2022**, 1–9, doi:10.1080/02640414.2022.2107816.

28. Schmida, E.A.; Wille, C.M.; Stiffler-Joachim, M.R.; Kliethermes, S.A.; Heiderscheit, B.C. Vertical Loading Rate Is Not Associated with Running Injury, Regardless of Calculation Method. *Med. Sci. Sports Exerc.* **2022**, *54*, 1382–1388, doi:10.1249/MSS.0000000000002917.

29. Saunders, P.U.; Pyne, D.B.; Telford, R.D.; Hawley, J.A. Factors Affecting Running Economy in Trained Distance Runners: *Sports Med.* **2004**, *34*, 465–485, doi:10.2165/00007256-200434070-00005.

30. Williams, K.R.; Cavanagh, P.R. Relationship between Distance Running Mechanics, Running Economy, and Performance. *J. Appl. Physiol.* **1987**, *63*, 1236–1245, doi:10.1152/jappl.1987.63.3.1236.

31. Moore, I.S.; Jones, A.M.; Dixon, S.J. Mechanisms for Improved Running Economy in Beginner Runners. *Med. Sci. Sports Exerc.* **2012**, *44*, 1756–1763, doi:10.1249/MSS.0b013e318255a727.

32. Mann, R.; Malisoux, L.; Urhausen, A.; Statham, A.; Meijer, K.; Theisen, D. The Effect of Shoe Type and Fatigue on Strike Index and Spatiotemporal Parameters of Running. *Gait Posture* **2015**, *42*, 91–95, doi:10.1016/j.gaitpost.2015.04.013.

33. Winter, D.A. *Biomechanics and Motor Control of Human Movement*; John Wiley & Sons, 2009;

34. Hood, S.; McBain, T.; Portas, M.; Spears, I. Measurement in Sports Biomechanics. *Meas. Control* **2012**, *45*, 182–186, doi:10.1177/002029401204500604.

35. Dugan, S.A.; Bhat, K.P. Biomechanics and Analysis of Running Gait. *Phys. Med. Rehabil. Clin. N. Am.* **2005**, *16*, 603–621, doi:10.1016/j.pmr.2005.02.007.

36. Lord, M. Foot Pressure Measurement: A Review of Methodology. *J. Biomed. Eng.* **1981**, *3*, 91–99, doi:https://doi.org/10.1016/0141-5425(81)90001-7.

37. Dyer, P.S.; Bamberg, S.J.M. Instrumented Insole vs. Force Plate: A Comparison of Center of Plantar Pressure. In Proceedings of the 2011 Annual International Conference of the IEEE Engineering in Medicine and Biology Society; IEEE: Boston, MA, August 2011; pp. 6805–6809.

38. Tokita, F.; Yamakoshi, K.; Sasaki, T.; Ishii, S. Portable Instrument for Accurate Measurement of Plantar Force Distribution during Dynamic Activities. *Med. Biol. Eng. Comput.* **1995**, *33*, 618–621, doi:10.1007/BF02522524.

39. Rosenbaum, D.; Becker, H.-P. Plantar Pressure Distribution Measurements. Technical Background and Clinical Applications. *Foot Ankle Surg.* **1997**, *3*, 1–14, doi:10.1046/j.1460-9584.1997.00043.x.

40. Willems, P.A.; Gosseye, T.P. Does an Instrumented Treadmill Correctly Measure the Ground Reaction Forces? *Biol. Open* **2013**, *2*, 1421–1424, doi:10.1242/bio.20136379.

41. Wixted, A.J.; Billing, D.C.; James, D.A. Validation of Trunk Mounted Inertial Sensors for Analysing Running Biomechanics under Field Conditions, Using Synchronously Collected Foot Contact Data. *Sports Eng.* **2010**, *12*, 207–212, doi:10.1007/s12283-010-0043-2.

42. Tan, H.; Wilson, A.M.; Lowe, J. Measurement of Stride Parameters Using a Wearable GPS and Inertial Measurement Unit. *J. Biomech.* **2008**, *41*, 1398–1406, doi:10.1016/j.jbiomech.2008.02.021.

43. Lee, J.B.; Mellifont, R.B.; Burkett, B.J. The Use of a Single Inertial Sensor to Identify Stride, Step, and Stance Durations of Running Gait. *J. Sci. Med. Sport* **2010**, *13*, 270–273, doi:10.1016/j.jsams.2009.01.005.

44. Donahue, S.R.; Hahn, M.E. Estimation of Gait Events and Kinetic Waveforms with Wearable Sensors and Machine Learning When Running in an Unconstrained Environment. *Sci. Rep.* **2023**, *13*, 2339, doi:10.1038/s41598-023-29314-4.

45. Alcantara, R.S.; Edwards, W.B.; Millet, G.Y.; Grabowski, A.M. Predicting Continuous Ground Reaction Forces from Accelerometers during Uphill and Downhill Running: A Recurrent Neural Network Solution. *PeerJ* **2022**, *10*, e12752, doi:10.7717/peerj.12752.

46. Cavanagh, P.R.; Hewitt, F.G.; Perry, J.E. In-Shoe Plantar Pressure Measurement: A Review. *The Foot* **1992**, *2*, 185–194, doi:10.1016/0958-2592(92)90047-S.

47. Barnett, S.; Cunningham, J.L.; West, S. A Comparison of Vertical Force and Temporal Parameters Produced by an In-Shoe Pressure Measuring System and a Force Platform. *Clin. Biomech.* **2001**, *16*, 353–357.

48. Honert, E.C.; Hoitz, F.; Blades, S.; Nigg, S.R.; Nigg, B.M. Estimating Running Ground Reaction Forces from Plantar Pressure during Graded Running. *Sensors* **2022**, *22*, doi:10.3390/s22093338.

49. Han, T.R.; Paik, N.J.; Im, M.S. Quantification of the Path of Center of Pressure (COP) Using an F-Scan in-Shoe Transducer. *Gait Posture* **1999**, *10*, 248–254.

50. Debbi, E.M.; Wolf, A.; Goryachev, Y.; Yizhar, Z.; Luger, E.; Debi, R.; Haim, A. In-Shoe Center of Pressure: Indirect Force Plate vs. Direct Insole Measurement. *The Foot* **2012**, *22*, 269–275, doi:10.1016/j.foot.2012.07.001.

51. Chesnin, K.J.; Selby-Silverstein, L.; Besser, M.P. Comparison of an In-Shoe Pressure Measurement Device to a Force Plate: Concurrent Validity of Center of Pressure Measurements. *Gait Posture* **2000**, 6.

52. Burns, G.T.; Deneweth Zendler, J.; Zernicke, R.F. Validation of a Wireless Shoe Insole for Ground Reaction Force Measurement. *J. Sports Sci.* **2019**, *37*, 1129–1138, doi:10.1080/02640414.2018.1545515.

53. Santuz, A.; Ekizos, A.; Arampatzis, A. A Pressure Plate-Based Method for the Automatic Assessment of Foot Strike Patterns During Running. *Ann. Biomed. Eng.* **2016**, *44*, 1646–1655, doi:10.1007/s10439-015-1484-3.

54. Lake, M.J.; Apps, C.; Sterzing, T. Lower Limb Kinematics and Plantar Pressure Distribution with Different Foot Strike Patterns during Running. *Footwear Sci.* **2013**, *5*, S141–S142, doi:10.1080/19424280.2013.799608.

55. MDL-F-Scan-Datasheet.

56. Giacomozzi, C. Appropriateness of Plantar Pressure Measurement Devices: A Comparative Technical Assessment. *Gait Posture* **2010**, *32*, 141–144, doi:10.1016/j.gaitpost.2010.03.014.

57. El Kati, R.; Forrester, S.; Fleming, P. Evaluation of Pressure Insoles during Running. *Procedia Eng.* **2010**, *2*, 3053–3058, doi:10.1016/j.proeng.2010.04.110.

58. Stöggl, T.; Martiner, A. Validation of Moticon's OpenGo Sensor Insoles during Gait, Jumps, Balance and Cross-Country Skiing Specific Imitation Movements. *J. Sports Sci.* **2017**, *35*, 196–206, doi:10.1080/02640414.2016.1161205.

59. Seiberl, W.; Jensen, E.; Merker, J.; Leitel, M.; Schwirtz, A. Accuracy and Precision of Loadsol ® Insole Force-Sensors for the Quantification of Ground Reaction Force-Based Biomechanical Running Parameters. *Eur. J. Sport Sci.* **2018**, *18*, 1100–1109, doi:10.1080/17461391.2018.1477993.

60. Renner, K.; Williams, D.; Queen, R. The Reliability and Validity of the Loadsol® under Various Walking and Running Conditions. *Sensors* **2019**, *19*, 265, doi:10.3390/s19020265.

61. Pataky, T.C. Spatial Resolution and Peak-Pressure-Change Measurement Accuracy. *J. Foot Ankle Res.* **2012**, *5*, O30, doi:10.1186/1757-1146-5-S1-O30.

62. Howell, A.M.; Kobayashi, T.; Hayes, H.A.; Foreman, K.B.; Bamberg, S.J.M. Kinetic Gait Analysis Using a Low-Cost Insole. *IEEE Trans. Biomed. Eng.* **2013**, *60*, 3284–3290, doi:10.1109/TBME.2013.2250972.

63. Hu, X.; Zhao, J.; Peng, D.; Sun, Z.; Qu, X. Estimation of Foot Plantar Center of Pressure Trajectories with Low-Cost Instrumented Insoles Using an Individual-Specific Nonlinear Model. *Sensors* **2018**, *18*, 421, doi:10.3390/s18020421.

64. Ostadabbas, S.; Nourani, M.; Pompeo, M. Continuous Plantar Pressure Modeling Using Sparse Sensors. In Proceedings of the 2012 IEEE 12th International Conference on Bioinformatics & Bioengineering (BIBE); IEEE: Larnaca, Cyprus, November 2012; pp. 309–314.

65. Hausdorff, J.M.; Ladin, Z.; Wei, J.Y. Footswitch System for Measurement of the Temporal Parameters of Gait. *J. Biomech.* **1995**, *28*, 347–351, doi:10.1016/0021-9290(94)00074-E.

66. Tirosh, O.; Sparrow, W.A. Identifying Heel Contact and Toe-Off Using Forceplate Thresholds with a Range of Digital-Filter Cutoff Frequencies. *J. Appl. Biomech.* **2003**, *19*, 178–184, doi:10.1123/jab.19.2.178.

67. Khandakar, A.; Mahmud, S.; Chowdhury, M.E.H.; Reaz, M.B.I.; Kiranyaz, S.; Mahbub, Z.B.; Ali, S.H.; Bakar, A.A.A.; Ayari, M.A.; Alhatou, M.; et al. Design and Implementation of a Smart Insole System to Measure Plantar Pressure and Temperature. *Sensors* **2022**, *22*, 7599, doi:10.3390/s22197599.

68. Arndt, A. Correction for Sensor Creep in the Evaluation of Long-Term Plantar Pressure Data. *J. Biomech.* **2003**, *36*, 1813–1817, doi:10.1016/S0021-9290(03)00229-X.

69. Hreljac, A. Impact and Overuse Injuries in Runners: *Med. Sci. Sports Exerc.* **2004**, 845–849, doi:10.1249/01.MSS.0000126803.66636.DD.

70. Bredeweg, S.W.; Kluitenberg, B.; Bessem, B.; Buist, I. Differences in Kinetic Variables between Injured and Noninjured Novice Runners: A Prospective Cohort Study. *J. Sci. Med. Sport* **2013**, *16*, 205–210, doi:10.1016/j.jsams.2012.08.002.

71. Barnett, S.; Cunningham, J.L.; West, S. A Comparison of Vertical Force and Temporal Parameters Produced by an In-Shoe Pressure Measuring System and a Force Platform. *Clin. Biomech.* **2000**, 5.

72. Donath, L.; Faude, O.; Lichtenstein, E.; Nüesch, C.; Mündermann, A. Validity and Reliability of a Portable Gait Analysis System for Measuring Spatiotemporal Gait Characteristics: Comparison to an Instrumented Treadmill. *J. NeuroEngineering Rehabil.* **2016**, *13*, 6, doi:10.1186/s12984-016-0115-z.

73. Weart, A.N.; Miller, E.M.; Freisinger, G.M.; Johnson, M.R.; Goss, D.L. Agreement Between the OptoGait and Instrumented Treadmill System for the Quantification of

Spatiotemporal Treadmill Running Parameters. *Front. Sports Act. Living* **2020**, *2*, 571385, doi:10.3389/fspor.2020.571385.

74. Weizman, Y.; Tan, A.M.; Fuss, F.K. Benchmarking Study of the Forces and Centre of Pressure Derived from a Novel Smart-Insole against an Existing Pressure Measuring Insole and Force Plate. *Measurement* **2019**, *142*, 48–59, doi:10.1016/j.measurement.2019.03.023.

75. Cramer, L.A.; Wimmer, M.A.; Malloy, P.; O'Keefe, J.A.; Knowlton, C.B.; Ferrigno, C. Validity and Reliability of the Insole3 Instrumented Shoe Insole for Ground Reaction Force Measurement during Walking and Running. *Sensors* **2022**, *22*, 2203, doi:10.3390/s22062203.

76. Brindle, R.A.; Bleakley, C.M.; Taylor, J.B.; Queen, R.M.; Ford, K.R. Validity of Estimating Center of Pressure during Walking and Running with Plantar Load from a Three-Sensor Wireless Insole. *Wearable Technol.* **2022**, *3*, e8, doi:10.1017/wtc.2022.5.

77. Tahir, A.M.; Chowdhury, M.E.H.; Khandakar, A.; Al-Hamouz, S.; Abdalla, M.; Awadallah, S.; Reaz, M.B.I.; Al-Emadi, N. A Systematic Approach to the Design and Characterization of a Smart Insole for Detecting Vertical Ground Reaction Force (vGRF) in Gait Analysis. *Sensors* **2020**, *20*, 957, doi:10.3390/s20040957.

78. Brimacombe, J.M.; Wilson, D.R.; Hodgson, A.J.; Ho, K.C.T.; Anglin, C. Effect of Calibration Method on Tekscan Sensor Accuracy. *J. Biomech. Eng.* **2009**, *131*, 034503, doi:10.1115/1.3005165.

79. Hsiao, H.; Guan, J.; Weatherly, M. Accuracy and Precision of Two In-Shoe Pressure Measurement Systems. *Ergonomics* **2002**, *45*, 537–555, doi:10.1080/00140130210136963.

80. Lin, F.; Wang, A.; Zhuang, Y.; Tomita, M.R.; Xu, W. Smart Insole: A Wearable Sensor Device for Unobtrusive Gait Monitoring in Daily Life. *IEEE Trans. Ind. Inform.* **2016**, *12*, 2281–2291, doi:10.1109/TII.2016.2585643.

81. Braun, B.J.; Veith, N.T.; Hell, R.; Döbele, S.; Roland, M.; Rollmann, M.; Holstein, J.; Pohlemann, T. Validation and Reliability Testing of a New, Fully Integrated Gait Analysis Insole. *J. Foot Ankle Res.* **2015**, *8*, 54, doi:10.1186/s13047-015-0111-8.

82. Schofield, J.S.; Evans, K.R.; Hebert, J.S.; Marasco, P.D.; Carey, J.P. The Effect of Biomechanical Variables on Force Sensitive Resistor Error: Implications for Calibration and Improved Accuracy. *J. Biomech.* **2016**, *49*, 786–792, doi:10.1016/j.jbiomech.2016.01.022.

83. Urry, S. Plantar Pressure-Measurement Sensors. *Meas. Sci. Technol.* **1999**, *10*, R16–R32, doi:10.1088/0957-0233/10/1/017.

84. Price, C.; Parker, D.; Nester, C. Validity and Repeatability of Three In-Shoe Pressure Measurement Systems. *Gait Posture* **2016**, *46*, 69–74, doi:10.1016/j.gaitpost.2016.01.026.

85. Hurkmans, H.L.P.; Bussmann, J.B.J.; Benda, E.; Verhaar, J.A.N.; Stam, H.J. Accuracy and Repeatability of the Pedar Mobile System in Long-Term Vertical Force Measurements. **2006**, 8.

86. Asmussen, M.J.; Kaltenbach, C.; Hashlamoun, K.; Shen, H.; Federico, S.; Nigg, B.M. Force Measurements during Running on Different Instrumented Treadmills. *J. Biomech.* **2019**, *84*, 263–268, doi:10.1016/j.jbiomech.2018.12.025.

87. Hafer, J.F.; Lenhoff, M.W.; Song, J.; Jordan, J.M.; Hannan, M.T.; Hillstrom, H.J. Reliability of Plantar Pressure Platforms. *Gait Posture* **2013**, *38*, 544–548, doi:10.1016/j.gaitpost.2013.01.028.

88. Kluitenberg, B.; Bredeweg, S.W.; Zijlstra, S.; Zijlstra, W.; Buist, I. Comparison of Vertical Ground Reaction Forces during Overground and Treadmill Running. A Validation Study. *BMC Musculoskelet. Disord.* **2012**, *13*, 235, doi:10.1186/1471-2474-13-235.

89. Selinger, J.C.; Hicks, J.L.; Jackson, R.W.; Wall-Scheffler, C.M.; Chang, D.; Delp, S.L. Running in the Wild: Energetics Explain Ecological Running Speeds. *Curr. Biol.* **2022**, *32*, 2309-2315.e3, doi:10.1016/j.cub.2022.03.076.

90. Alvim, F.; Cerqueira, L.; Netto, A.D.; Leite, G.; Muniz, A. Comparison of Five Kinematic-Based Identification Methods of Foot Contact Events During Treadmill Walking and Running at Different Speeds. *J. Appl. Biomech.* **2015**, *31*, 383–388, doi:10.1123/jab.2014-0178.

91. Mills, P.M.; Barrett, R.S.; Morrison, S. Agreement between Footswitch and Ground Reaction Force Techniques for Identifying Gait Events: Inter-Session Repeatability and the Effect of Walking Speed. *Gait Posture* **2007**, *26*, 323–326, doi:10.1016/j.gaitpost.2006.09.077.

92. Jor, A.; Das, S.; Bappy, A.S.; Rahman, A. Foot Plantar Pressure Measurement Using Low Cost Force Sensitive Resistor (FSR): Feasibility Study. *J. Sci. Res.* **2019**, *11*, 311–319, doi:10.3329/jsr.v11i3.40581.

93. Fong, D.T.-P.; Chan, Y.-Y.; Hong, Y.; Yung, P.S.-H.; Fung, K.-Y.; Chan, K.-M. Estimating the Complete Ground Reaction Forces with Pressure Insoles in Walking. *J. Biomech.* **2008**, *41*, 2597–2601, doi:10.1016/j.jbiomech.2008.05.007.

94. Forner Cordero, A.; Koopman, H.J.F.M.; van der Helm, F.C.T. Use of Pressure Insoles to Calculate the Complete Ground Reaction Forces. *J. Biomech.* **2004**, *37*, 1427–1432, doi:10.1016/j.jbiomech.2003.12.016.

95. Koch, M.; Lunde, L.-K.; Ernst, M.; Knardahl, S.; Veiersted, K.B. Validity and Reliability of Pressure-Measurement Insoles for Vertical Ground Reaction Force Assessment in Field Situations. *Appl. Ergon.* **2016**, *53*, 44–51, doi:10.1016/j.apergo.2015.08.011.

96. Morin, P.; Muller, A.; Pontonnier, C.; Dumont, G. Evaluation of the Foot Center of Pressure Estimation from Pressure Insoles during Sidestep Cuts, Runs and Walks. *Sensors* **2022**, *22*, 5628, doi:10.3390/s22155628.

97. Hanlon, M.; Anderson, R. Real-Time Gait Event Detection Using Wearable Sensors. *Gait Posture* **2009**, *30*, 523–527, doi:10.1016/j.gaitpost.2009.07.128.

98. Blades, S.; Marriott, H.; Hundza, S.; Honert, E.C.; Stellingwerff, T.; Klimstra, M. Evaluation of Different Pressure-Based Foot Contact Event Detection Algorithms across Different Slopes and Speeds. *Sensors* **2023**.

99. Aqueveque, P.; Germany, E.; Osorio, R.; Pastene, F. Gait Segmentation Method Using a Plantar Pressure Measurement System with Custom-Made Capacitive Sensors. *Sensors* **2020**, *20*, 656, doi:10.3390/s20030656.

100. Arampatzis, A.; Knicker, A.; Metzler, V.; Bru, G.-P. Mechanical Power in Running: A Comparison of Di!Erent Approaches. *J. Biomech.* **2000**, 7.

101. Martins, N.R.A.; Annaheim, S.; Spengler, C.M.; Rossi, R.M. Fatigue Monitoring Through Wearables: A State-of-the-Art Review. *Front. Physiol.* **2021**, *12*, 25.

102. Burnie, L.; Chockalingam, N.; Holder, A.; Claypole, T.; Kilduff, L.; Bezodis, N. Commercially Available Pressure Sensors for Sport and Health Applications: A Comparative Review. *The Foot* **2023**, *56*, 102046, doi:10.1016/j.foot.2023.102046.

103. Pataky, T.C. Spatially Continuous Analysis of In-Shoe Plantar Pressure Data. *Footwear Sci.* **2011**, *3*, S127–S128, doi:10.1080/19424280.2011.575803.

104. Wang, E.-T.; Hsieh, C.-H.; Yang, W.-W.; Shih, Y.; Chan, M.-S.; Shiang, T.-Y. Estimating Center of Pressure from Limited Number of Pressure Sensors for Gait Tasks. *Footwear Sci.* **2019**, *11*, S118–S120, doi:10.1080/19424280.2019.1606110.

105. Tan, A.M.; Fuss, F.K.; Weizman, Y.; Azari, M.F. Centre of Pressure Detection and Analysis with a High-Resolution and Low-Cost Smart Insole. *Procedia Eng.* **2015**, *112*, 146–151, doi:10.1016/j.proeng.2015.07.190.

106. Wang, D.; Cai, P.; Mao, Z. The Configuration of Plantar Pressure Sensing Cells for Wearable Measurement of COP Coordinates. *Biomed. Eng. OnLine* **2016**, *15*, 116, doi:10.1186/s12938-016-0237-3.

107. Keijsers, N.L.W.; Stolwijk, N.M.; Pataky, T.C. Linear Dependence of Peak, Mean, and Pressure–Time Integral Values in Plantar Pressure Images. *Gait Posture* **2010**, *31*, 140–142, doi:10.1016/j.gaitpost.2009.08.248.

108. Lord, M. Spatial Resolution in Plantar Pressure Measurement. *Med. Eng. Phys.* **1997**, *19*, 140–144, doi:10.1016/S1350-4533(96)00057-4.

109. Claverie, L.; Ille, A.; Moretto, P. Discrete Sensors Distribution for Accurate Plantar Pressure Analyses. *Med. Eng. Phys.* **2016**, *38*, 1489–1494, doi:10.1016/j.medengphy.2016.09.021.

110. Carter, J.; Chen, X.; Cazzola, D.; Trewartha, G.; Preatoni, E. ESTIMATION OF GROUND REACTION FORCE DURING RUNNING USING CONSUMER-LEVEL WEARABLE INSOLES AND MACHINE LEARNING. **2023**.

111. Jurca, A.; Žabkar, J.; Džeroski, S. Analysis of 1.2 Million Foot Scans from North America, Europe and Asia. *Sci. Rep.* **2019**, *9*, 19155, doi:10.1038/s41598-019-55432-z.

112. Pataky, T.C.; Maiwald, C. Spatiotemporal Volumetric Analysis of Dynamic Plantar Pressure Data. *Med. Sci. Sports Exerc.* **2011**, *43*, 1582–1589, doi:10.1249/MSS.0b013e3182112f40.

113. Strohmeier, P.; Håkansson, V.; Honnet, C.; Ashbrook, D.; Hornbæk, K. Optimizing Pressure Matrices: Interdigitation and Interpolation Methods for Continuous Position Input. In Proceedings of the Proceedings of the Thirteenth International Conference on Tangible, Embedded, and Embodied Interaction; ACM: Tempe Arizona USA, March 17 2019; pp. 117–126.

114. Chen, B.-H.; Chang, C.-H.; Huang, S.-C. Denoising Using Inverse-Distance Weighting with Sparse Approximation. In Proceedings of the 2016 IEEE International Symposium on Multimedia (ISM); IEEE: San Jose, CA, USA, December 2016; pp. 439–444.

115. Yeon Ju Lee; Jungho Yoon Nonlinear Image Upsampling Method Based on Radial Basis Function Interpolation. *IEEE Trans. Image Process.* **2010**, *19*, 2682–2692, doi:10.1109/TIP.2010.2050108.

116. JASP Team JASP (Version 0.18.0)[Computer Software] 2023.

117. Mann, R.; Malisoux, L.; Nührenbörger, C.; Urhausen, A.; Meijer, K.; Theisen, D. Association of Previous Injury and Speed with Running Style and Stride-to-stride Fluctuations. *Scand. J. Med. Sci. Sports* **2015**, *25*, doi:10.1111/sms.12397.

118. Mills, P.M.; Barrett, R.S.; Morrison, S. Agreement between Footswitch and Ground Reaction Force Techniques for Identifying Gait Events: Inter-Session Repeatability and the Effect of Walking Speed. *Gait Posture* **2007**, *26*, 323–326, doi:10.1016/j.gaitpost.2006.09.077.

119. Zifchock, R.A.; Davis, I.; Higginson, J.; McCaw, S.; Royer, T. Side-to-Side Differences in Overuse Running Injury Susceptibility: A Retrospective Study. *Hum. Mov. Sci.* **2008**, *27*, 888–902, doi:10.1016/j.humov.2008.03.007.

120. Harle, R.; Taherian, S.; Pias, M.; Coulouris, G.; Hopper, A.; Cameron, J.; Lasenby, J.; Kuntze, G.; Bezodis, I.; Irwin, G.; et al. Towards Real-Time Profiling of Sprints Using Wearable Pressure Sensors. *Comput. Commun.* **2012**, *35*, 650–660, doi:10.1016/j.comcom.2011.03.019.

121. Leitch, J.; Stebbins, J.; Paolini, G.; Zavatsky, A.B. Identifying Gait Events without a Force Plate during Running: A Comparison of Methods. *Gait Posture* **2011**, *33*, 130–132, doi:10.1016/j.gaitpost.2010.06.009.

122. Fellin, R.E.; Rose, W.C.; Royer, T.D.; Davis, I.S. Comparison of Methods for Kinematic Identification of Footstrike and Toe-off during Overground and Treadmill Running. *J. Sci. Med. Sport Sports Med. Aust.* **2010**, *13*, 646–650, doi:10.1016/j.jsams.2010.03.006.

123. Hong, Y.; Wang, L.; Li, J.X.; Zhou, J.H. Comparison of Plantar Loads during Treadmill and Overground Running. *J. Sci. Med. Sport* **2012**, *15*, 554–560, doi:10.1016/j.jsams.2012.01.004.

124. Gottschall, J.S.; Kram, R. Ground Reaction Forces during Downhill and Uphill Running. *J. Biomech.* **2005**, *38*, 445–452.

125. Zhou, P.; Zhang, X. A Novel Technique for Muscle Onset Detection Using Surface EMG Signals without Removal of ECG Artifacts. *Physiol. Meas.* **2014**, *35*, 45–54, doi:10.1088/0967-3334/35/1/45.

126. Hendershot, B.D.; Mahon, C.E.; Pruziner, A.L. A Comparison of Kinematic-Based Gait Event Detection Methods in a Self-Paced Treadmill Application. *J. Biomech.* **2016**, *49*, 4146–4149, doi:10.1016/j.jbiomech.2016.10.046.

127. Milner, C.E.; Paquette, M.R. A Kinematic Method to Detect Foot Contact during Running for All Foot Strike Patterns. *J. Biomech.* **2015**, *48*, 3502–3505, doi:10.1016/j.jbiomech.2015.07.036.

128. Jones, A.M.; Kirby, B.S.; Clark, I.E.; Rice, H.M.; Fulkerson, E.; Wylie, L.J.; Wilkerson, D.P.; Vanhatalo, A.; Wilkins, B.W. Physiological Demands of Running at 2-Hour Marathon Race Pace. *J. Appl. Physiol.* **2021**, *130*, 369–379, doi:10.1152/japplphysiol.00647.2020.

129. Hurkmans, H.L.P.; Bussmann, J.B.J.; Selles, R.W.; Horemans, H.L.D.; Benda, E.; Stam, H.J.; Verhaar, J.A.N. Validity of the Pedar Mobile System for Vertical Force Measurement during a Seven-Hour Period. *J. Biomech.* **2006**, *39*, 110–118, doi:10.1016/j.jbiomech.2004.10.028.

130. Mundt, M. Bridging the Lab-to-Field Gap Using Machine Learning: A Narrative Review. *Sports Biomech.* **2023**, 1–20, doi:10.1080/14763141.2023.2200749.

7. Appendices

7.1 Appendix A

Link to foot contact event detection algorithms used in chapter 4.

https://github.com/samuelblades/In-shoe-pressure-foot-contact-event-detection/tree/main

7.2 Appendix B

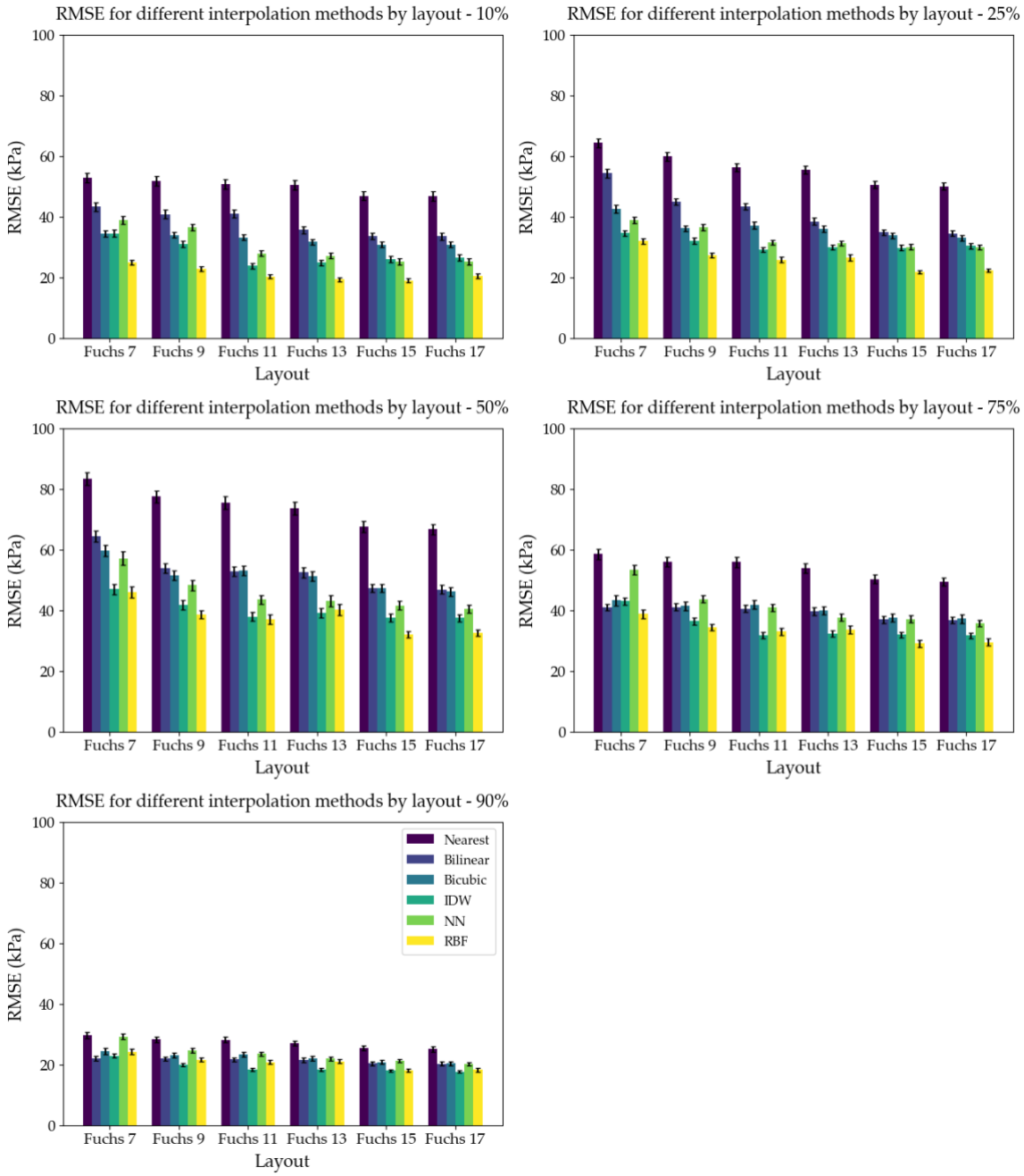

Figure 7-1 Root mean squared error (RMSE) across different layouts and interpolation methods at each of the points in the stance phase.

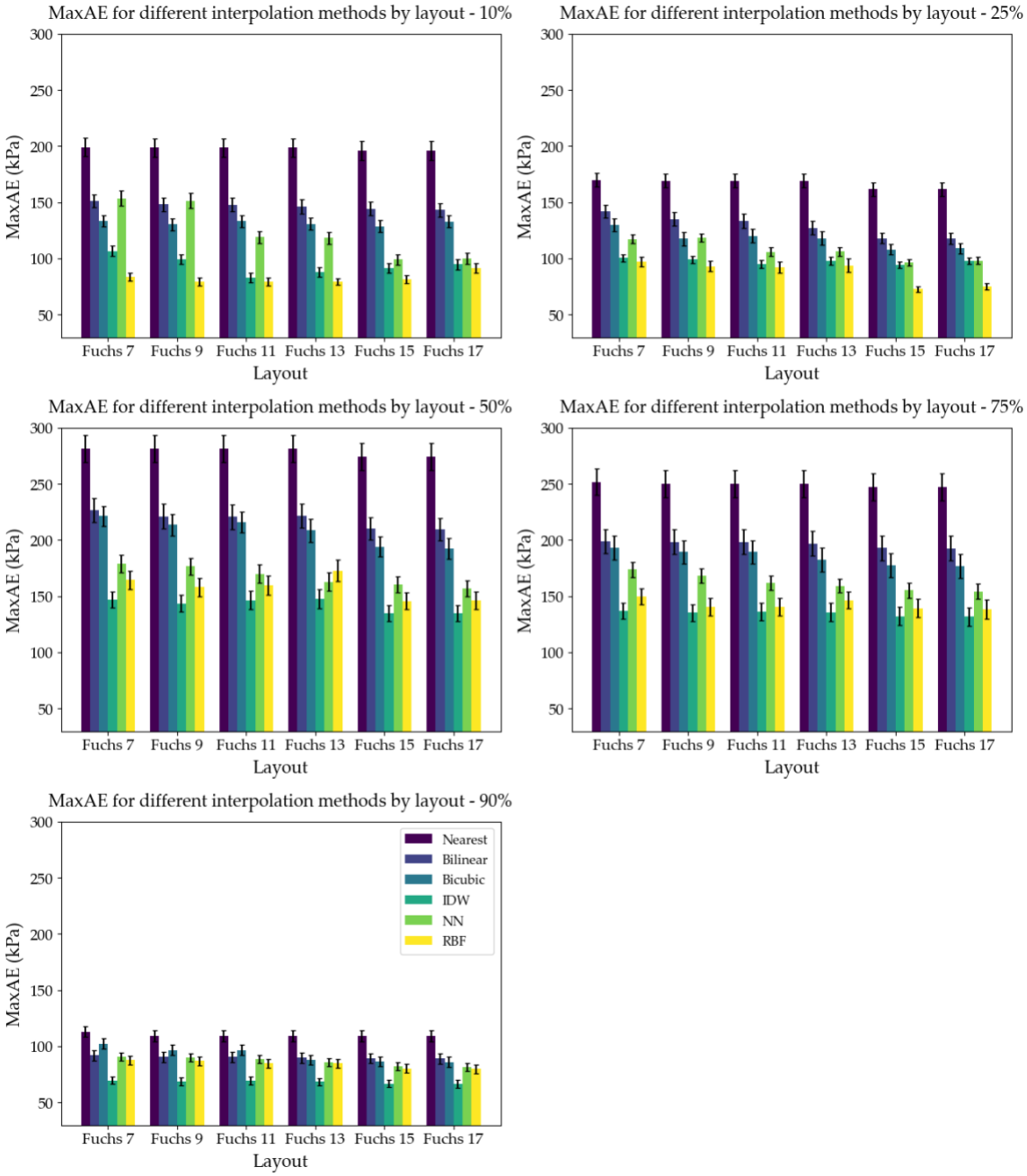

Figure 7-2 Max absolute error (MaxAE) across different layouts and interpolation methods at each of the points in the stance phase.

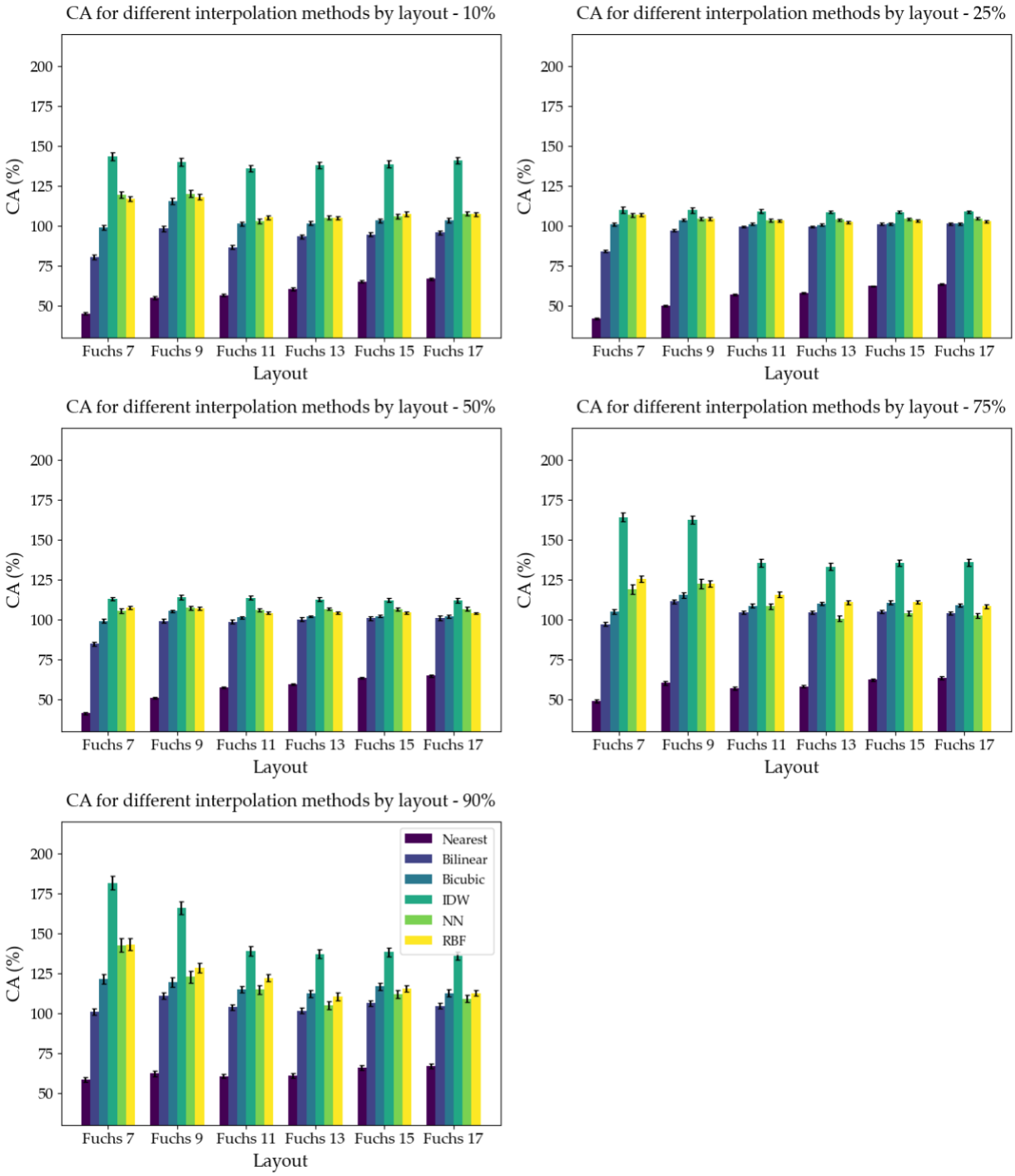

Figure 7-3 Percent difference in contact area (CA) across different layouts and interpolation methods at each of the points in the stance phase.

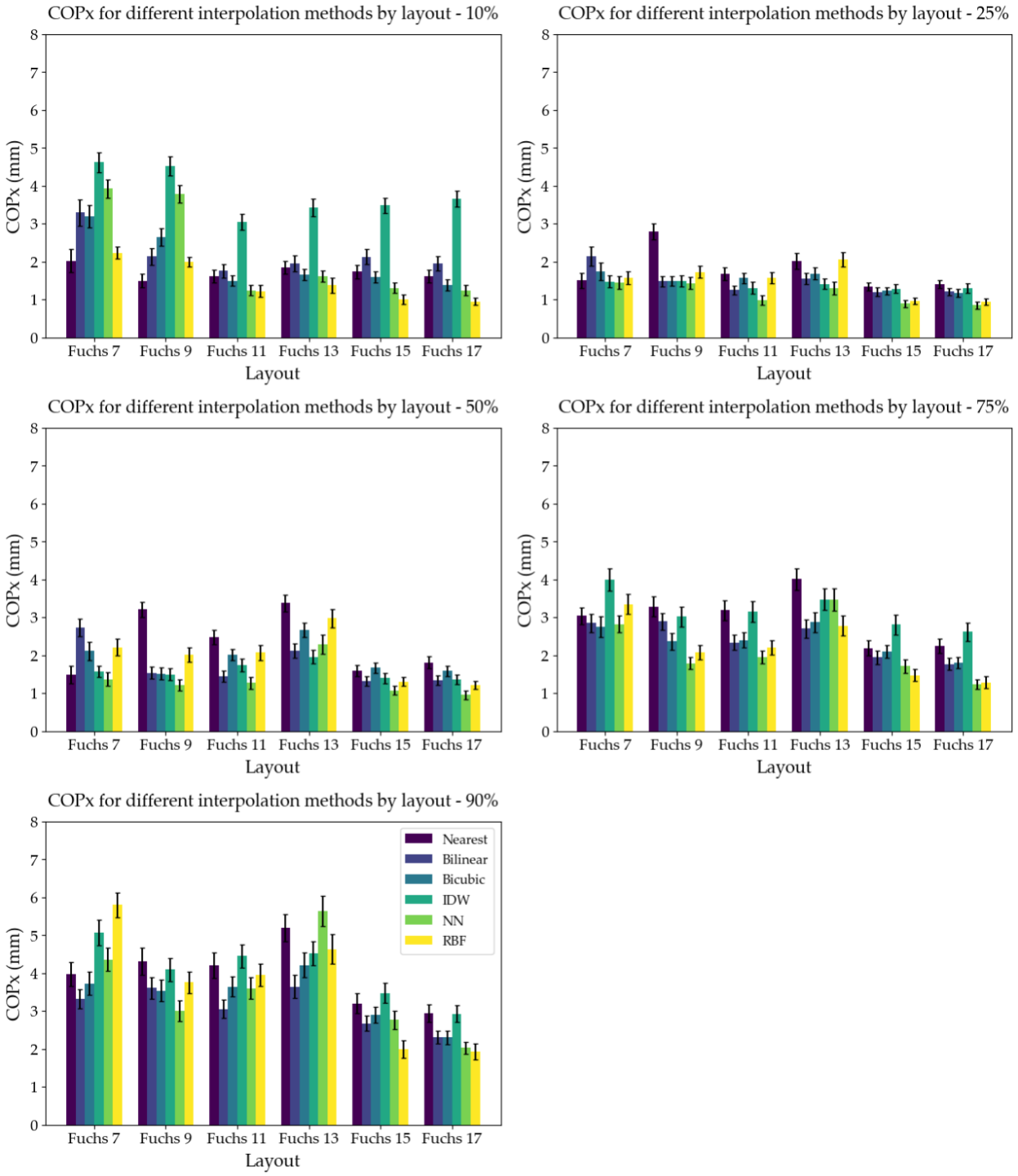

Figure 7-4 Error in medial-lateral center of pressure (COPx) across different layouts and interpolation methods at each of the points in the stance phase.

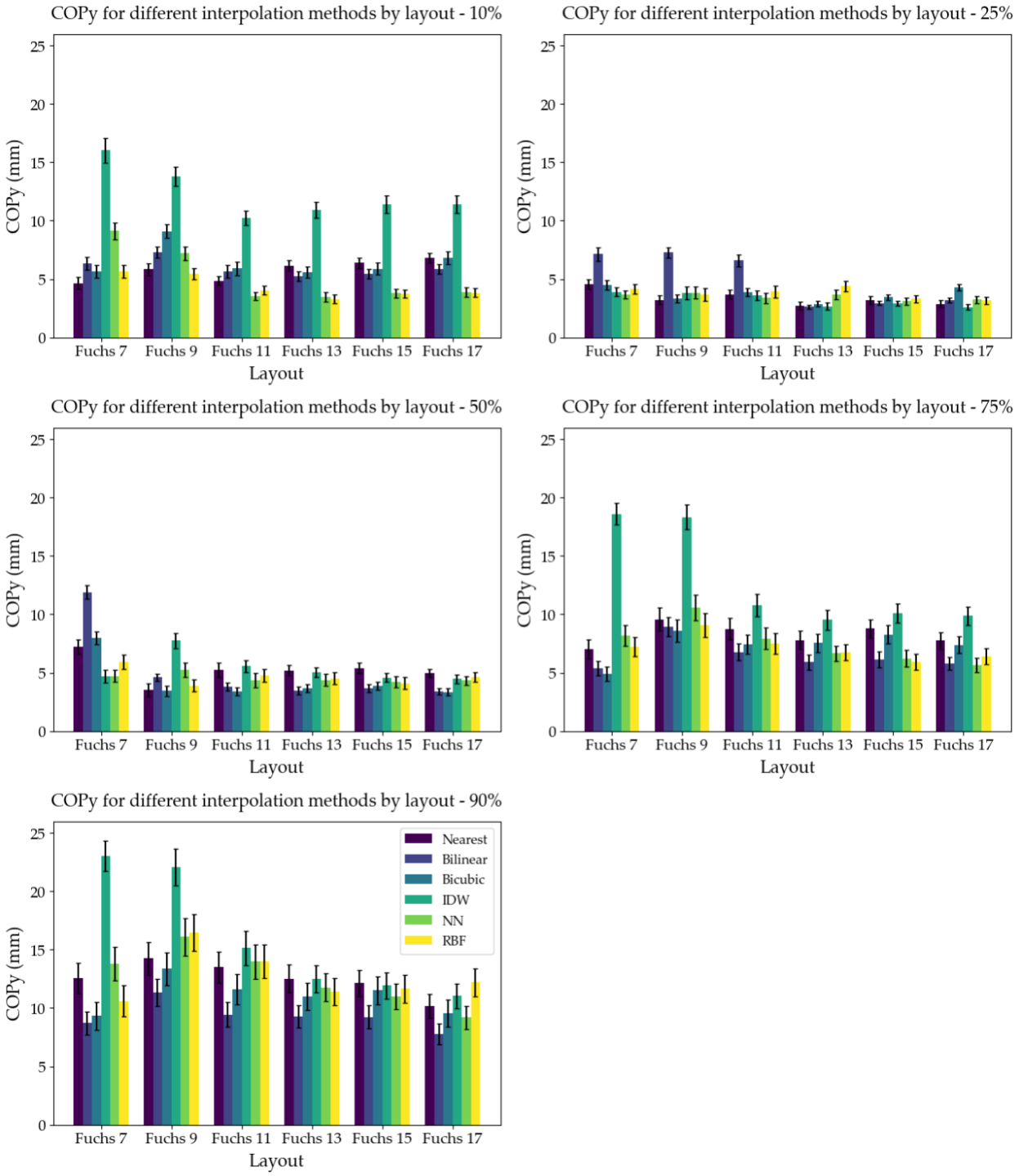

Figure 7-5 Error in anterior-posterior center of pressure (COPy) across different layouts and interpolation methods at each of the points in the stance phase.

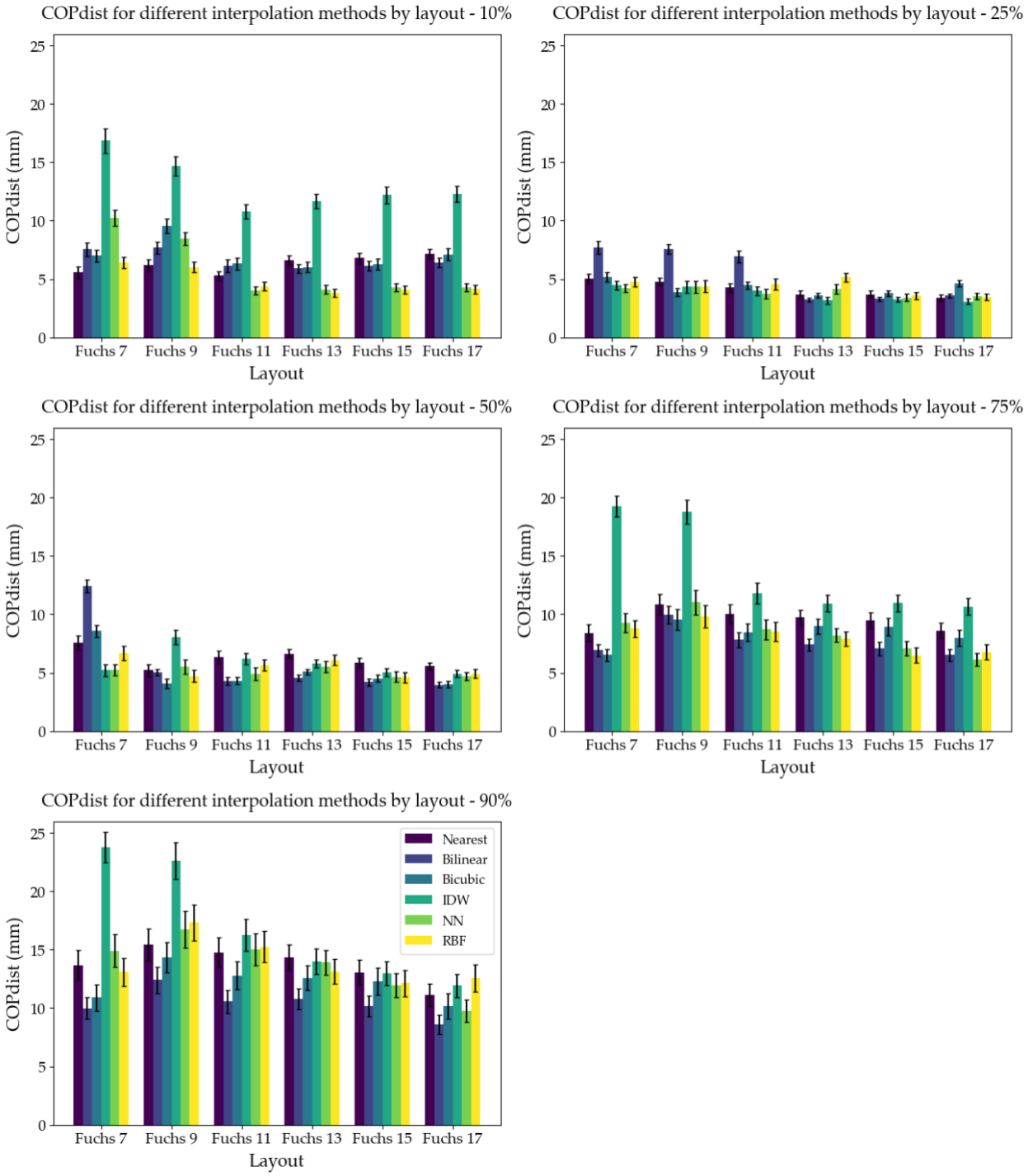

Figure 7-6 Error in distance between estimated center of pressure and reference (COPdist) across different layouts and interpolation methods at each of the points in the stance phase.

7.3 Appendix C

This appendix contains a list of the relevant patents that are either a partial or direct result of the research contained in this dissertation.

System and method for synthesizing sensor readings
US Provisional 63/282,234

System and method for analyzing force sensor data
US Provisional 63/291,424, US Provisional 63/315,847

System and method for determining running power
US Provisional 63/291,517

System and method for determining cycling power
US Provisional 63/291,994

Sensorized insert for footwear
US 29/824,064 (design patent application)
CA 212,745 (industrial design application)

System and method for determining user-estimation weights for synthesizing sensor readings
US Provisional 63/320,805

System and method for creating custom footwear
US Provisional 63/326,101

System and method for quantifying injury recovery state
US Provisional 63/356,

7.4 Appendix D

Preface

The following chapters contained in this dissertation are based on scientific publications:

Chapter 2 **S. Blades**, M. Jensen, T. Stellingwerff, S. Hundza, and M. Klimstra, 'Characterization of the Kinetyx SI Wireless Pressure-Measuring Insole during Benchtop Testing and Running Gait', Sensors, vol. 23, no. 4, p. 2352, 2023.

Statement of contribution: Conceptualization, S.B., T.S., S.H. and M.K.; methodology, S.B., S.H. and M.K.; software, S.B. and M.J.; validation, S.B. and M.K.; formal analysis, S.B. and M.K.; investigation, S.B. and M.K.; resources, S.B., S.H. and M.K.; data curation, S.B.; writing—original draft preparation, S.B. and M.K.; writing—review and editing, S.B., S.H., T.S. and M.K.; visualization, S.B. and M.K. supervision, S.H. and M.K.; project administration, S.B.; funding acquisition, S.B., S.H., T.S. and M.K. All authors have read and agreed to the published version of the manuscript.

Chapter 4 **S. Blades**, H. Marriott, S. Hundza, E. C. Honert, T. Stellingwerff, and M. Klimstra, 'Evaluation of Different Pressure-Based Foot Contact Event Detection Algorithms across Different Slopes and Speeds', Sensors, vol. 23, no. 5, p. 2736, 2023.

Statement of contribution: Conceptualization, S.B., T.S., S.H. and M.K.; methodology, S.B., S.H. and M.K.; software, S.B. and H.M.; validation, S.B., H.M. and M.K.; formal analysis, S.B., H.M. and M.K.; investigation, S.B. and M.K.; resources, S.B., H.M., E.C.H., S.H. and M.K.; data curation, S.B., E.C.H. and H.M.; writing—original draft preparation, S.B. and M.K.; writing—review and editing, S.B., H.M., E.C.H., S.H., T.S. and M.K.; visualization, S.B., H.M. and M.K. supervision, S.H. and M.K.; project administration, S.B.; funding acquisition, S.B., S.H., T.S. and M.K. All authors have read and agreed to the published version of the manuscript.

Copywrite statement: Articles published under an open access Creative Common CC BY license, any part of the article may be reused without permission provided that the original article is clearly cited. For more information, please refer to https://www-mdpi-com.ezproxy.library.uvic.ca/openaccess.

Co-author permission statement: All co-authors of Chapters 2 and 4 have agreed that the manuscripts contained in these chapters may be included in this dissertation.